Supplementary Information

Dynamic Covalent Disulfide Exchange Mediates Oral Delivery of Biomacromolecules

Chen Chen,[1,†] Tingjing Huang,[1,†] Zheng Liu,[1,†] Hongjun Li,[2] Yang Zhang,[3] Xia Liu,[1] Yuheng Guo,[1] Jingying Li,[1] Ting Wu,[1] Wen He,[1] Hao Chen,[1] Elena A. Rozhkova,[4] Guojun Chen,[5] Zhitong Chen,[6] Zhaowei Chen,[1,2,*] Zhen Gu,[2,7,*] and Huanghao Yang[1,*]

[1]MOE Key Laboratory for Analytical Science of Food Safety and Biology, New Cornerstone Science Laboratory, Fujian Provincial Key Laboratory of Analysis and Detection Technology for Food Safety, and State Key Laboratory of Photocatalysis on Energy and Environment, College of Chemistry, Fuzhou University, Fuzhou 350108, P. R. China

[2] National Key Laboratory for Advanced Drug Delivery and Release Systems, College of Pharmaceutical Sciences, Zhejiang University, Hangzhou 310058, P. R. China

[3]School of Materials Science and Engineering, Center of Advanced Analysis & Gene Sequencing, Zhengzhou University, Zhengzhou 450001, P. R. China

[4]Center for Nanoscale Materials, Argonne National Laboratory, Argonne, Illinois 60439, United States

[5]Department of Biomedical Engineering and the Rosalind & Morris Goodman Cancer Research Centre, McGill University, Montreal, QC H3A 1A3, Canada

[6]Institute of Biomedical and Health Engineering, Shenzhen Institute of Advanced Technology, Chinese Academy of Sciences, Shenzhen, 518055, China

[7]Jinhua Institute of Zhejiang University, Jinhua 321299, China

[†]These authors contributed equally: Chen Chen, Tingjing Huang, Zheng Liu

*Corresponding authors. e-mail: hhyang@fzu.edu.cn; guzhen@zju.edu.cn; chenzw@fzu.edu.cn

Materials and Methods

Materials. Deionized ultrapure water (18.2 MΩ·cm^{-1}; Millipore Co., USA) was used in all experiments. Lipoic acid, 1,1'-carbonyldiimidazole, dichloromethane, ethylenediamine, sodium chloride, anhydrous sodium sulphate, 1H-pyrazole-1-carbox-amidine hydrochloride, diethyl ether, fluorescein isothiocyanate (FITC), chlorpromazine, methyl-β-cyclodextrin, wortmannin, sodium azide, Exo 1, Endosidin 2, egg phosphatidylcholine, 1,2-dioleoyl-sn-glycero-3-phosphoethanolamine, and cholesterol were purchased from Sigma-Aldrich Co. Ltd. Recombinant human insulin was purchased from Psaitong (catalogue no. I10022). Cy5.5 NHS ester was purchase from ApexBio Technology. All these agents were used directly without further purification unless notified.

Statistical analysis. Two-tailed student's *t*-test (two group) and one-way ANOVA with Tukey post-hoc tests (multiple comparison) were performed to determine statistical significance between different groups. Data are presented as means ± s.d. as indicated in the figure legends. All statistical analyses were performed using the software GraphPad Prism. Significance was denoted in Figures as $*P < 0.05$, $**P < 0.01$, $***P < 0.001$, and $****P < 0.0001$.

Synthesis of lipoic acid-guanidinium (LG) derivatives. The procedure for synthesis of LGs was shown in Supplementary Fig. 2. In the first step, lipoic acid (4.13 g, 20 mmol) and 1,1'-carbonyldiimidazole (4.06 g, 25.0 mmol) were dissolved in anhydrous dichloromethane (100 ml) and kept at 0 °C. This solution was added dropwise into 35 ml anhydrous dichloromethane containing 10 ml (150 mmol) ethylenediamine at 0 °C. The reaction mixture was stirred for 40 min at 0 °C and for another 30 min at room temperature. Afterwards, the mixture was washed with saturated brine (3 × 100 ml). The organic phase was dried over anhydrous sodium sulphate and concentrated under reduced pressure to obtain a yellow oil (2.32 g, 47%). In the second step, lipoic acid-ethylenediamine conjugates (2.32 g, 9.4 mmol) were dissolved in anhydrous dichloromethane (150 ml) and 1H-pyrazole-1-carbox-amidine hydrochloride (1.38 g, 9.4 mmol) was then added to the solution. The suspension was stirred for 6 h at room temperature. Solvent was removed under reduced pressure and the residue was dissolved in 4 ml of methanol. Diethyl ether (50 ml) were added to induce precipitation. The solid was collected and washed with diethyl ether (50 ml) for four times to obtain pure LGs (1.78 g, 58%). The characterization of the compounds synthesized at each step are shown in Supplementary Figs. 3-8.

Preparation and characterization of LG/insulin-*x*. A stock solution of insulin (20 mg ml^{-1}) was first prepared by dissolving in 0.01 M HCl solution. Then, 100 μl of insulin was withdrawn from the stock solution, titrated with 0.01 M NaOH to pH 7.4, and diluted in Tris-HCl buffer (20 mM, pH 7.4). Thereafter, LGs dissolved in Tris-HCl buffer at different concentrations were added to the insulin solution under magnetic stirring at 400 rpm, with a final volume of 1 ml. In the preliminary study, the starting molar ratio (*x*) of LG to insulin was set as 10, 20, 40, 60, and 80. After stirring for 15 min, LG/insulin-*x* complex coacervates were separated by centrifugation at 3,000~8,000 × *g* for 10 min at 4 °C, and the complex coacervates were washed with Tris-HCl buffer for three times. Scale-up preparation of LG/insulin-40 with a formulation volume of 1 liter was performed by a similar process at the same concentrations of insulin and LG. Fluorophore-tagged LG/insulin-40 was prepared in a similar way. Changes in turbidity of the mixtures of LGs and insulin and the control solutions was recorded by measuring the absorbance at 600 nm in a time-course mode by a UV-Vis spectrometer (Cary 3500 UV-Vis, Agilent Technologies, Inc). To

monitor the ring opening kinetics of LGs, 50 μl of the reaction suspension was pipetted, mixed with 150 μl acetate buffer (pH 4.0, 50 mM), and the absorption of the resulting solution at 330 nm was measured by a plate reader (Infinite 200 PRO multimode plate reader, Tecan). The molecular weights of the poly(disulfide)s in the complex coacervates were analyzed by Bruker ultraflextreme MALDI-TOF/TOF mass spectroscopy (Bruker Daltonics, Bremen, Germany) using sinapinic acid as the matrix. The hydrodynamic size and zeta potential of LG/insulin-*x* were characterized by Malvern Zetasizer NanoZS (Malvern Instruments). The morphology of LG/insulin-*x* was characterized by Cryo-EM (Krios G3i, Thermoscientific). The secondary structure of insulin in the complex coacervates was studied by CD spectroscopy (Jasco J-1500).

The encapsulation efficiency (EE) was determined after centrifugation of LG/insulin-*x* and the concentration of free insulin in the supernatant was quantified by reverse-phase high-performance liquid chromatography (HPLC, Waters 1850, Waters). The HPLC was equipped with a C18 column (particle size, 5 μm; pore size, 300 Å; length by inner diameter, 250 mm × 4.6 mm, BDS Hypersil™) and a UV detector. The mobile phase was consisted of NaH_2PO_4 buffer (0.2 M, pH 2.3, containing 0.1 M Na_2SO_4) and acetonitrile at a ratio of 73: 27, degassed and then ran at a flow rate of 1.0 ml min^{-1} at 35 °C. All chromatograms were recorded by measuring the ultraviolet absorption at wavelength λ = 214 nm. EE was calculated using the following equation:

$$EE\ (\%) = \frac{weight_{\text{total insulin}} - weight_{\text{free insulin}}}{weight_{\text{total insulin}}} \times 100 \quad (\mathbf{1})$$

where $weight_{\text{total insulin}}$ was the starting amount of insulin added, and $weight_{\text{free insulin}}$ was the amount of insulin measured in the supernatant.

Loading capacity (LC) was calculated using the following equation:

$$LC\ (\%) = \frac{weight_{\text{total insulin}} - weight_{\text{free insulin}}}{weight_{\text{LG/insulin}-x}} \times 100 \quad (\mathbf{2})$$

where $weight_{\text{LG/insulin-}x}$ was measured after lyophilization of the complex coacervates.

To label insulin with fluorophores (*i.e.*, FITC and Cy5.5), 100 μl of isocyanate-substituted fluorophores (FITC, 25 mM) or N-hydroxysuccinimide ester of fluorophore (Cy5.5 NHS ester, 25 mM) dissolved in dimethyl sulfoxide was mixed with insulin solutions (10 mg ml^{-1}) in 5 ml sodium bicarbonate buffer (0.1 M, pH 8.3) at room temperature overnight under dark conditions. Fluorophore-tagged insulin was purified by dialysis, followed by lyophilization, and stored at 4 °C for further utilization.

Cell culture. Caco-2 human colon cells and 4T1 cells were provided by Cell Bank/Stem Cell Bank, Chinese Academy of Sciences, and used without further reauthentication. Caco-2 cells were cultured in minimum essential medium (MEM, Corning, 10009CV) containing 20% (v/v) fetal bovine serum (Gibco, Invitrogen), 100 mg ml^{-1} streptomycin (Gibco, Invitrogen) and 100 U ml^{-1} penicillin (Gibco, Invitrogen) in an incubator (Thermo Scientific) at 37 °C in a humidified atmosphere containing 5% (v/v) CO_2. 4T1 cells were cultured in Dulbecco's Modified Eagle Medium (DMEM, Gibco, 11965092) containing 10% (v/v) fetal bovine serum (Gibco, Invitrogen) and other culture conditions were the same to that of Caco-2 cells. Cells were checked every three months for potential mycoplasma contamination.

Caco-2 monolayers in Transwells. Caco-2 cells were seeded at a density of 50,000 cells per well on Corning Transwell polyester membrane cell culture insert (diameter 12 mm, pore size 0.4 μm) placed inside 12-well plates and cultured for 15-24 days to allow for differentiation. The transepithelial electrical resistance (TEER) of cell monolayers was monitored every three days to confirm barrier formation using a Millicell ERS voltmeter (Millipore Corp., Bedford, MA, USA) connected to a pair of chopstick electrodes. When the TEER exceeded 500 Ω·cm^2, sufficient tight junction integrity between cells were considered formed and further studies were performed.

***In vitro* transepithelial transport.** Prior to the transepithelial transport study, the Caco-2 monolayers were washed with Hanks's balanced salt solution (HBSS, pH 7.4) and then prewarmed MEM was added to the apical and basolateral chambers. After equilibration at 37 °C for 30 min, the medium in the apical chambers were replaced with MEM containing FITC-tagged LG/insulin-*x* (*x* = 10, 20, 40, 10 μg ml^{-1} of insulin), equivalent FITC-tagged free insulin (10 μg ml^{-1}), or FITC-tagged insulin (10 μg ml^{-1}) plus sodium caprate (2 mg ml^{-1}). After certain time intervals, 20 μl of culture medium was taken out from the basolateral chambers and was replaced with equal volume of fresh MEM. The amount of insulin transported across each Caco-2 monolayer was determined by measuring the fluorescence intensity of FITC using a microplate reader at 488/520 nm excitation/emission wavelengths and calculated from the calibration curve of FITC-tagged insulin in MEM. During the transepithelial transport study, the TEER values of Caco-2 monolayers treated with different insulin formulations were recorded at indicated time points. TEER changes of each group were normalized to their values measured before the transport assays.

The apparent permeability coefficient (P_{app}) of each group was calculated according to previous protocols[1]. For groups with final concentrations in the acceptor chambers that did not exceed 10% of the concentrations in the donor chambers, the P_{app} values were calculated using the following equation:

$$P_{app} = \frac{dQ}{dt} \times \frac{1}{A \times C_0} \quad (3)$$

where dQ/dt is the steady-state flux of insulin from the donor chamber to the acceptor chamber, A is the membrane area of transwell insert (cm^2), and C_0 is the initial concentration of insulin in the donor chamber.

For groups with final concentrations in the acceptor chambers that exceeded 10% of the concentrations in the donor chambers, the P_{app} values were calculated using the following equation:

$$C_a(t) = \frac{M}{V_d + V_a} + \left(C_{a,0} - \frac{M}{V_d + V_a}\right) e^{-P_{app} A (1/V_d + 1/V_a) t} \quad (4)$$

Where V_d is the volume of the donor chamber, V_a is the volume of the acceptor chamber, A is the area membrane area of the transwell insert, M is the total amount of insulin added in the transwell system, $C_{a,0}$ is the initial concentration of insulin in the acceptor chamber, and $C_a(t)$ is the concentration of insulin in the acceptor chamber at time t measured at different time intervals.

To study the effect of inhibitors on the transepithelial transport of LG/insulin-*x*, the Caco-2 monolayers were first incubated with endocytosis inhibitors including chlorpromazine (10 μg ml^{-1}), methyl-β-cyclodextrin (50 μM), wortmannin (50 nM) and sodium azide (NaN_3, 10 mM), exocytosis inhibitors including Exo 1 (20 μM) and Endosidin 2 (40 μM), DTNB (2 mg ml^{-1}), and DTNB-loaded fusogenic liposomes (2 mg ml^{-1} of DTNB) for 30 min. Thereafter, the medium in the basolateral chambers was

replaced with fresh MEM while the medium in the apical side was replaced with MEM containing FITC-tagged LG/insulin-*x* (*x* = 10, 20, 40; 10 μg ml^{-1} of insulin) and equal concentrations of the corresponding inhibitors. The amount of insulin transported across Caco-2 monolayers in each transwell was determined as described above.

The DTNB-loaded fusogenic liposomes were prepared as following[2]. Lipid solution was prepared in chloroform with the composition of EPC/DOTAP/CH 5:1:0.1 (w/w/w, total = 24.4 mg), the solvent was then removed by rotary evaporation under vacuum. The formed lipid film was hydrated with 4 ml Hepes buffer (5 mM, 150 mM NaCl, pH 7.4) containing DTNB (6 mg ml^{-1}). The suspension was then extruded three times through membrane filters with progressively decreasing pore size: 0.80, 0.45, and 0.20 μm (all surfactant-free cellulose; Corning). Nonencapsulated DTNB was removed by three cycles of centrifugation at 34,000 × g for 1 h at 4 °C (Micro Ultracentrifuge CS120FNX, Hitachi) followed by resuspension in Hepes buffer. Non-loaded liposomes were prepared in a similar way except that no DTNB was added in the buffer during hydration.

Tight junction protein immunostaining. After washing the formed Caco-2 monolayers twice with PBS, 0.5 ml MEM containing LG/insulin-*x* (*x* = 10, 20, 40, 10 μg ml^{-1} of insulin) or insulin (10 μg ml^{-1}) plus sodium caprate (2 mg ml^{-1}) were added to the transwell inserts. Then, the transwell inserts were transferred to 12-well plates containing 1.5 mL MEM per well and the cells were further incubated at 37 °C for 6 h. After that, Caco-2 monolayers were washed with PBS twice and then stained Alexa Fluor 488™ ZO-1 monoclonal antibody (Invitrogen, catalogue no. MA3-39100-A488), Alexa Fluor 488™ claudin-5 monoclonal antibody (Invitrogen, catalogue no. 352588), and Alexa Fluor 488™ occludin monoclonal antibody (Invitrogen, catalogue no. 331588) according to manufacturer's instructions. The nuclei were stained with Hoechst 33342 (1 μg ml^{-1}). Thereafter, the PET membranes of transwell inserts were cut carefully by a scalpel, and invertedly placed on a cover slip for imaging by a Nikon A1 confocal laser scanning microscope.

Cell viability assay. The potential cytotoxicity of LG/insulin-*x* (*x* = 10, 20, 40) towards Caco-2 cells during the transepithelial transport was assessed by the 3-(4,5)-dimethylthiahiazo(-z-y1)-3,5-di-phenytetrazoliumromide (MTT) assay. At the end of transepithelial transport study, the culture media of the basolateral and apical chambers were replaced with MEM containing 0.5 mg ml^{-1} MTT and the cells were incubated for an additional 4 h. The culture medium was then removed and DMSO was added to each well to dissolve the formazan crystals. 100 μl of the solution was withdrawn from each well and transferred to a 96-well plate. The absorbance at 570 nm, which is proportional to the viable cell number, was measured in a microplate reader. Cell viability was expressed as percentage of absorbance normalized to the untreated controls. To measure the *in vitro* biocompatibility of LG/insulin-*x* (*x* = 10, 20, 40), Caco-2 cells were seeded in 96-well plates at a density of 10,000 cells per well. LG/insulin-*x* of different concentrations was added and then incubated with the cells for 24 h. Thereafter, the cell viability was measured by MTT assay.

Lactate dehydrogenase (LDH) leakage assay. At the end of transepithelial transport studies, the culture medium from apical chamber and lateral chamber were mixed, 50 μl of this mixture was taken out and the LDH leakage was quantified using an LDH assay kit (Sigma-Aldrich, catalogue no. MAK066) according to the manufacturer's instructions. Nontreated Caco-2 monolayers and 1% Triton X-100 treated monolayers were used as negative and positive controls, respectively. Results were expressed as percentage of LDH

leakage normalized to the positive control. To evaluate the effect of LG/insulin-*x* of different concentrations, Caco-2 cells were seeded in 96-well plates at a density of 10,000 cells per well. LG/insulin-*x* of different concentrations was added and then incubated with the cells for 24 h. Thereafter, the LDH leakage was quantified using an LDH assay kit, where 1% Triton X-100 treated Caco-2 cells were used as the control.

Cellular uptake studies. Caco-2 cells were seeded in 35 mm glass bottom confocal dishes at a density of 100,000 cells per dish and incubated at 37 °C until over 80% confluent (~7 days). Caco-2 cells were first incubated with MemGlow™ NR12A (a membrane lipid order probe, 100 nM; Cytoskeleton, catalogue no. MG07)[3] for 10 min; then, Cy5.5-tagged LG/insulin-*x* (10 μg ml^{-1} of insulin) was added to the culture medium and the cells were further incubated for 10 min before imaging under Zeiss LSM 900 confocal microscope (Carl Zeiss). The fluorescence of Cy5.5-tagged LG/insulin-*x* was used to locate the regions for recording lipid order. Ratiometric confocal images were obtained under the excitation of 488 nm laser, and the fluorescence was recorded at two wavelength ranges: 550-600 and 600-650 nm in a sequential mode by rapid switching to minimize the drift effect. Ratiometric images were produced by dividing the intensity of the 550-600 nm channel by that of the 600-650 nm channel. For each pixel, the ratio was coded using a pseudocolor scale, and the intensity is defined by the integral intensity recorded for both channels at the corresponding pixel. For groups studying the effect of endocytosis inhibitors and DTNB, the cells were incubated with inhibitors and DTNB at concentrations used above for 30 min before washing and further incubated with MemGlow™ NR12A and Cy5.5-tagged LG/insulin-*x* in the presence of inhibitors and DTNB. To measure the lipid flip-flop in membrane regions binding LG/insulin-*x* and the membrane permeability during the initial uptake, Caco-2 cells incubated with Cy5.5-tagged LG/insulin-*x* (10 μg ml^{-1} of insulin) in the presence of Annexin V-Alexa Fluor 488 (10 μl; Invitrogen, Catalogue no. A23204) in Annexin V buffer (10 mM HEPES, 140 mM NaCl, and 2.5 mM $CaCl_2$, pH 7.4.), and propidium iodide (1 μg ml^{-1}) for 10 min before imaging under a confocal microscope.

To study the uptake kinetics of LG/insulin-*x* and the correlations between LG/insulin-*x* and organelles in confluent cells, the cell nuclei, endo-lysosomes, mitochondria, endoplasmic reticulum (ER), Golgi apparatus and microtubules were stained by Hoechst 33342 (1 μg ml^{-1}, Invitrogen, catalogue no. H3570, 405⁄461 nm), LysoTracker Deep Red (10 ng ml^{-1}, 647/668 nm, Invitrogen, catalogue no. L12492), MitoTracker Red CMXRos (200 nM, 579⁄599 nm, Invitrogen, catalogue no. M7512), ER-Tracker Red (500 nM, 587⁄615 nm, Invitrogen, catalogue no. E34250), Golgi-Tracker Red (167 μg ml^{-1}, 589⁄615 nm, Invitrogen, catalogue no. D7540) and Tubulin-Tracker Deep Red (1×, 652⁄669 nm, Invitrogen, catalogue no. T34077) according the manufactures' instructions, respectively. For groups treated with inhibitors, Caco-2 cells were first incubated with endo/exocytosis inhibitors, DTNB, or DTNB-loaded fusogenic liposomes at concentrations used above for 30 min. Then, the culture medium in each dish was replaced with MEM containing FITC-tagged LG/insulin-*x* (10 μg ml^{-1} of insulin) and equal concentration of the corresponding inhibitor. Thereafter, the cells were incubated for another 2 h before imaging. The obtained confocal microscopy images were analyzed following routine procedures to extract Pearson's correlation coefficients using ImageJ software, equipped with a JACoP plugin.

To study the localization of LG/insulin-*x* at the basal plasma membrane during the transepithelial delivery, the monolayers were examined by confocal laser scanning microscope and the *x*-*z* sections were created by a *Z*-stacking method with a 1-μm interval after incubated with FITC-tagged LG/insulin-*x* (10 μg

ml^{-1}) in the absence or presence of exocytosis inhibitors (Exo 1, 20 μM; Endosidin 2, 40 μM) or DTNB-loaded fusogenic liposomes (2 mg ml^{-1} of DTNB). In this section, to avoid potential disturbance caused by the transported LG/insulin-*x* that could reroute back from the acceptor to donor chamber *via* DCDE-mediated uptake from the basolateral plasma membrane, home-made 3D-printed acceptor chambers equipped with perfusion systems were used (Supplementary Fig. 31). The chambers with an inner volume of about 5 mL fitting the transwell inserts were printed by a 3D printer (Fromlabs 3+, Formlabs Inc., Massachusetts, USA) using Clear Resin (Formlabs Inc., Massachusetts, USA) according to the manufacture's protocol. After 1 h incubation, the transwell inserts were withdrawn, and the basolateral and apical surface of monolayers were washed by HBSS in transwell plates. Then, cells were fixed with 4% formaldehyde for 15 min, washed with HBSS and stained with Alexa Fluor-555 Wheat Germ Agglutinin (10 μg mL^{-1}, 555/565 nm, Invitrogen, catalogue no. W32464) for 10 min to stain the cellular membranes and then washed with HBSS. Subsequently, the nuclei were stained with Hoechst 33342 (1 μg ml^{-1}) for 10 min and washed with HBSS. After staining, the PET membranes of transwell inserts were cut carefully by a scalpel, and invertedly placed on a cover slip for confocal imaging.

Animal experiments. Animal experiments were performed according to animal protocols approved by the Institutional Animal Care and Use Committee of Fuzhou University (protocol no. 013-20200610-002). C57BL/6J mice (male, 6-8 weeks old) and BALB/c mice (female, 6-8 weeks old) were purchased from Beijing Vital River Laboratory Animal Technology Co. Ltd. Bama minipigs (female, 6 months old, 20-25 kg) were purchased from Wuhan Origin of Life Technology Co. Ltd. To establish type-1 diabetic mice, C57BL/6J mice were fasted overnight but had free access to water, then streptozotocin (10 mg ml^{-1}) was intraperitoneally injected at a dose of 170 mg kg^{-1} in sterilized citrate buffer solution (100 mM, pH 4.4). After one week, mice with fasting blood glucose levels higher than 300 mg dl^{-1} were considered to be diabetic and used for further experiments. The diabetic minipig model was established by intraperitoneal injection of two doses of streptozotocin (75 mg kg^{-1} for the first administration and 150 mg kg^{-1} for the second administration) in sterilized citrate buffer solution (75 mg ml^{-1}, 100 mM, pH 4.4) with an 8-day interval. After about one week of recovery, the blood glucose levels were monitored using a continuous glucose monitoring system (288 data points per day; SiJoy GS1 CGM system, Shenzhen SiBionics Technology Co. Ltd.) to confirm the induction of insulin-deficient diabetes Bama minipig model (fasting blood glucose levels higher than 250 mg dl^{-1}). For all the diabetes treatment studies, mice and minipigs were randomly allocated to each group. Animal experiments involved exclusively objective measurements and the researchers were not blinded to group application during the animal studies. All data from *in vivo* experiments were collected and analyzed by at least three researchers.

Intraintestinal insulin delivery. After overnight fasting, the initial blood glucose levels of diabetic mice were measured before being placed on a warm pad and kept anesthetized by isoflurane inhalation. The intestines of mice were surgically exposed and insulin of different formulations, including LG/insulin-40, free insulin, or mixture of sodium caprate (100 mg kg^{-1}) and insulin in 0.1 ml PBS buffer, were injected into the jejunum lumen at an insulin dose of 20 IU kg^{-1}. Intrajejunal injection of an equal volume of PBS was used as a control. The abdominal wall was seamed with PGA suture, and the skin wound was closed with wound clips. Thereafter, the mice were woken up from anesthesia, and the blood glucose levels of the mice were monitored with a Sinocare Safe AQ Smart Blood Glucose Meter (Sinocare Inc., Changsha, China) by collecting ~3 μl blood samples from the tail vein at predetermined time intervals. For comparison to the

current standard of insulin delivery, 5 IU kg^{-1} of insulin was subcutaneously injected to the dorsum of additional diabetic mice. The area above the curves (AACs) of the blood glucose levels for each mouse was calculated by trapezoidal integration to sum the areas between the initial blood glucose value and known points in the blood glucose profile. The pharmacological availability compared to subcutaneous injection was calculated using the following equation:

$$Pharmacological\ availability\ (\%) = \left(\frac{AAC_{\text{test}}}{Dose_{\text{test}}}\right) / \left(\frac{AAC_{\text{s.c.}}}{Dose_{\text{s.c.}}}\right) \times 100 \quad (\mathbf{5})$$

where AAC_{test} and $AAC_{\text{s.c.}}$ represent the AACs yielded from the blood glucose profiles of mice treated with intrajejunal injection or oral administration of insulin (in the following sections) of different formulations and subcutaneous insulin injection (5 IU kg^{-1}), respectively; $Dose_{\text{test}}$ and $Dose_{\text{s.c.}}$ represent the dose of insulin administered by intrajejunal injection or oral administration and subcutaneous injection, respectively.

TEM examination of tight junctions. For transmucosal delivery studies, 2 h after intrajejunal injection of LG/insulin-40 or sodium caprate plus insulin, mice were euthanized and small parts of jejunum tissues near the injection site were collected and washed with PBS. The samples were fixed by 2.5% glutaraldehyde in PBS. After washed with PBS, the tissues were postfixed in 1% buffered osmium tetroxide, dehydrated, and embedded in epoxy resin within embedding capsules. Thereafter, the embedded tissues were cut with an ultra-microtome to obtain ultrathin sections with thicknesses of 70-100 nm. These sections were loaded onto copper grids, contrasted with uranyl acetate, and examined by transmission electron microscope operated at 80.0 kV (HT7700, Hitachi, Japan).

Stability of LG/insulin-40 in simulated gastric/intestinal fluids. Stimulated gastric fluid (SGF) and simulated intestinal fluid (SIF) were prepared according to the United States Pharmacopeia and National Formulary USP 35-NF 30 (The United States Pharmacopeial Convention, Inc.: Rockville, MD, 2012). Briefly, to prepare SGF, 3.2 g pepsin and 2.0 g NaCl in 1 liter of deionized water, and the pH of the solution was adjusted to 1.2 with hydrochloric acid. SIF was prepared by dissolving 6.8 g of KH_2PO_4, 0.896 g NaOH and 10 g trypsin in 1 liter deionized water and the pH of the solution was adjusted to 6.8. 200 μl aliquots of LG/insulin-40 (10 mg ml^{-1} of insulin) was added to 1.8 ml of SGF and SIF, respectively. Samples were incubated at 37 °C under shaking (100 rpm) over 6 h. At indicated time intervals, 20 μl of the suspensions were taken out, immediately mixed with 50 μl Pepstatin A (0.04 mg ml^{-1}) or Aprotinin (1.0 mg ml^{-1}) in 0.2 M NaH_2PO_4 buffer (pH 2.3, containing 0.1 M Na_2SO_4). Meanwhile, equal volume of fresh stimulated fluid was added to the reaction solution. After that, the insulin content was analyzed by HPLC. Studies with free insulin in SGF and SIF were used as controls.

The stability of LG/insulin-40 in the simulated fluids was also studied by measuring the changes in turbidity and hydrodynamic sizes. Due to the fast dissociation rate of LG/insulin-40 in SGF, changes in turbidity were recorded by a UV-Vis spectrometer in time-course mode. 1.5 ml LG/insulin-40 (2 mg ml^{-1}) was first placed in the cuvette, then the time-course recording mode of UV-Vis spectrometer was turned on. After a short while, 1.5 ml SGF (2 ×) was added, the changes in turbidity were recorded until reaching steady. Thereafter, the solutions were drawn and analyzed by Malvern Zetasizer NanoZS. The turbidity changes of LG/insulin-40 suspensions (1 mg ml^{-1}) in stimulated intestinal fluid over 6-h incubation were recorded by microplate reader at indicated time points. After the 6-h incubation, the suspensions were analyzed by Malvern Zetasizer NanoZS.

Translocation across reconstituted mucus. Type II mucin, which is the primary component of intestinal mucus[4], from porcine stomach (Sigma-Aldrich, catalogue no. M2378) was used to reconstitute the *in vitro* mucus 3D migration model. Briefly, mucin was dissolved in PBS (50 mg ml^{-1}) to prepare the reconstituted mucus. For permeation studies, 50 µl of the prepared mucin solution was added to each transwell insert to give a mucus layer with a thickness of about 0.45 mm. Then, the transwell inserts were placed in a plate containing 1.5 ml PBS in the acceptor chambers and 500 µl suspensions of FITC-tagged LG/insulin-40 or free insulin in PBS were added to the apical surface of the mucus layer in the donor chambers at a insulin concentration of 10 µg ml^{-1}. At indicated time intervals, 20 µl of samples were taken out from the basolateral chambers and replaced with equal volumes of PBS. The amount of insulin transported across the mucus layers was determined by measuring the fluorescence intensity of FITC using a microplate reader and calculated from the calibration curve of FITC-tagged insulin in PBS. To study the effect of thiol-blocking agents, similar experimental processes were conducted except that DTNB (2 mg ml^{-1}) were mixed with the mucus 1 h before added to transwell inserts.

For 3D confocal imaging, mucus was stained by Alexa Fluor-555 Wheat Germ Agglutinin 1 h before added into glass bottom dish (200 µl) to give a *c.a.* 0.6-mm deep layer. Then, 100 µl suspensions of FITC-tagged LG/insulin-40 or free insulin in PBS were gently dropped to the apical surface of the mucus layer within the visual field of confocal microscope objective. After sitting for 15 minutes, *Z*-stack scanning was carried out with a 1-µm interval, starting from the planes showing observable green fluorescence signals to the apical surfaces. This scanning process was performed to record the diffusion of FITC-tagged LG/insulin-40 within the mucus. For groups studying the effect of thiol-blocking agents, DTNB and Alexa Fluor-555 Wheat Germ Agglutinin were mixed with the mucus 1 h before added confocal dishes.

Mucus rheology. To study if the permeation of LG/insulin-40 through mucus was gained by the mucus thinning effect, the viscosity of mucus in the presence of LG/insulin-40 of different concentrations was measured. 950 µl aliquots of reconstituted mucus (50 mg ml^{-1}) were mixed with 50 µl of LG/insulin-40 with final concentrations of 0–1.0 mg ml^{-1} in PBS and incubated for 3 h. Thereafter, the viscosities of the samples were measured across the shear rate of 0.05-100 1/s at room temperature using an AR-G2 rheometer equipped with a 60-mm diameter steel cone plate geometry, with the gap set at 0.35 mm (TA Instruments, New Castle, DE).

Electrophoresis. To check whether LG/insulin-40 had mucolytic effect, sodium dodecyl sulfate–polyacrylamide gel electrophoresis (SDS-PAGE) analysis was leveraged to study the integrity of mucin after incubated with LG/insulin-40 of different concentrations. Briefly, aliquots of 100 µl reconstituted mucus (50 mg ml^{-1}) were mixed with 10 µl of LG/insulin-40 in PBS, with final concentrations of 0-1.0 mg ml^{-1}. After incubation at 37 °C for 3 h, the solutions were analyzed by SDS-PAGE on 4-15% precast polyacrylamide gel (Bio-Rad, catalogue no. 4561083). Thereafter, the gel was stained by periodic acid-Schiff's reagent (PAS, Thermo Fisher Scientific, catalogue no. 24562).

Capsule preparation and characterization. Before packing into capsules, LG/insulin-40 suspensions were concentrated to 10 mg ml^{-1} (of insulin) by centrifugation and re-suspension. For mice, Torpac gelatin capsules of size M were used (Braintree Scientific Inc., MA, USA, catalogue no. A-CT M). Before loading LG/insulin-40 concentrate, both the inner and outer surfaces of capsules were wetted with Eudragit® L 100-55 (Evonik) methanol solution (15% w/w) at room temperature to form the enteric coating and placed under

gentle air flow to dry completely. The enteric coating process was repeated for three times. For Bama minipigs, enterosoluble vacant gelatin capsules of size 2 (Shaoxing Kangke Capsule Co., Ltd, Zhejiang, China) were used for loading LG/insulin-40 concentrate. To prepare capsules loaded with free insulin, similar procedures were conducted. These capsules were immediately utilized for animal or release studies after preparation.

To mimic the dissolution of size M capsules in murine gastrointestinal trials, FITC-tagged LG/insulin-40-loaded enteric capsules were first placed into 2 ml SGF without pepsin. The samples were shaken at 100 rpm and 37 °C for 1 h, 10 μl of the supernatants was taken out and mixed with 200 μl PBS at indicated time points for FITC fluorescence readout. Capsules were then transferred into SIF without trypsin and the samples were shaken again and sampled for FITC-tagged LG/insulin-40 in the supernatant at indicated time intervals. The amount of insulin released from the capsules was determined by measuring the fluorescence intensity of FITC using a microplate reader at 488/520 nm excitation/emission wavelengths and calculated from the calibration curve. For measurement of the dissolution of size 2 capsules, similar procedures were conducted except that 5 ml of simulated fluids was utilized.

Oral insulin delivery in diabetic mice. After fasting overnight, diabetic mice were treated with LG/insulin-40-loaded enteric capsules (20 IU kg^{-1}) at predetermined insulin doses by oral gavage with a capsule dosing syringe (Braintree Scientific Inc., MA, USA, catalogue no. X-SYR M). The mice remained fasted during experiments but had free access to water. The blood glucose levels of mice were monitored with a glucose meter by collecting ~3 μl blood samples from the tail vein at predetermined time intervals. For control groups, free insulin-loaded enteric capsules (20 IU kg^{-1}) or blank enteric capsules were orally administered *via* a capsule dosing syringe, and LG/insulin-40 solutions (20 IU kg^{-1}) were orally administrated *via* an oral gavage syringe. For comparison to the current standard of insulin delivery, 5 IU kg^{-1} of insulin was subcutaneously injected to the dorsum of additional diabetic mice. The AACs of the blood glucose levels for mice after receiving different treatments were calculated by trapezoidal integration to sum the areas between the initial blood glucose values and known points in the blood glucose profiles. The pharmacological availability compared to subcutaneous injection was calculated using Equation (**5**).

To measure the plasma insulin levels *in vivo*, ~25 μl of blood samples were collected from the tail veins of mice at indicated time points. The plasma was isolated and stored at -20 °C until being assayed. The plasma insulin concentrations were measured with a Human Insulin ELISA kit (Invitrogen, Catalogue No. KAQ1251) according to the manufacturer's protocol. The areas under the plasma insulin concentration curves (AUCs) for mice after different treatments were calculated by trapezoidal integration to sum the areas between the initial plasma insulin concentration values and known points in the plasma insulin concentration time profiles. The relative bioavailability compared to subcutaneous injection was calculated using the following Equation:

$$Relative\ bioavailability\ (\%) = \left(\frac{AUC_{\text{test}}}{Dose_{\text{test}}}\right) / \left(\frac{AUC_{\text{s.c.}}}{Dose_{\text{s.c.}}}\right) \times 100 \quad (\mathbf{6})$$

where AUC_{test} and $AUC_{\text{s.c.}}$ represent the AUCs derived from the plasma insulin concentration time profiles of mice treated with oral gavage of insulin of different formulations and subcutaneous insulin injection, respectively; $Dose_{\text{test}}$ and $Dose_{\text{s.c.}}$ represent of the dose of insulin administered by oral administration and subcutaneous injection, respectively.

***Ex vivo* imaging.** After fasting overnight, diabetic mice were treated with Cy5.5-tagged LG/insulin-40-loaded enteric capsules by oral gavage. At different time intervals post administration, mice were euthanized, the entire intestine and major organs including liver, heart, kidneys, spleen, and lung were harvested and visualized with an IVIS Lumina III Series system (PerkinElmer) by recording the fluorescence at 710 nm under the excitation of 660 nm. Meanwhile, mid parts of the lighted intestinal segments, including duodenum (1 h after dosing), jejunum (2 h after dosing), ileum (4 h after dosing), and colon (6 h after dosing), and liver (4 h after dosing) were collected for cryosection preparation, nucleus staining and confocal microscopy imaging.

***Ex vivo* absorption.** The absorption of LG/insulin-40 across different intestinal regions (duodenum, jejunum, ileum, and colon) was studied using the Ussing Chamber System (Beijing Jingong Hongtai Technology Co., LTD., China). After fasting overnight, diabetic mice were euthanized, and the intestines were immediately collected. 2-3 cm of the mid parts of the four intestinal segments were isolated, cut open into planar sheets and washed carefully with ice-cold Krebs-Ringer buffer (117 mM NaCl, 4.7 mM KCl, 1.2 mM Na_2HPO_4, 25 mM $NaHCO_3$, 1.2 mM $MgCl_2$, 2.5 mM $CaCl_2$, 11 mM glucose) to remove the luminal contents. Then, the tissues were mounted between the donor and acceptor chambers with a surface area of 0.20 cm^2 without stripping off the muscle and serosal layers. The chambers were filled with 5 ml Krebs-Ringer buffer, kept at 37 °C, and continuously bubbled with carbogen (95% oxygen and 5% carbon dioxide) to stabilize the buffer pH. After an equilibration period to achieve a stable short-circuit current (10-15 min), FITC-tagged LG/insulin-40 (5 μg ml^{-1} of insulin) was added to the donor chambers. At predetermined time intervals, 100 μl of solutions were withdrawn from the acceptor chamber and replaced with equal volume of prewarmed fresh Krebs-Ringer buffer. The amounts of insulin transported across each region were determined by measuring the fluorescence intensity of FITC using a microplate reader and calculated from the calibration curve of FITC-tagged insulin in Krebs-Ringer buffer. For groups studying the effect of thiol-blocking reagents, DTNB or DTNB-loaded fusogenic liposomes (2 mg ml^{-1} of DTNB) were added to the acceptor chamber and incubated for 30 min. Then, the solutions in both sides were replaced with fresh prewarmed Krebs-Ringer buffer. Thereafter, FITC-tagged LG/insulin-40 plus DTNB or DTNB-loaded fusogenic liposomes (2 mg ml^{-1} of DTNB) were added to the donor chambers for measuring the transport kinetics of insulin. The P_{app} value of each group was calculated using Equation (**3**) or (**4**), except that A represented the tissue area (0.2 cm^2) between the donor and acceptor chambers. During the experiments, the donor and acceptor chambers were connected to Ag/AgCl electrodes *via* 3 M KCl agar bridges, and the TEER's of intestinal segments were recorded in real time by the equipped VCC MC6Plus clamp patch to assess the integrity of tissues.

Hepatic glucose utilization in mice. The effect of oral insulin on murine hepatic glucose utilization was studied by measuring the hepatic glycogen contents after consecutively treating diabetic mice for different days. Mice were deprived of food for 1.5 h before dosing at around 9:00 a.m. and p.m. but free to food at other times. Two hours after receiving LG/insulin-40-loaded enteric capsules (20 IU kg^{-1}) or 0.5 h after receiving subcutaneous injection of insulin (5 IU kg^{-1}), mice were free to food. For glycogen measurement, mice were euthanized 4 h after the meal post the last insulin dosing on the indicated day, their livers were harvested immediately, and the hepatic glycogen contents were measured by a glycogen assay kit (Abcam, catalogue no. ab65620) according to the manufacturer's instructions. Nontreated diabetic mice and healthy mice experiencing similar feeding procedures were used as the control.

Long-term biosafety evaluation. To evaluate the long-term biosafety of orally delivered LG/insulin-40, diabetic mice were treated with LG/insulin-40-loaded enteric capsules (20 IU kg^{-1}) twice daily for two weeks. Mice were deprived of food for 1.5 h before each dosing at around 9:00 a.m. and p.m. but free to food at other times. Diabetic mice receiving saline were used as the control. During the course, the body weight of mice was measured every other day. On day 0 before oral dosing and at 12 h after the last oral dosing on day 14, blood samples were collected for analyzing the levels of endotoxin and proinflammatory factors in the plasma and the blood biochemical parameters. Endotoxins were detected using a Pierce™ chromogenic endotoxin quant kit (Invitrogen, catalogue no. A39553) according to the manufacturer's instructions. For immunological analysis, representative inflammatory factors, including TNF-α, IL-1β, IL-6, and IFN-γ were measured by ELISA kits (Invitrogen, Thermo Fisher Scientific) according to the manufacturer's instructions. Blood biochemical parameters were analyzed by H7600-020 automatic analyzer (Hitachi, Japan) for evaluating potential toxicity toward the liver and kidneys. The major organs (heart, liver, spleen, lung, and kidneys) and pieces of different intestinal segments (duodenum, jejunum, ileum, and colon) were harvested, fixed in 4% paraformaldehyde, embedded in paraffin, cut into 5-μm sections, and stained with hematoxylin and eosin for histological analysis. For intestinal microstructure analysis, pieces from the mid parts of different intestinal regions were isolated and their ultrathin sections were prepared by the protocol described above for TEM imaging.

Oral insulin delivery in large animals. Streptozotocin-induced diabetic Bama minipigs were used as the large animal model. The diabetic minipigs were fed with two daily meals (around 9:00 a.m. and 7:00 p.m.) and provided with drinking water all the time. Before pharmacodynamic and pharmacokinetics studies, all diabetic minipigs were fasted overnight but had free access to water. The continuous glucose monitoring system (288 data points per day) was applied on the back according to the procedure shown in Supplementary Fig. 50. Minipigs were treated with LG/insulin-40-loaded enteric capsules (size 2) at predetermined insulin doses (2 IU kg^{-1}) by oral gavage with a capsule dosing syringe. Additional water (20-40 ml) was used to flush the capsules into the stomach of minipigs. For control groups, free insulin-loaded enteric capsules or blank enteric capsules were orally administered *via* a capsule dosing syringe, and LG/insulin-40 solutions were directly orally administrated *via* an oral gavage syringe. For comparison to the current standard of insulin delivery, 0.5 IU kg^{-1} of insulin was subcutaneously injected behind the base of ears of control diabetic minipigs. The AACs of the blood glucose levels for minipigs after different treatments were calculated by trapezoidal integration to sum the areas between the initial blood glucose values and known points in the blood glucose profiles. The pharmacological availability compared to subcutaneous injection was calculated using Equation (**5**).

To measure the plasma human insulin levels *in vivo*, ~50 μl of blood samples were collected from the external jugular vein at the indicated time points. The plasma was isolated and stored at -20 °C until analysis. The plasma insulin concentrations were measured with a Human Insulin ELISA kit according to the manufacturer's protocol. The AUCs of plasma insulin levels for minipigs after different treatments were calculated by trapezoidal integration to sum the areas between the initial plasma insulin concentration values and known points in the plasma insulin concentration time profiles. The relative bioavailability compared to subcutaneous injection was calculated using Equation (**6**).

Multi-day oral dosing in large animal. For multi-day oral dosing studies, minipigs were orally gavaged

with LG/insulin-40-loaded enteric capsules 2 h before each meal (4 IU kg^{-1}, drug dosing time around 7:00 a.m. and 5:00 p.m.) for two weeks. Diabetic minipigs receiving subcutaneously injected insulin (1 IU kg^{-1}) 0.5 h before each meal were used as the control. During the course, the blood glucose levels were recorded using continuous glucose monitoring systems (CGMSs). Typically, the SiJoy GS1 continuous glucose monitoring system (CGMS) has a duration of 14 days before it expires. To ensure uninterrupted monitoring, a new CGMS was applied to the other side of the back one day prior to the expiration of the old one. Once the blood glucose readout from the new CGMS stabilized, the old CGMS was removed. The blood glucose readings from both CGMS devices were then merged and utilized for the following analysis. The magnitude of average glucose excursions on each day were calculated using EasyGV kindly shared by Nathan R Hill © University of Oxford 2010+[5]. The behavior and stooling patterns of the minipigs were monitored at least two times a day by a veterinary staff, where no abnormalities were observed. On day 0 before oral dosing and 12 h after the last oral dosing on day 14, blood samples were collected from the external jugular vein for blood biochemical and hematology analysis. To quantitatively measure the levels of glycated albumin over the total albumin concentrations, serum isolated from the blood samples were analyzed using the porcine glycated albumin ELISA kit (Coibo Bio, Shanghai, China; catalogue no. CB10752-Pg) according to the manufacturer's instructions. At the end of these experiments, minipigs were euthanized, pieces of different intestinal segments (duodenum, jejunum, ileum, and colon) and the major organs (heart, liver, spleen, lung, and kidneys) were collected, fixed in 4% paraformaldehyde, embedded in paraffin, cut into 5-μm sections, and stained with hematoxylin and eosin for histological analysis.

Formulation of other biologics with poly(disulfide)s. *HSA/poly(disulfide)s complexes.* Similar to the process of preparing LG/insulin-*x*, the oral formulation of HSA was prepared at a molar ratio of LG:HSA = 200:1. To test the systemic absorption of HSA using this poly(disulfide)s-formulated oral biologic, Cy5.5-tagged HSA was used for bioimaging studies in 4T1-tumor bearing mice. The 4T1 tumor-bearing mice model was built by subcutaneously injecting 1×10^6 4T1 cells into the right flank of C57BL/6J mice. When tumor size reached about 50-100 mm^3, the mice were randomly divided into three groups. After overnight fasting, mice in the first group were gavaged with size M enteric capsules loaded with the concentrate of Cy5.5-tagged HSA/poly(disulfide)s complexes (20 mg kg^{-1} of HSA). In the second group, free Cy5.5-tagged HSA-loaded enteric capsules were administered by oral gavage (20 mg kg^{-1}). In the third group, 4 mg kg^{-1} Cy5.5-tagged HSA was intravenously injected to the tail vein of mice. At indicated time points, the accumulation of HSA in tumor was visualized with an IVIS Lumina III Series system, PerkinElmer.

sCT/poly(disulfide)s complexes. To prepare the oral formulation of sCT using poly(disulfide)s, we synthesized alendronate-conjugated lipoic acid (AL) as the disulfide monomer. AL monomers were synthesized by dissolving 100 mg lipoic acid-*N*-hydroxysuccinimide ester[6] in 20 ml acetone, followed by addition of 90 mg alendronate sodium trihydrate in 35 ml water, 71.08 mg *N*,*N*-diisopropylethylamine, and 2 ml NaOH solution (0.1 M). The mixture was stirred at room temperature overnight. Then, the solvent was removed by rotary evaporation and lyophilization. After that, the crude product was redissolved in water and precipitated with dimethylformamide. The solid part was isolated by centrifugation, redissolved in water, and precipitated with acetone. The final product was afforded by washing with acetone twice and was stored at 4 °C for further use. sCT was formulated with in-situ polymerized AL monomers similar to the process of preparing LG/insulin-*x* using a staring molar ratio of AL/sCT = 20:1 (AL/sCT-20). The obtained AL/sCT-20 was characterized by TEM. For oral delivery, concentrated AL/sCT-20 was packed

into size M enteric capsules and administered to overnight-fasted healthy BALB/c mice at a dose of 0.25 mg kg^{-1}. For the control group, free sCT-loaded enteric capsules were orally administered. For comparison, 0.05 mg kg^{-1} of sCT was subcutaneously injected to the right flank of additional mice. At indicated time points, ~30 μl of blood samples were collected from the orbital sinus of mice and the serum calcium levels were quantified using a calcium assay kit (Sigma-Aldrich, catalogue no. MAK022) according to the manufacturer's instructions.

Supplementary Figures:

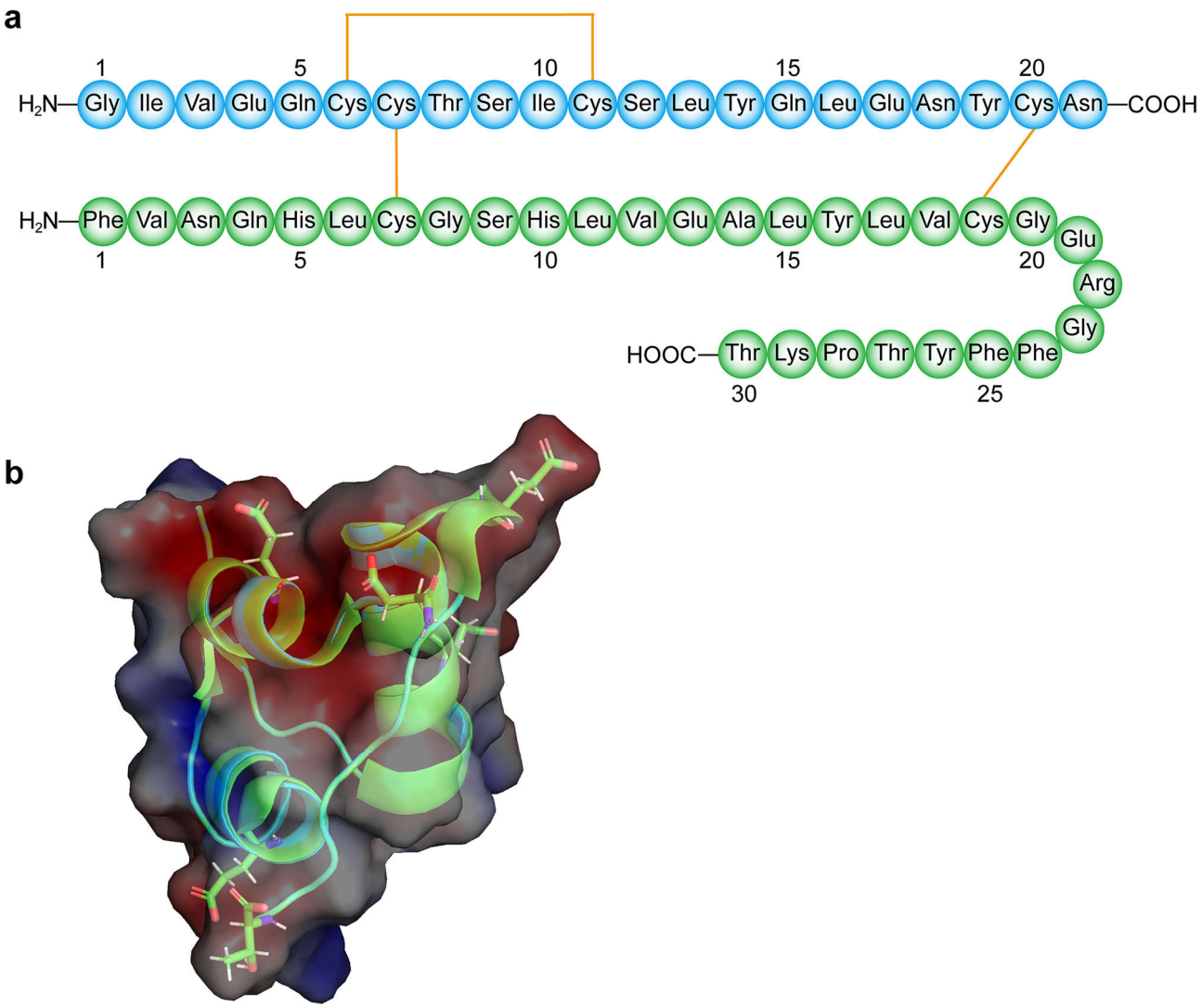

Supplementary Fig. 1 | The amino acid sequence and electrostatic surface potential of recombinant human insulin. **a**, The amino acid sequence of recombinant human insulin. **b**, Ball-and-stick presentation of the six carboxylate groups (*i.e.*, Glu^{A18}, Glu^{A17}, Asn^{A21}, Glu^{B13}, Glu^{B21}, and Thr^{B30}) lying on the insulin surface and forming negatively charged patches. C, N, and O atoms are in green, blue, and red, respectively. The calculated electrostatic surface potentials of insulin are colored from –3 kT/e (dark red) to +3 kT/e (dark blue), where *k, T,* and *e* are the Boltzmann constant, temperature, and magnitude of the electron charge, respectively. The image was generated by PyMOL using 2jv1 PDB file.

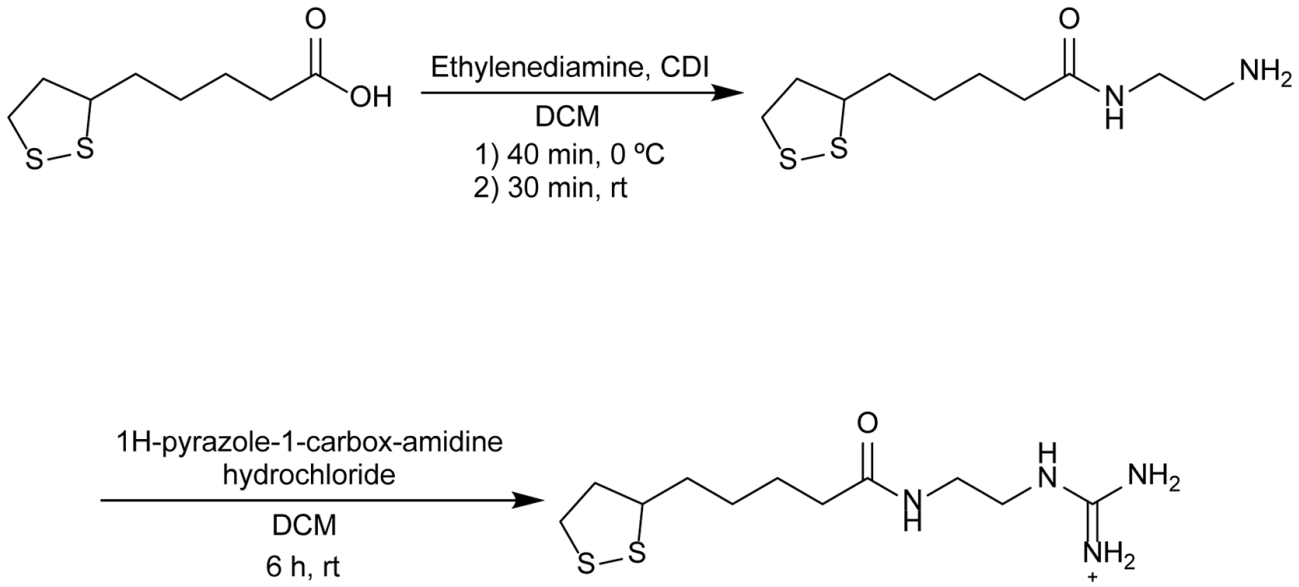

Supplementary Fig. 2 | Schematic illustration of the procedure for synthesizing the LG. CDI, 1,1'-carbonyldiimidazole; DCM, dichloromethane.

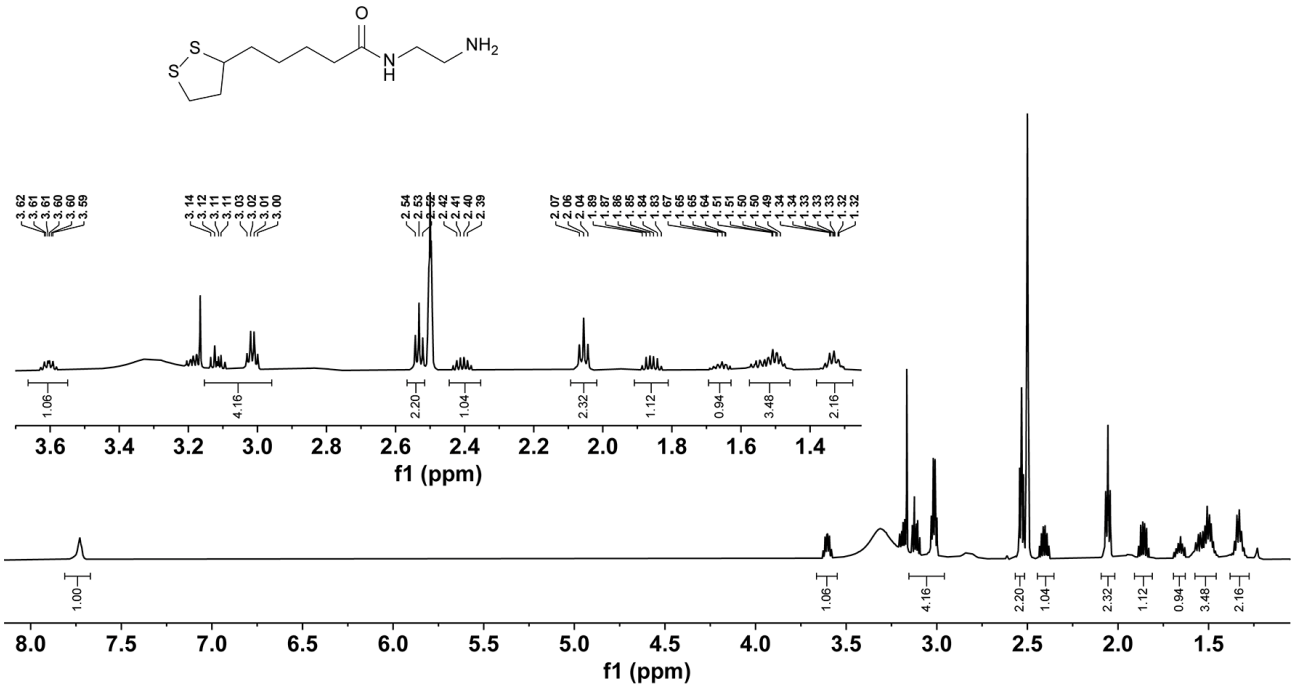

Supplementary Fig. 3 | ^{1}H NMR (600 MHz, DMSO-d_6) spectrum of the lipoic acid-ethylenediamine conjugate. δ (ppm): 7.73 (t, J = 5.8 Hz, 1H), 3.66–3.55 (m, 1H), 3.15–2.96 (m, 4H), 2.53 (t, J = 6.5 Hz, 2H), 2.44–2.35 (m, 1H), 2.06 (t, J = 7.4 Hz, 2H), 1.86 (dq, J = 13.5, 6.9 Hz, 1H), 1.66 (t, J = 7.0 Hz, 1H), 1.58–1.46 (m, 3H), 1.38–1.28 (m, 2H).

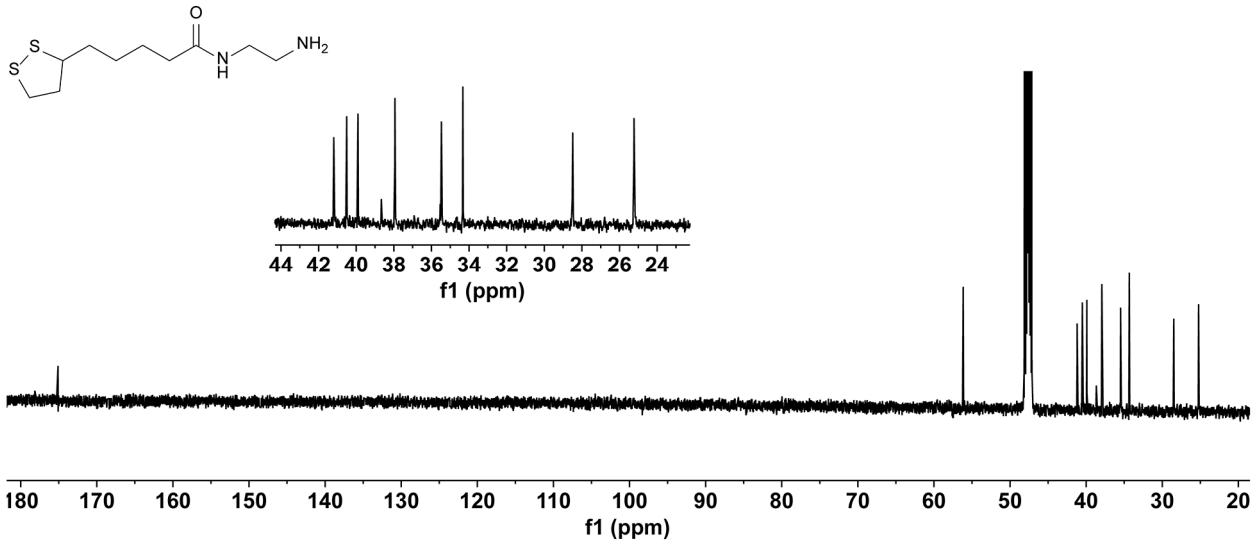

Supplementary Fig. 4 | ^{13}C NMR (151 MHz, MeOD) spectrum of the lipoic acid-ethylenediamine conjugate. δ (ppm): 175.09, 56.16, 41.19, 40.51, 39.91, 37.94, 35.47, 34.33, 28.49, 25.23.

Supplementary Fig. 5 | Mass spectrum (ESI, MeOH) of the lipoic acid-ethylenediamine conjugate which is matched by the peak at 249.1085.

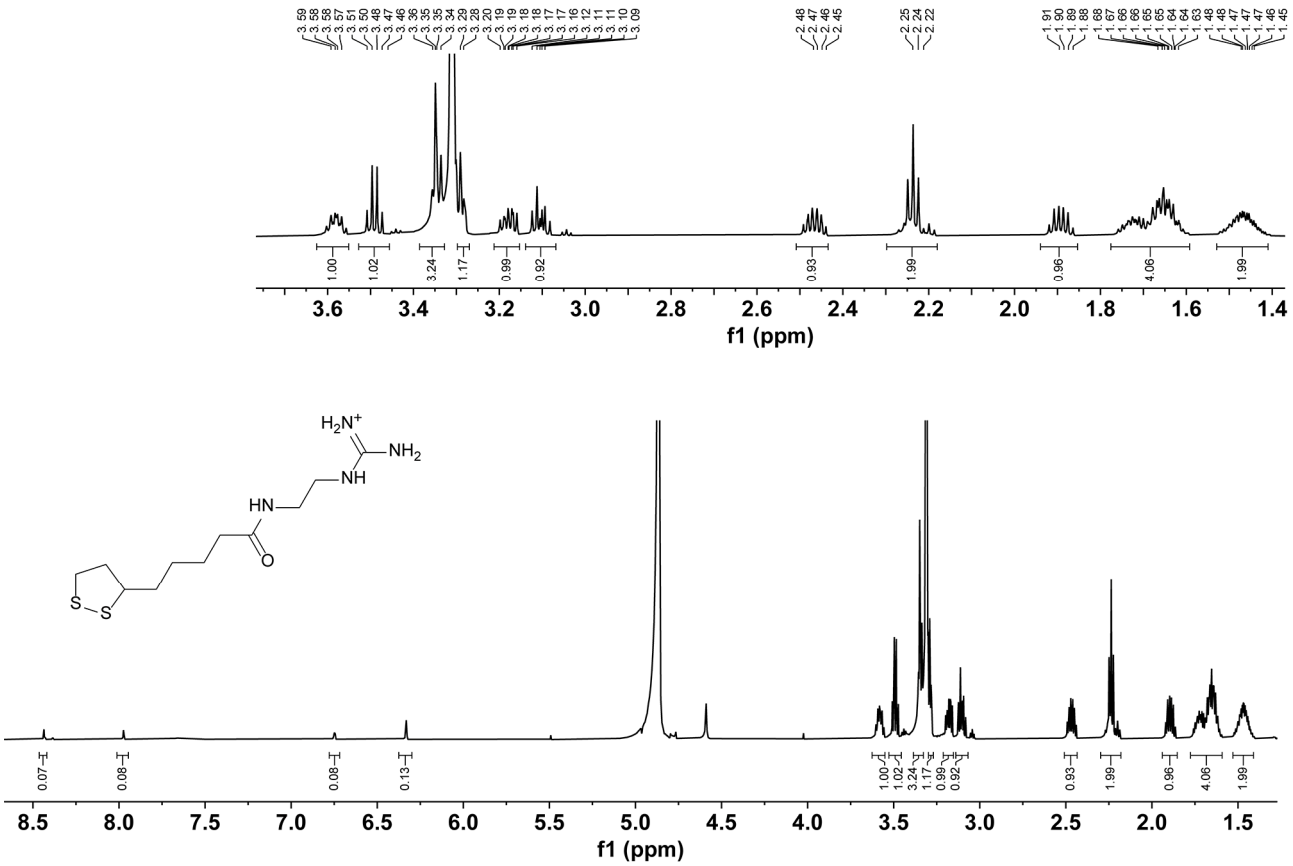

Supplementary Fig. 6 | ^{1}H NMR (600 MHz, MeOD) spectrum of the LG. δ (ppm): 3.58 (dd, *J* = 9.1, 5.7 Hz, 1H), 3.49 (q, *J* = 7.0 Hz, 1H), 3.39–3.33 (m, 3H), 3.29 (d, *J* = 4.4 Hz, 1H), 3.21–3.15 (m, 1H), 3.14–3.07 (m, 1H), 2.47 (dd, *J* = 12.2, 5.8 Hz, 1H), 2.24 (t, *J* = 7.5 Hz, 2H), 1.89 (dd, *J* = 12.9, 6.6 Hz, 1H), 1.65 (ddd, *J* = 13.6, 9.4, 6.0 Hz, 4H), 1.53–1.41 (m, 2H).

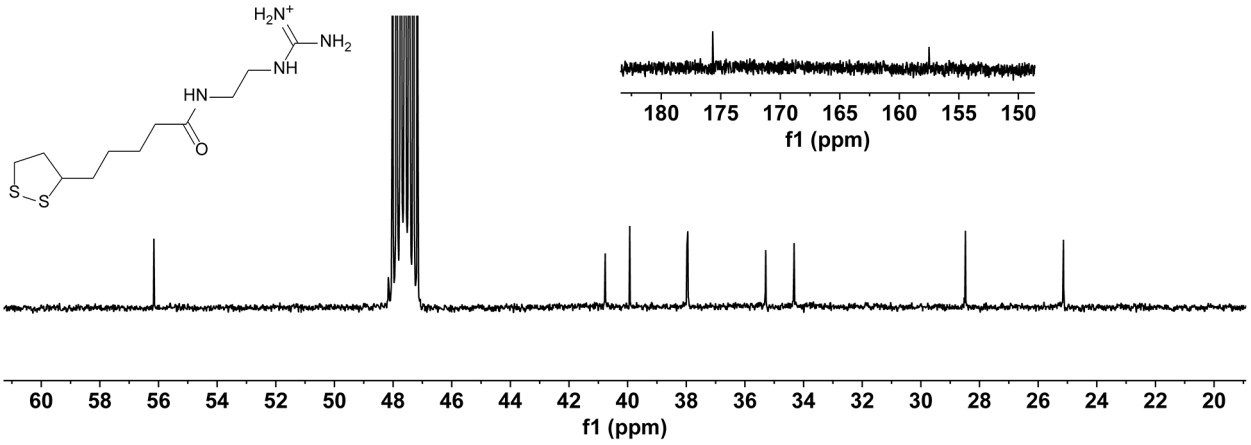

Supplementary Fig. 7 | ^{13}C NMR (151 MHz, MeOD) spectrum of the LG. δ (ppm): 175.68, 157.51, 56.16, 40.77, 39.93, 37.96, 35.29, 34.32, 28.48, 25.14.

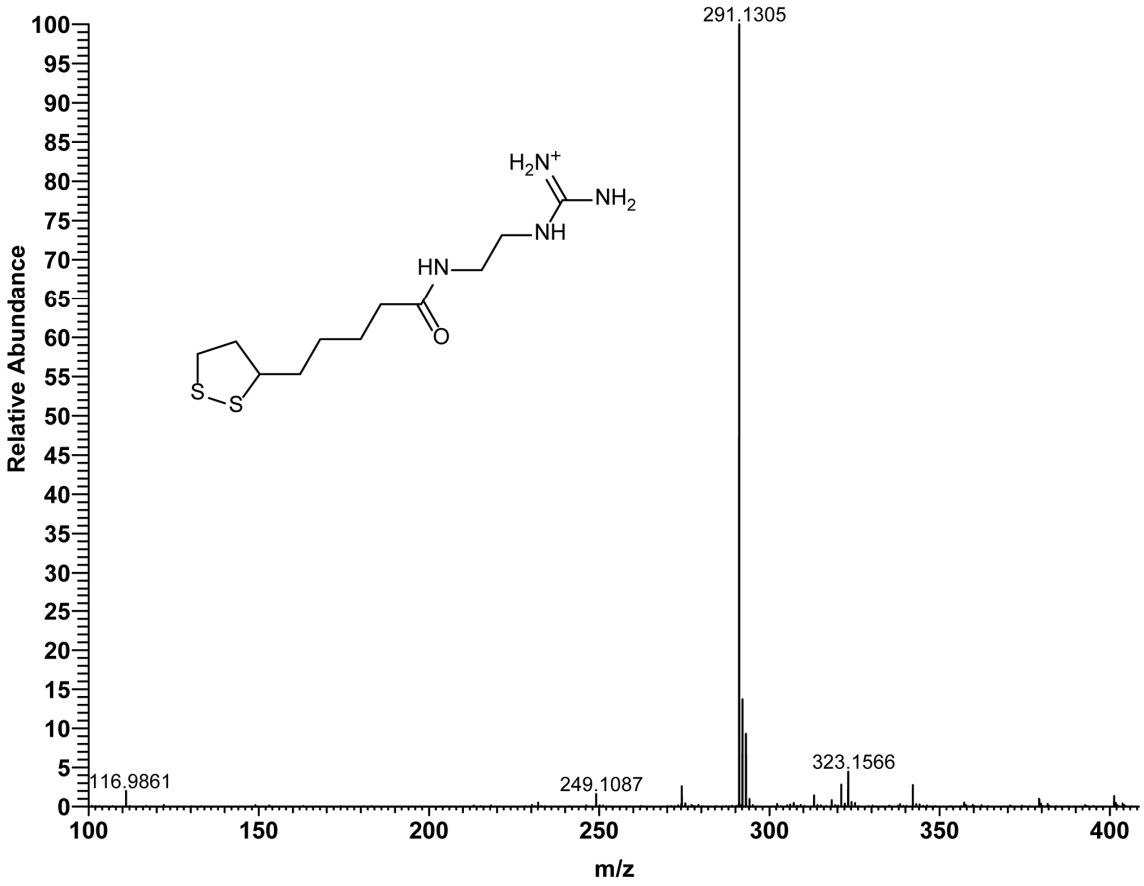

Supplementary Fig. 8 | Mass spectrum (ESI, 0.1% HCOOH in MeOH) of the LG which is matched by the peak at 291.1305.

Supplementary Fig. 9 | Real-time monitoring the changes in the turbidity of solutions containing different substrates. **a**, Evolution of the turbidity (indicated by the absorbance at 600 nm) of solutions containing LGs and insulin at different starting molar ratios (designated LG/insulin-*x*, *x* = 10, 20, 40, 60, and 80). Inset photographs show the solutions containing LGs and insulin at different starting molar ratios after mixing for 2 and 15 min, respectively. The solutions turned turbid rapidly after mixing, indicating the occurrence of preliminary phase separation. **b-f**, Evolution of the turbidity of control groups: mixtures of LGs and insulin in acetate buffer (20 mM, pH 4.0; designated LG + insulin-*x*, pH 4.0; **b**), guanidinium chloride plus insulin (designated Gu^+ + insulin-*x*; **c**), lipoic acid plus insulin (designated LA + insulin-*x*; **d**), LGs alone (designated LG-*x*; **e**) or insulin alone (**f**), where *x* represents the molar ratio of control excipients relative to the insulin concentration used in **a**. Inset photographs show the control solutions after mixing for 2 min and 1 h, respectively, which remained clear throughout even prolonging the aging time. For control groups, the concentrations of each

constituent are the same to their counterparts used for preparing LG/insulin-*x*. The inset cartoons in the first-column panel are the schematic illustrations showing the substrates in the solution of each group. Data points represent mean ± s.d. (n = 3 independent experiments). At pH lower than the isoelectric point of insulin (pI ~5.3), the non-occurrence of phase separation was attributed to the protonation of the carboxyl groups being blocked the binding of LGs. Together with the other groups which utilized agents lacked the guanidinium groups or the hydrophobic dithiolane groups confirmed our hypothesis that the binding of the amphiphilic LGs onto the negatively charged domains of insulin surface led to the preliminary phase separation.

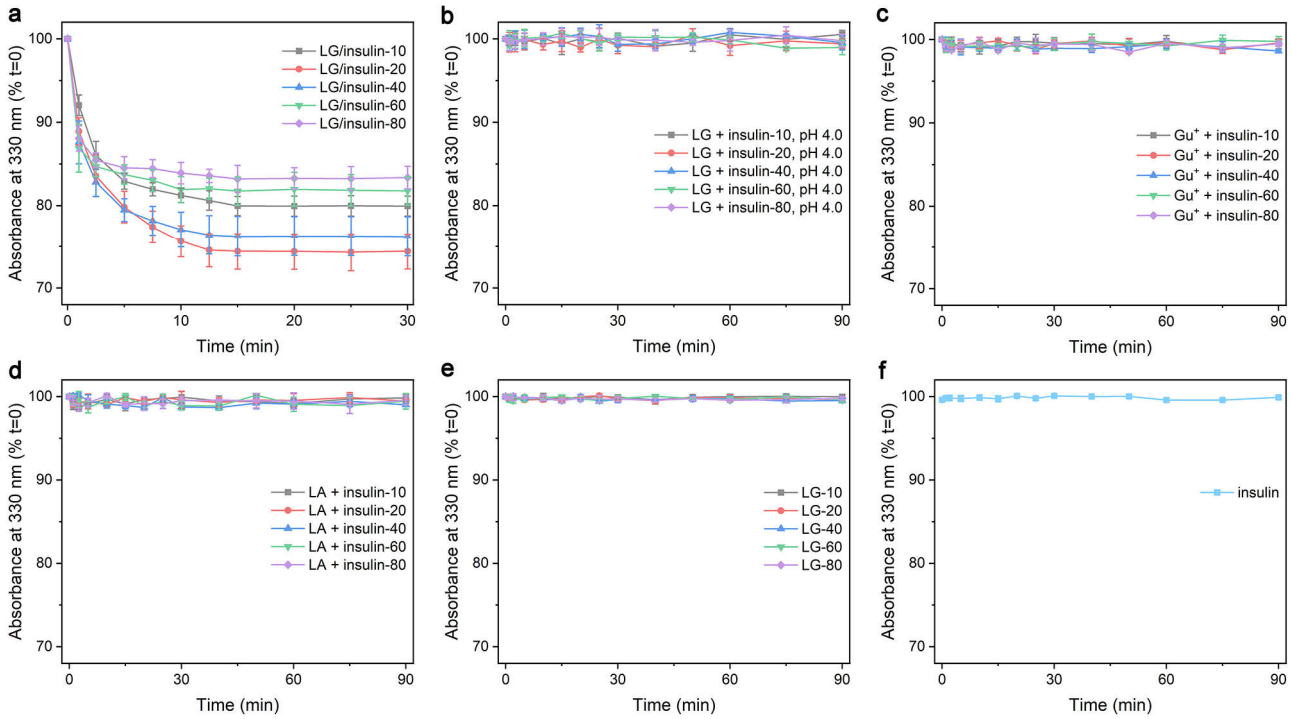

Supplementary Fig. 10 | a, Kinetics of ring-opening of the 1,2-dithilane group of the LG. Changes in the absorption at λ = 330 nm after mixing LGs with insulin at different molar ratios. **b-f**, Changes in the absorption at λ = 330 nm of control groups: mixtures of LGs and insulin in acetate buffer (20 mM, pH 4.0; designated LG + insulin-*x*; pH 4.0; **b**), guanidinium chloride plus insulin (designated Gu^+ + insulin-*x*; **c**), lipoic acid plus insulin (designated LA + insulin-*x*; **d**), LGs alone (designated LG-*x*; **e**) or insulin alone (**f**), where *x* represents the molar ratio of control excipients relative to the insulin concentration used in **a**. Data were shown by the percentage of absorption intensity at λ = 330 nm at indicated time points compared to the initial values. Data points represent mean ± s.d. (n = 3 independent experiments). Compared to the complexation of insulin and LGs which occurred instantly after mixing and reached equilibrium within about 3 min, the ring-opening of the dithiolanes lagged. This proved our formulation hypothesis that after the preliminary phase separation the locally concentrated dithiolanes underwent energy-favored disulfide-exchange ring-opening polymerization to give rise to the formation of multivalent interaction-stabilized complex coacervates. Moreover, after mixing LGs and insulin, the absorbance at λ = 330 nm declined gradually and plateaued within 15 min, while that of the control groups remained nearly unchanged even after 1.5 h.

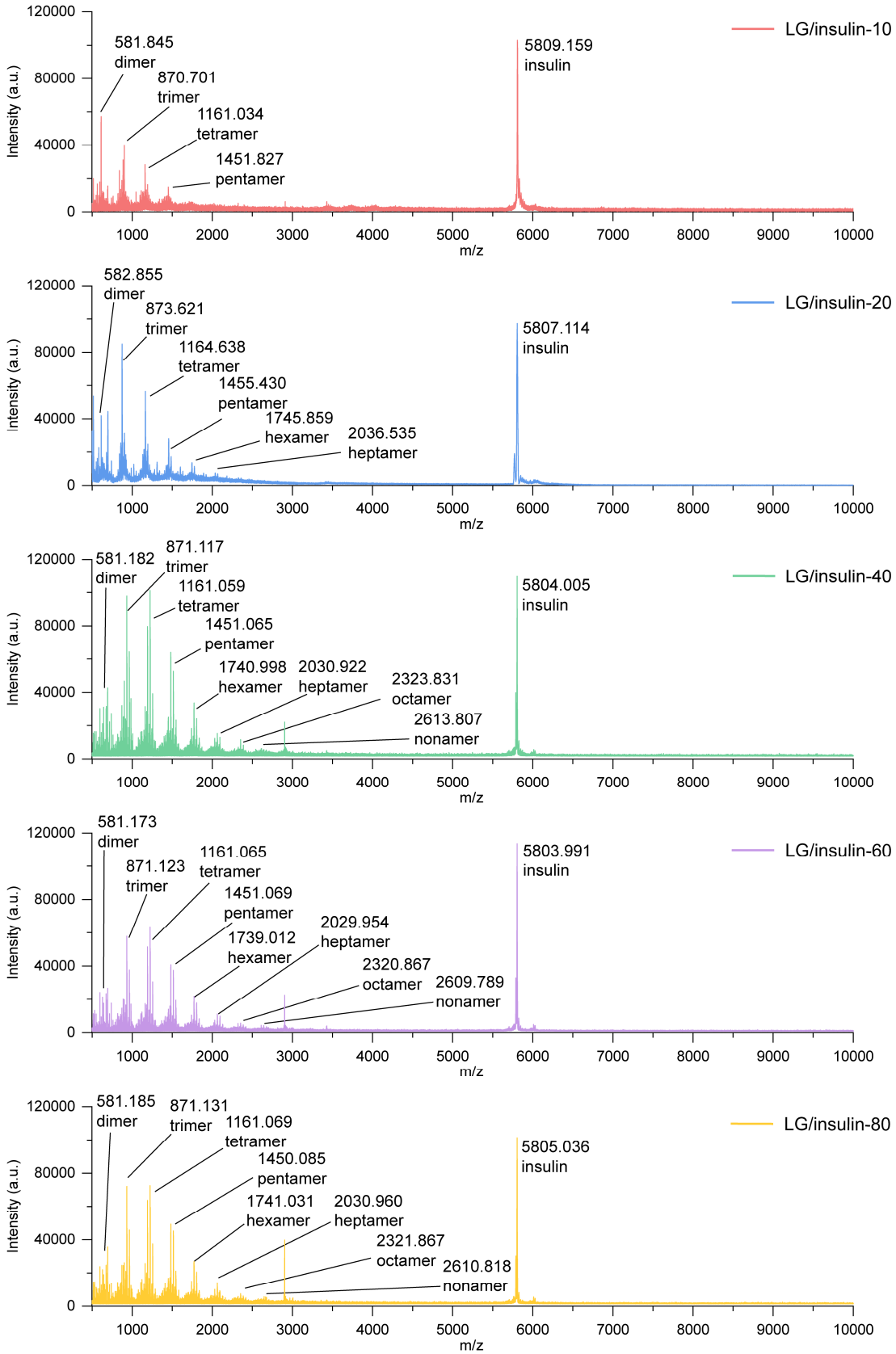

Supplementary Fig. 11 | MALDI-TOF mass spectra of LG/insulin-*x* (*x* = 10, 20, 40, 60, and 80) complex coacervates. From the spectra, there are oligomeric poly(disulfide)s of 2-5, 2-7, and 2-9 repeating units detected for LG/insulin-10, LG/insulin-20 and LG/insulin-40–80, respectively.

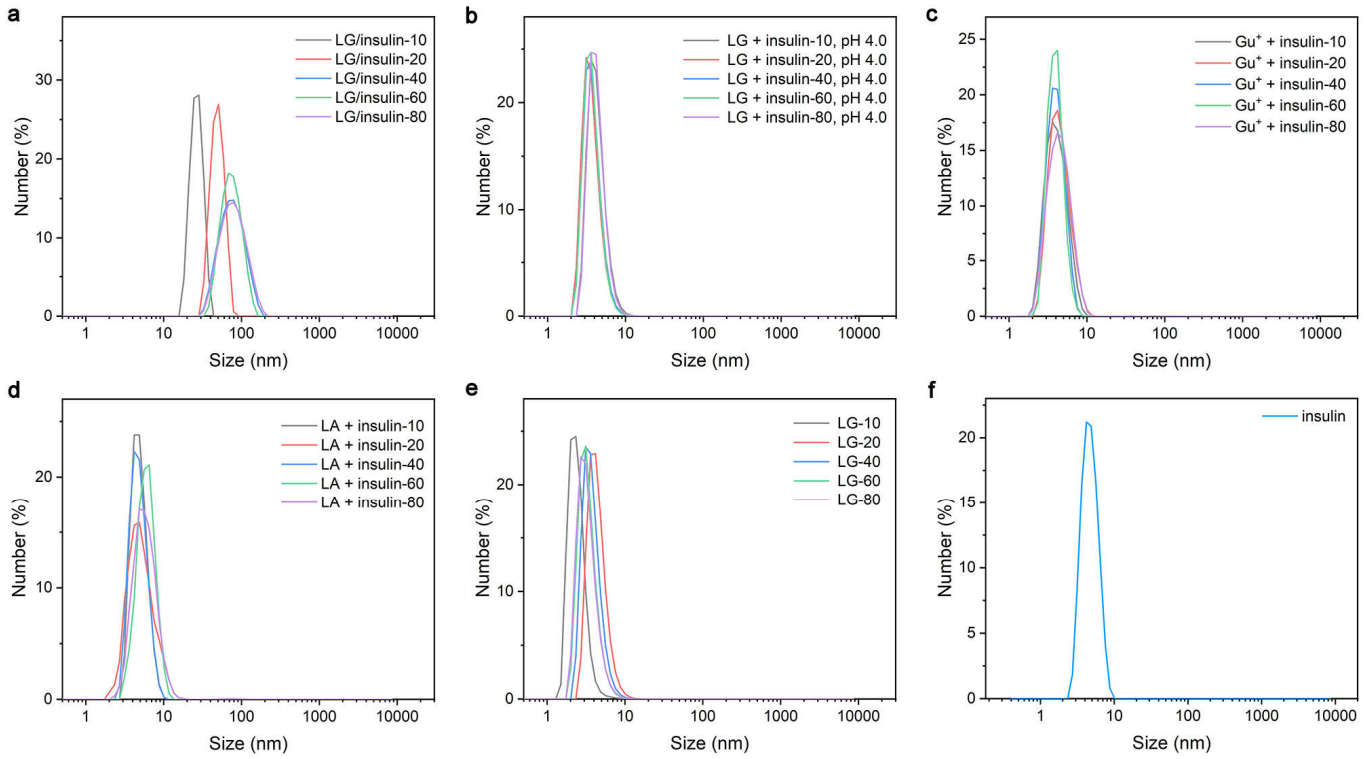

Supplementary Fig. 12 | Dynamic light scattering analysis of the solutions containing insulin and different substrates. **a-f**, Hydrodynamic size distribution of (**a**) LG/insulin-*x* (*x* = 10, 20, 40, 60, and 80), (**b**) mixtures of LGs and insulin in acetate buffer (20 mM, pH 4.0) (designated LG + insulin-*x*, pH 4.0), (**c**) guanidinium chloride plus insulin (designated Gu^+ + insulin-*x*), (**d**) lipoic acid plus insulin (designated LA + insulin-*x*), (**e**) LGs alone (designated LG-*x*) and (**f**) insulin alone. For **b-e**, *x* represents the molar ratio of the control substrates relative to the insulin concentration used in **a**. From **a**, the sizes of LG/insulin-10–80 are 26.7 ± 8.2, 49.6 ± 5.7, 79.3 ± 10.2, 76.2 ± 8.9, 80.3 ± 8.2 nm, respectively. For control groups (**b-f**), the concentrations of each constituent are the same to their counterparts used for preparing LG/insulin-*x*. The appearance of much smaller sized nanostructures in the solution of LGs (**e**) were attributed to the formation of micelles from amphiphilic LGs.

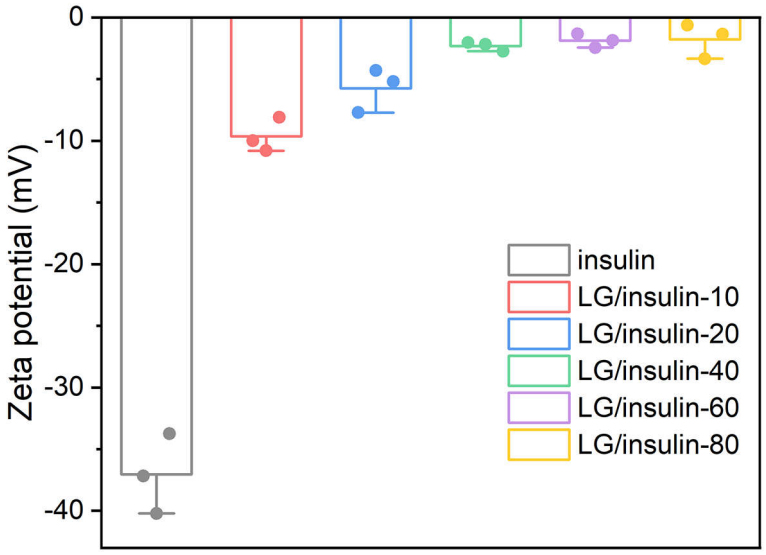

Supplementary Fig. 13 | Surface charges of the complex coacervates formed between insulin and LGs. The zeta-potentials of LG/insulin-10–80 are –9.6 ± 1.4, –5.7 ± 1.8, –2.3 ± 0.4, –1.9 ± 0.6, –1.8 ± 1.4 mV, respectively. Data points represent mean ± s.d. (n = 3 independent experiments).

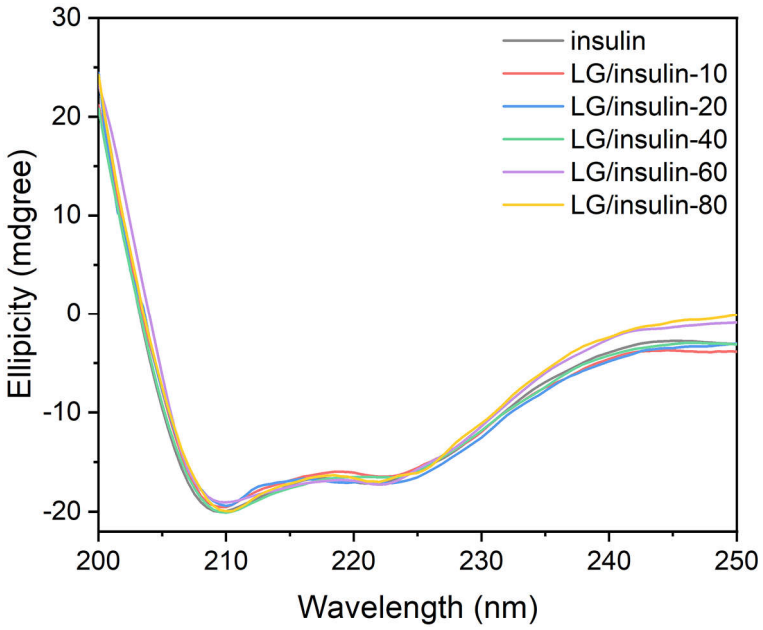

Supplementary Fig. 14 | Analysis of the secondary structure of insulin in the complex coacervates formed between insulin and LGs. Optical circular dichroism spectra of insulin and LG/insulin-*x* (*x* = 10, 20, 40, 60, and 80). The optical circular spectra of LG/insulin-*x* are similar to that of native insulin, showing two negative extrema around 209 and 222 nm that are assigned to the α-helix of insulin molecules. These results demonstrated that insulin's secondary structure was preserved in complex coacervates, indicating that insulin's disulfide bridges were unlikely disturbed by the ring-opening polymerization because they have much lower tension than dithiolanes[7] and thus are less reactive.

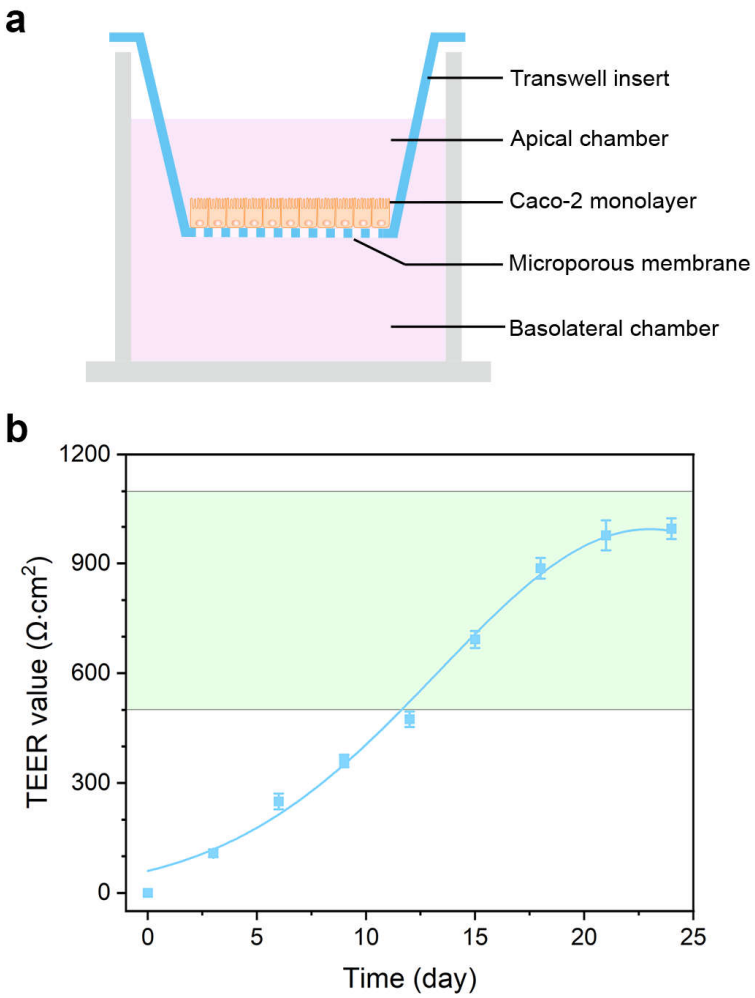

Supplementary Fig. 15 | Construction of Caco-2 cell monolayers in transwells. **a**, Schematic of the Caco-2 cell monolayer model. **b**, The transepithelial electrical resistance (TEER) values of Caco-2 monolayers measured every 3 days for confirming the formation of proper barrier. Green windows represent the range of acceptable TEER values (500-1100 Ω cm^2) for further studies. Data points represent mean ± s.d. (n = 5 independent experiments).

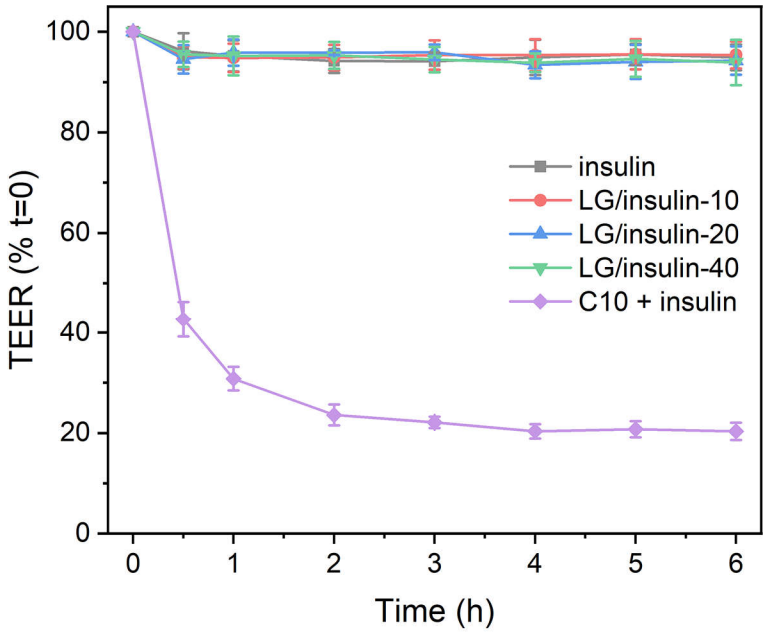

Supplementary Fig. 16 | Variation of TEER of Caco-2 monolayers during the transepithelial transport study. Changes in TEER values of Caco-2 monolayers at different time points after incubated with insulin of different formulations including LG/insulin-*x* (*x* = 10, 20, 40), free insulin, and sodium caprate (C10) plus free insulin. TEER changes of each group were normalized to their values measured before the addition of samples. Sodium caprate drastically reduced the TEER of Caco-2 monolayers by approximately 80%, whereas LG/insulin-*x* and free insulin has no obvious effect. Data points represent mean ± s.d. (n = 3 independent experiments).

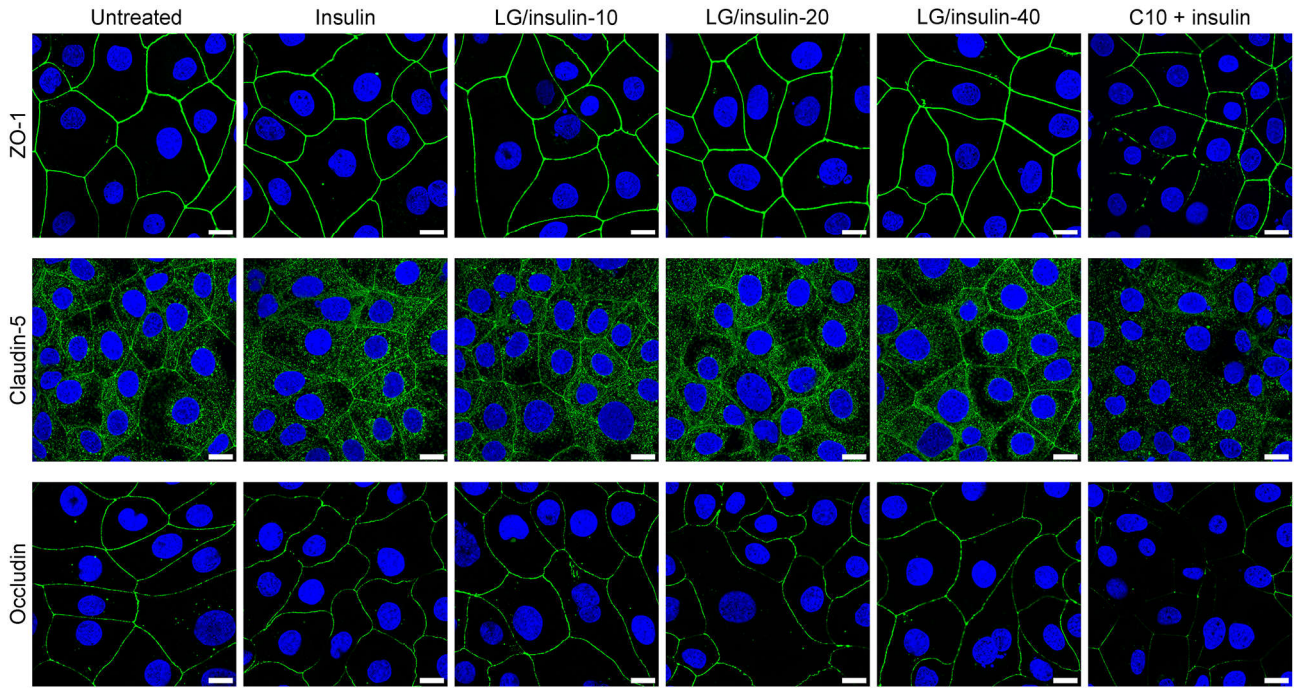

Supplementary Fig. 17 | Immunofluorescence assay of the conformation of tight junction proteins. Representative confocal laser microscopy images showing the patterns of tight junction proteins, including zonula occludens-1 (ZO-1), claudin-5, and occludin of Caco-2 monolayers after incubated with different insulin formulations including LG/insulin-*x* (*x* = 10, 20, 40), free insulin, and sodium caprate (C10) plus free insulin. Untreated Caco-2 monolayers were used as the blank control. ZO-1, claudin-5, occludin, and the nuclei were stained with Alexa Fluor™ 488 ZO-1 monoclonal antibody (green), Alexa Fluor™ 488 claudin-5 monoclonal antibody (green), Alexa Fluor™ 488 occludin monoclonal antibody (green), and Hoechst 33342 (blue), respectively. Scale bars, 20 μm. The results indicated that, in contrast to sodium caprate which caused large gaps in the normally continuous rings at the boundary between adjacent cells, no significant opening of the tight junctions was caused by LG/insulin-*x*.

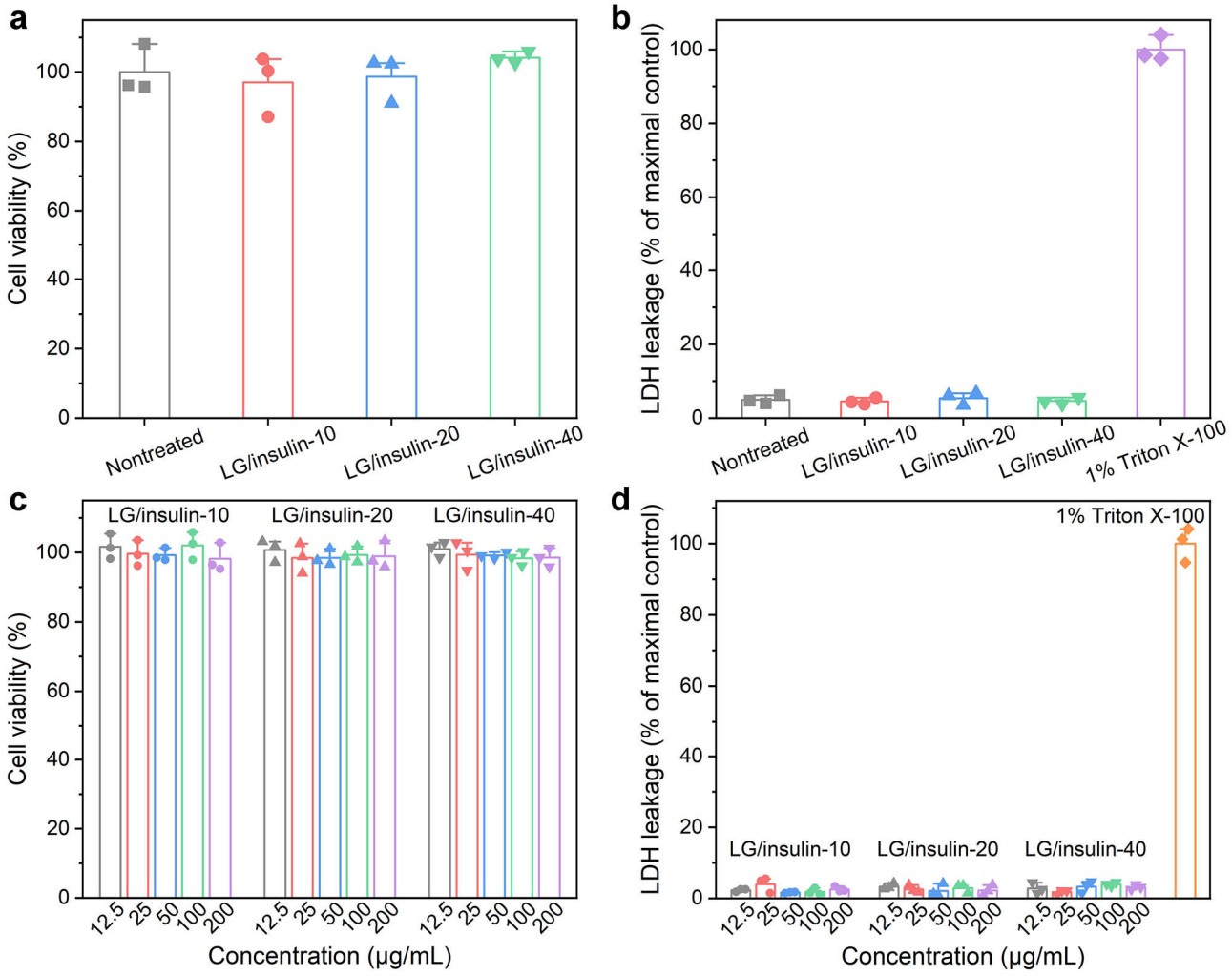

Supplementary Fig. 18 | *In vitro* biocompatibility of LG/insulin-*x* (*x* = 10, 20, 40). **a-d**, MTT assay of the cell viability of Caco-2 monolayers (**a**) and LDH release assay of Caco-2 monolayers at the end of transepithelial transport of LG/insulin-*x* (**b**); MTT (**c**) and LDH release assays (**d**) of Caco-2 cells after incubating with LG/insulin-*x* at different concentrations. Data points represent mean ± s.d. (n = 3 independent experiments). These results demonstrated that LG/insulin-*x* showed negligible influence on the viability or membrane integrity of Caco-2 cells.

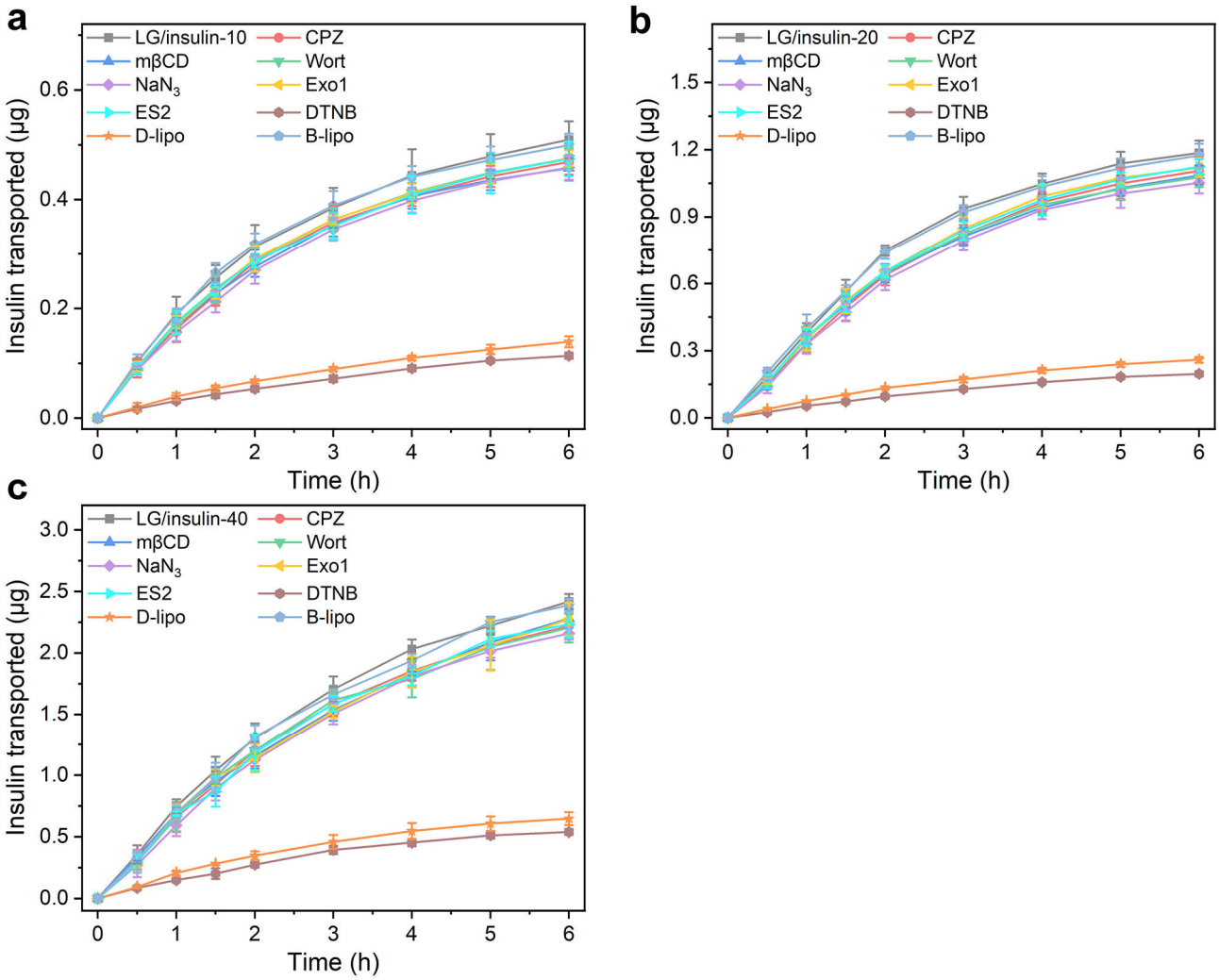

Supplementary Fig. 19 | Effect of inhibitors on the transcellular delivery of LG/insulin-*x* (*x* = 10, 20, 40) across the Caco-2 monolayers. **a-c**, Cumulative transcellular transport profiles of (**a**) LG/insulin-10, (**b**) LG/insulin-20, and (**c**) LG/insulin-40 across the Caco-2 monolayers in the presence of different inhibitors. Endocytosis inhibitors: chlorpromazine (CPZ) is a clathrin-mediated endocytosis inhibitor acting by inhibiting the relocation of clathrin and adaptor protein complex-2 from the plasma membrane to endosomes; methyl-β-cyclodextrin (mβCD) is a caveolar endocytosis inhibitor acting by removing cholesterol out the plasma membrane and hence destroying the structure of lipid rafts (or caveolae); wortmannin is a micropinocytosis inhibitor acting by blocking phosphoinositide 3-kinase which is involved in the initiation of membrane ruffling and macropinosomes formation; sodium azide (NaN_3) is an oxidative phosphorylation inhibitor acting by abolishing ATP-dependent processes and comprehensively inhibits energy-dependent endocytosis. Exocytosis inhibitors: Exo1 is an exocytosis inhibitor acting by inhibiting vesicular trafficking between the endoplasmic reticulum and the Golgi apparatus; endosidin 2 (ES2) inhibits exocytosis and endosomal recycling by binding to the exocyst component of 70 kDa subunit of the exocyst complex. DTNB is an inhibitor for thiol-mediated uptake which converts the exofacial thiols into disulfides and blocks DCDE on the cellular surface. DTNB-loaded fusogenic liposomes (D-lipo) were used to deliver thiol-blocking agents into the cytosol to deactivate the DCDE between the intracellular thiols and the poly(disulfide)s in the LG/insulin-*x* coacervates. Blank liposomes (B-lipo) without loading DTNB were used to exclude the possible effect of liposomes.

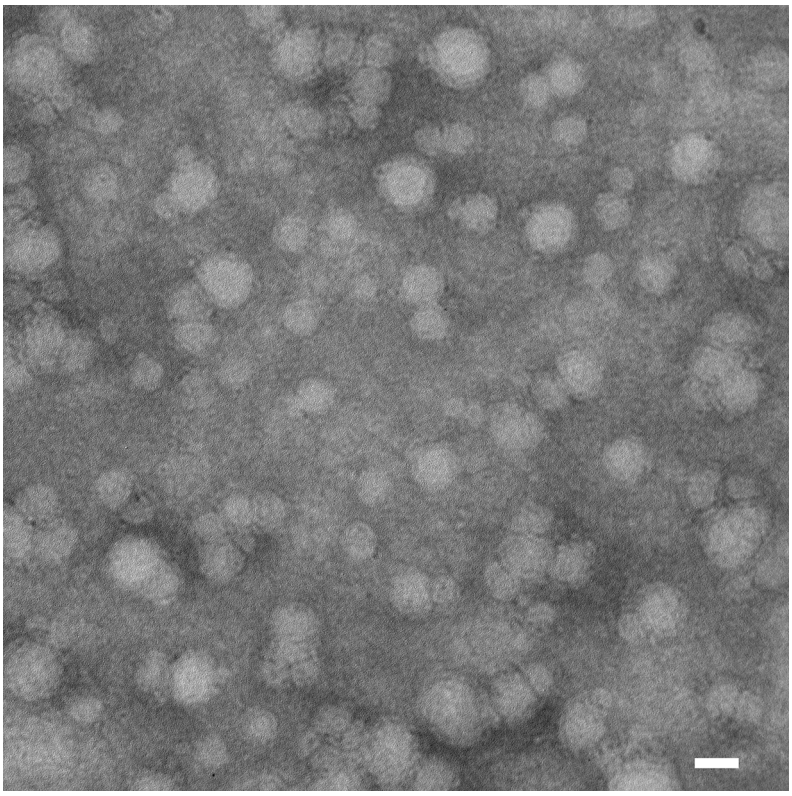

Supplementary Fig. 20 | Representative TEM image of the fusogenic liposomes used for intracellular delivery of DTNB. Scale bar, 100 nm. The samples were negatively stained by 1% phosphotungstic acid.

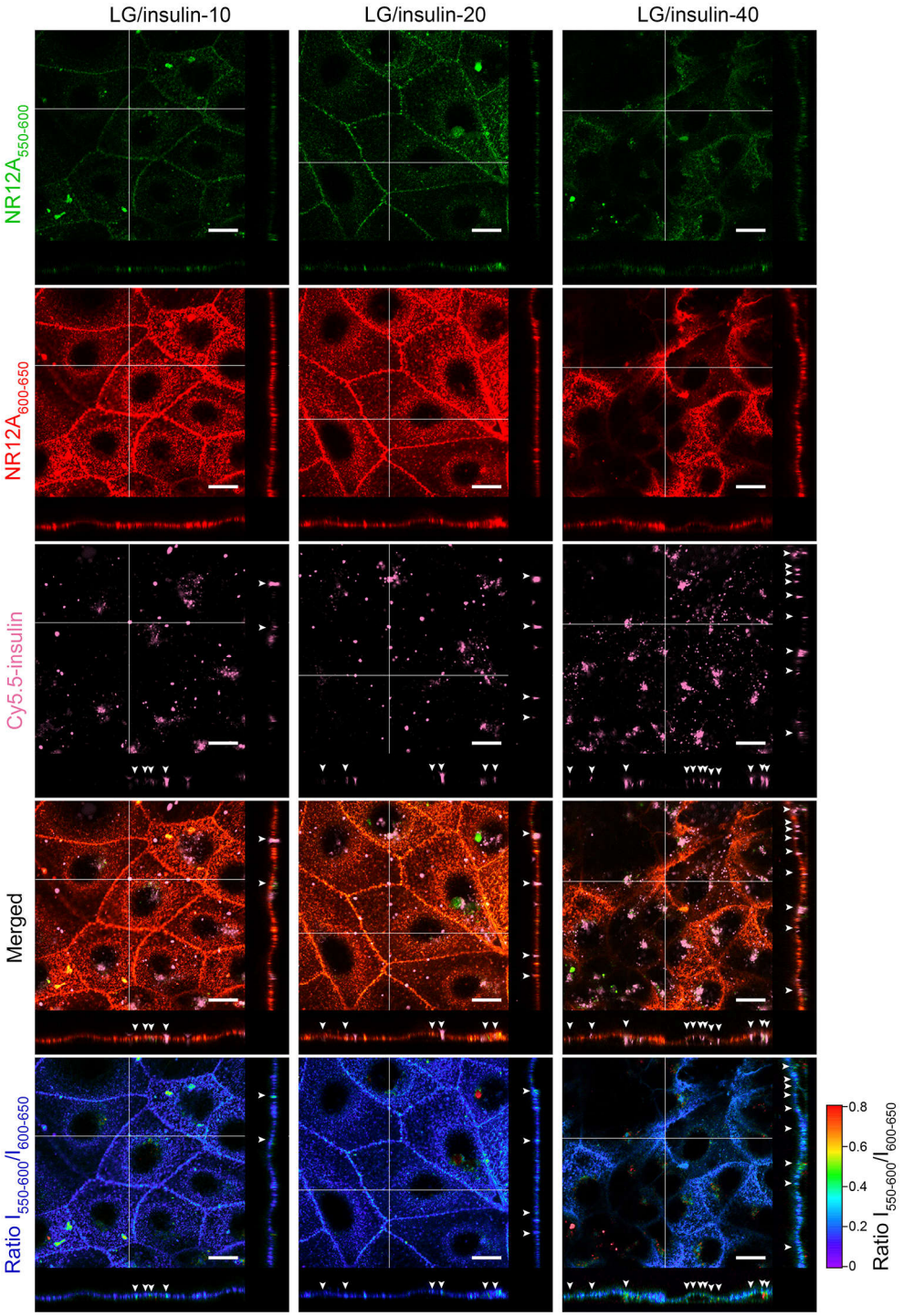

Supplementary Fig. 21 | Orthogonal projections of Caco-2 cells after incubated with Cy5.5-tagged LG/insulin-*x* (pink) for 10 min. In each panel, orthogonal views show the intersection planes at the position of the white crosshair. The plasma membrane was stained with MemGlow™ NR12A to show the lipid organization. Ratiometric images were generated by dividing the intensity of the 550-600 nm channel ($I_{550–600}$; green) by that of the 600-650 nm channel ($I_{600–650}$; red). The positions binding LG/insulin-*x* were indicated by white arrows. Compared to the non-binding areas, the blue shift in emission of NR12A in regions binding LG/insulin-*x* indicated a local increase in lipid order. The *x*-*z* orthogonal views were also shown in Fig. 2d. Scale bars, 20 μm.

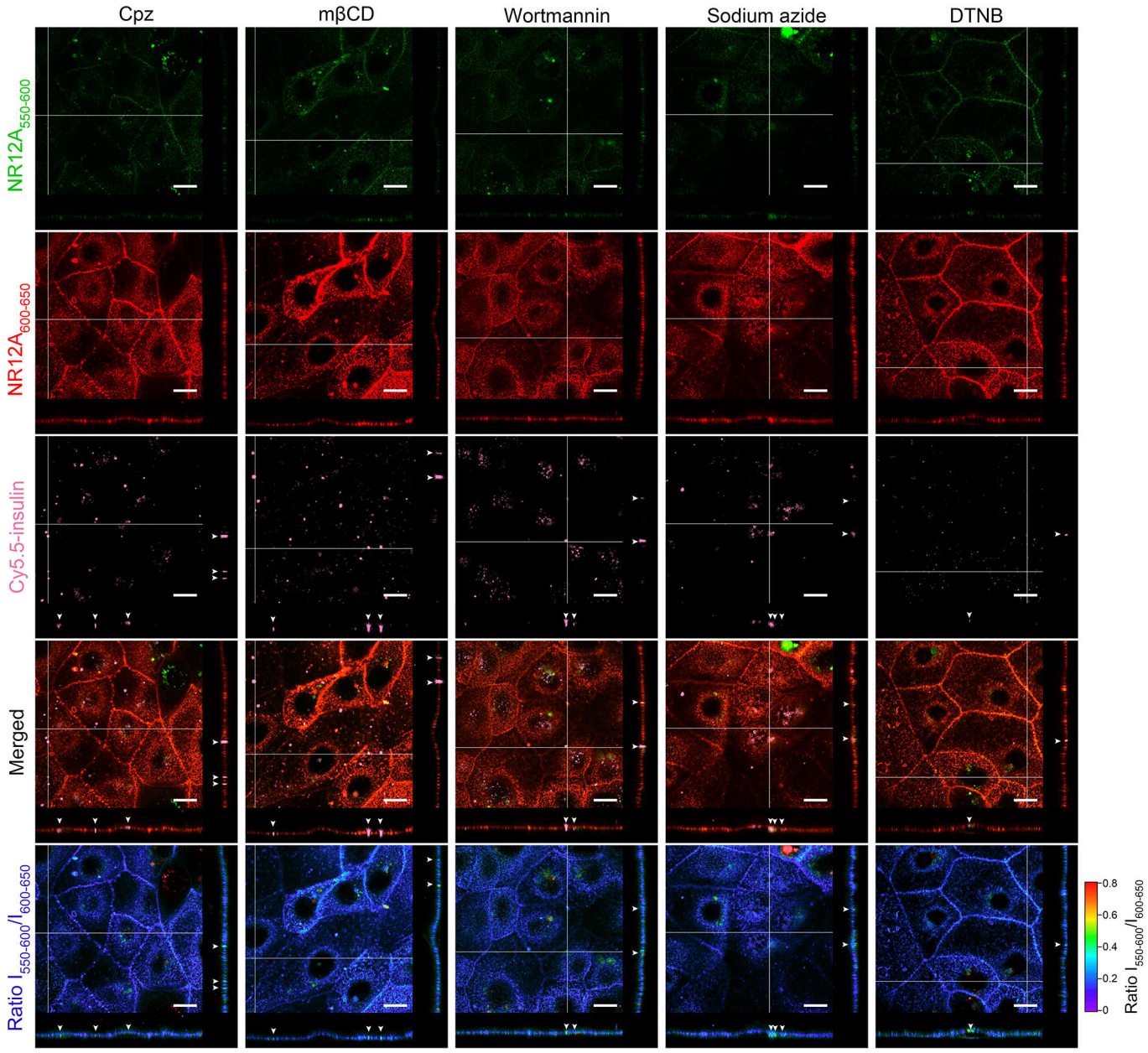

Supplementary Fig. 22 | Orthogonal projections of Caco-2 cells after incubated with Cy5.5-tagged LG/insulin-10 (pink) in the presence of endocytosis inhibitors and DTNB for 10 min. In each panel, orthogonal views show the intersection planes at the position of the white crosshair. The plasma membrane was stained with MemGlow™ NR12A to show the lipid organization. Ratiometric images were generated by dividing the intensity of the 550-600 nm channel ($I_{550–600}$; green) by that of the 600-650 nm channel ($I_{600–650}$; red). Compared to non-binding areas, the blue shift in emission of NR12A in regions binding LG/insulin-10 indicated a local increase in lipid order. Scale bars, 20 μm.

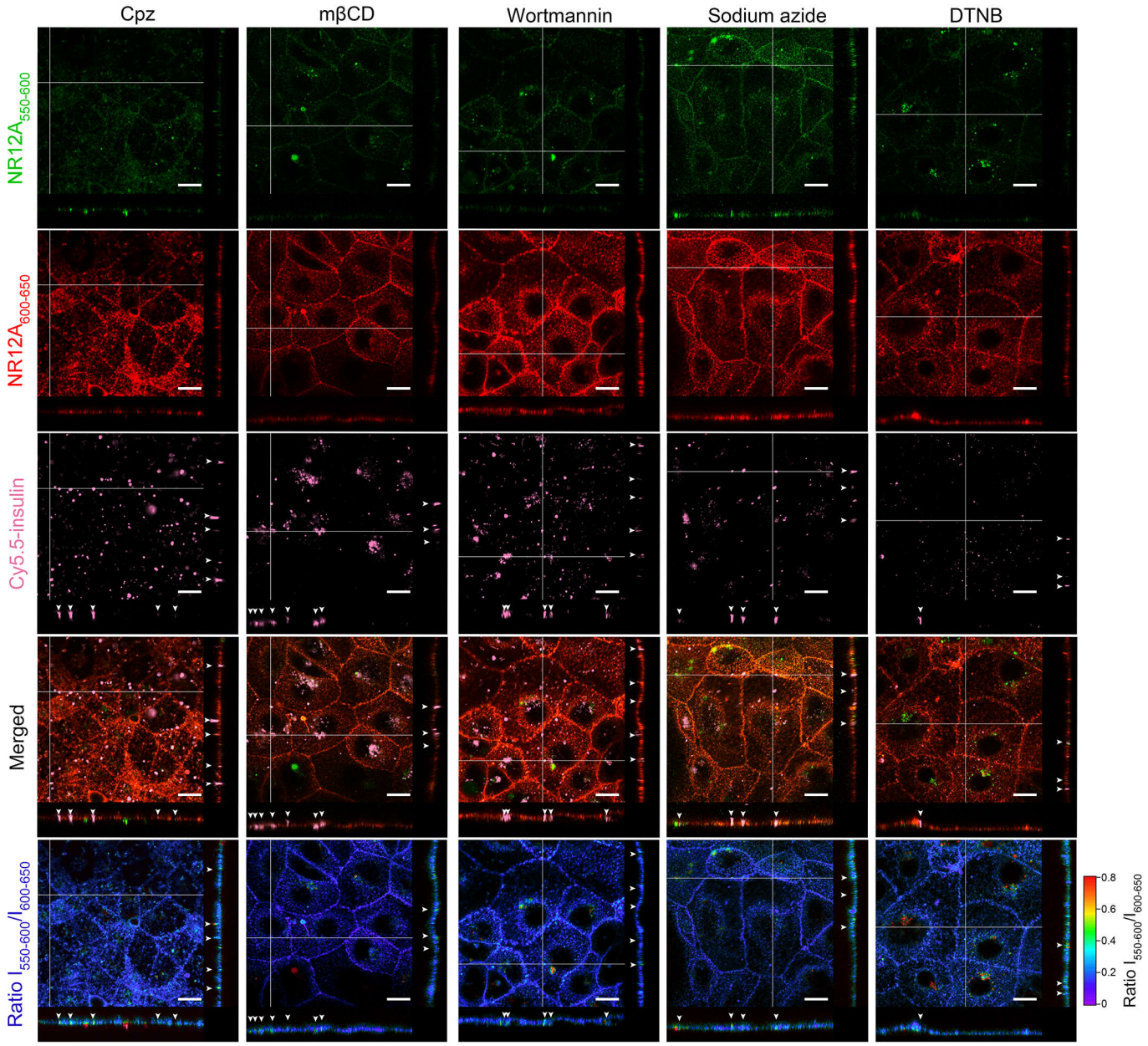

Supplementary Fig. 23 | Orthogonal projections of Caco-2 cells after incubated with Cy5.5-tagged LG/insulin-20 (pink) in the presence of endocytosis inhibitors and DTNB for 10 min. In each panel, orthogonal views show the intersection planes at the position of the white crosshair. The plasma membrane was stained with MemGlow™ NR12A to show the lipid organization. Ratiometric images were generated by dividing the intensity of the 550-600 nm channel ($I_{550–600}$; green) by that of the 600-650 nm channel ($I_{600–650}$; red). Compared to non-binding areas, the blue shift in emission of NR12A in regions binding LG/insulin-20 indicated a local increase in lipid order. Scale bars, 20 μm.

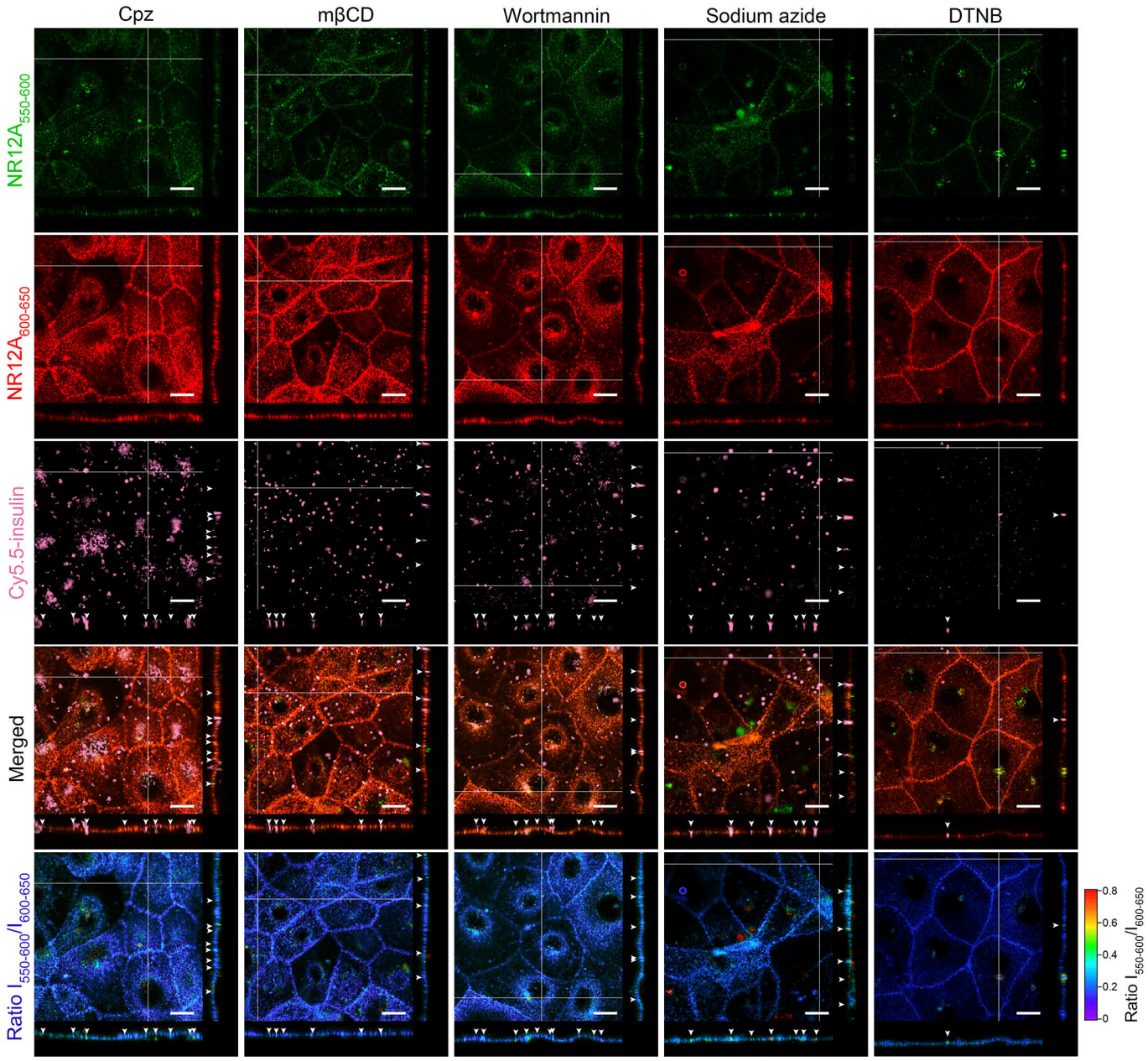

Supplementary Fig. 24 | Orthogonal projections of Caco-2 cells after incubated with Cy5.5-tagged LG/insulin-40 (pink) in the presence of endocytosis inhibitors and DTNB for 10 min. In each panel, orthogonal views show the intersection planes at the position of the white crosshair. The plasma membrane was stained with MemGlow™ NR12A to show the lipid organization. Ratiometric images were generated by dividing the intensity of the 550-600 nm channel ($I_{550–600}$; green) by that of the 600-650 nm channel ($I_{600–650}$; red). Compared to non-binding areas, the blue shift in emission of NR12A in regions binding LG/insulin-10 indicated a local increase in lipid order. Scale bars, 20 μm. From confocal imaging shown in Supplementary Fig. 22-24, the binding of LG/insulin-*x* on the plasma membrane was not obviously affected by common endocytosis inhibitors. However, this binding could be hampered by DTNB.

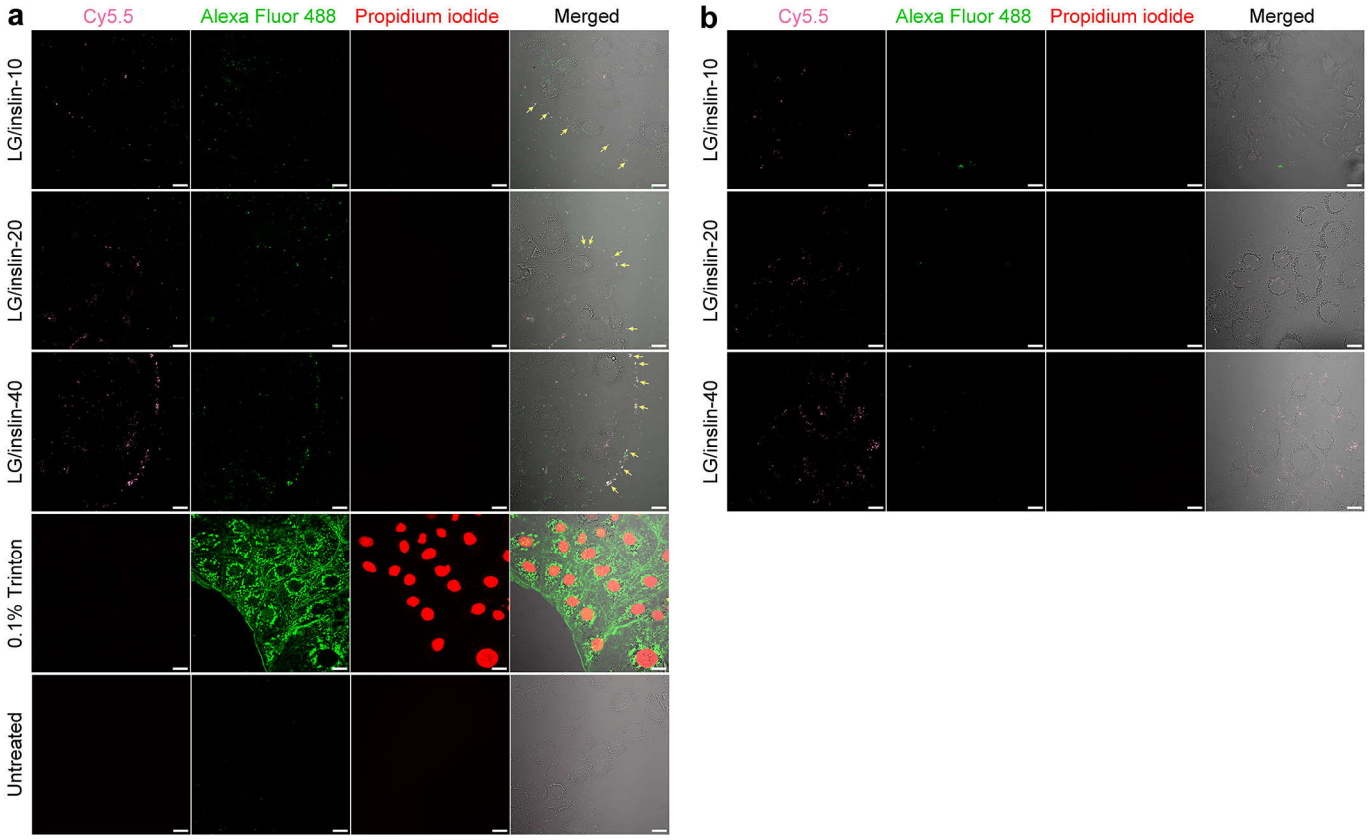

Supplementary Fig. 25 | Cellular uptake of LG/insulin-*x* in the presence of Annexin V and propidium iodide. **a**, Confocal imaging of Caco-2 cells after co-incubated with Cy5.5-tagged LG/insulin-*x* (pink), Annexin V-Alexa Fluor 488 conjugate (green) and propidium iodide (red) for 10 min. Compared to cells treated with Annexin V alone which showed insignificant binding to the cell membrane (the untreated group), colocalization of pink and green fluorescence was observed in the group treated with LG/insulin-*x*, indicating that flip-flop of lipids occurred in the binding regions. Moreover, no influx of the cell impermeant propidium iodide was observed in cells showing membrane binding of LG/insulin-*x*, indicating that the membrane regions binding LG/insulin-*x* kept sealed throughout. Cells treated with Triton-X 100 (0.1%) were set as a positive control. **b**, Caco-2 cells were first incubated with LG/insulin-*x* for 10 min, then LG/insulin-*x* was removed, and the cells were incubated in blank culture medium for 30 min. After that, the cells were stained with Annexin V- Alexa Fluor 488 conjugate and propidium iodide. There was much less binding of Annexin V observed after removal of the LG/insulin-*x*, indicating that the flip-flop of lipids accompanying the translocation of LG/insulin-*x* was transient and reversible. Scale bars, 20 μm.

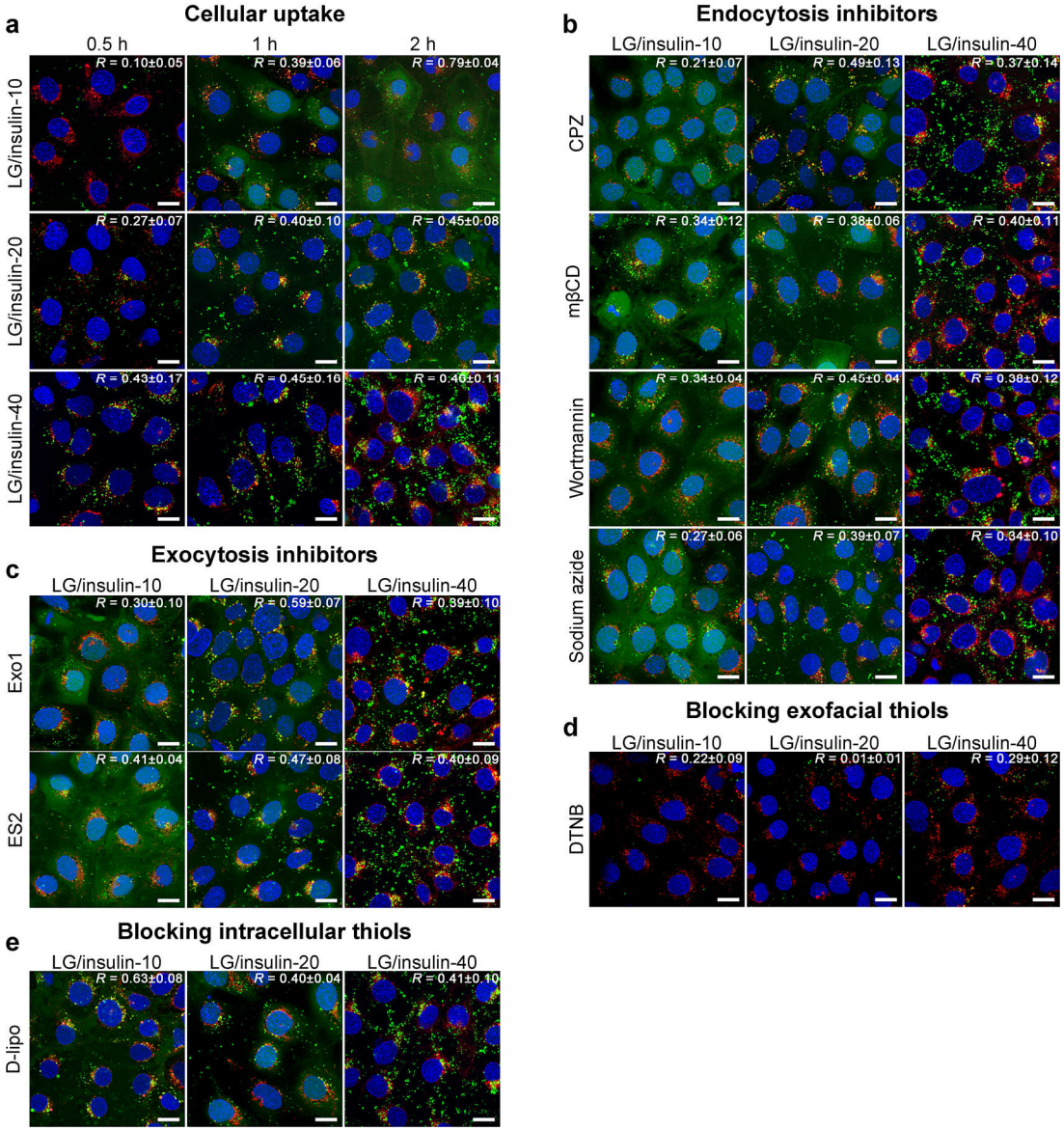

Supplementary Fig. 26 | Confocal microscopy images showing the cellular uptake of LG/insulin-*x* and the correlation of LG/insulin-*x* with endo-lysosomes after different incubation times (**a**), and the correlation of LG/insulin-*x* with endo-lysosomes after incubation for 2 h in the presence of endocytosis inhibitors (**b**), exocytosis inhibitors (**c**), DTNB (**d**), and DTNB-loaded fuosogenic liposomes (D-lipo; **e**). Green: FITC-tagged insulin; red: endo-lysosomes; blue: nuclei. Scale bars, 20 μm. The inset numerical value is the Pearson's correlation coefficient (*R*) between green and red fluorescence averaged from the cells in each panel (n = 10-18). The fluorescent signals of most LG/insulin-40 remained as puncta while the fluorescent signals of LG/insulin-10 or -20 became spread in the cytosol over time, which was due to their differences in sensitivity towards intracellular glutathione-mediated dissociation. The diffuse fluorescence produced by the dissociated LG/insulin-10 and -20 led to false correlation results. These discussions also explain the similar phenomena observed in Supplementary Figs. 27-30. From confocal imaging, for non-dissociated LG/insulin-*x*, particularly LG/insulin-40, only slight colocalization with endo-lysosomes were observed, agreeing with the quantification analysis which showed that Pearson's coefficients are below the colocalization threshold of >0.5. These results indicated that a minority of LG/insulin-*x* might enter cells *via* regular endocytosis pathways, as also evidenced by the slight effect of endocytosis inhibitors on the transepithelial delivery (Supplementary Fig. 19). However, the remarkable inhibitory effect of extracellularly added DTNB on the cellular uptake (**d**) and transcellular delivery of LG/insulin-*x* suggested DCDE-mediated uptake to be the predominant mode of cellular entry.

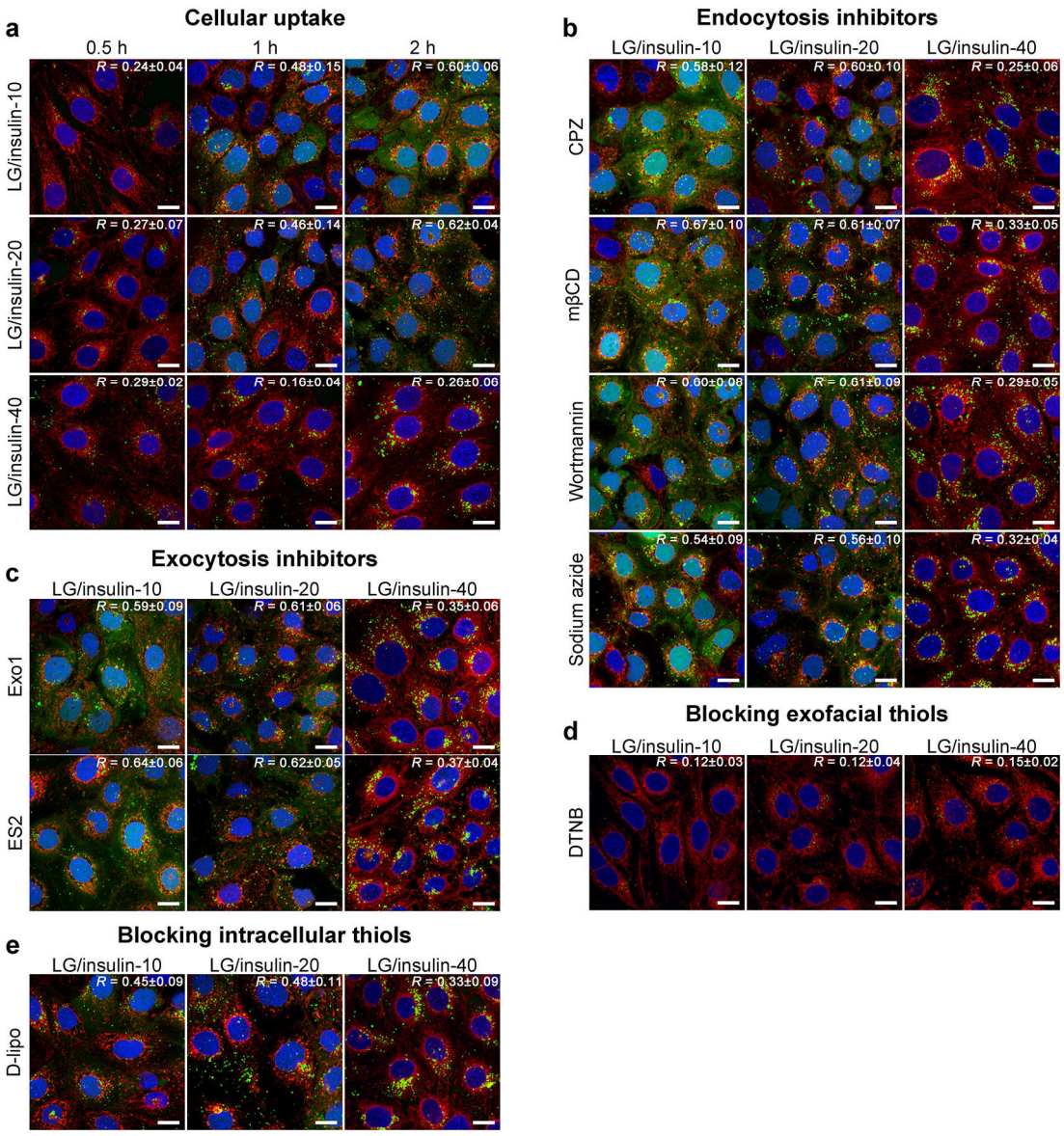

Supplementary Fig. 27 | Confocal microscopy images showing the cellular uptake of LG/insulin-*x* and the correlation of LG/insulin-*x* with the endoplasmic reticulum after different incubation time (**a**), and the correlation of LG/insulin-*x* with the endoplasmic reticulum after incubation for 2 h in the presence of endocytosis inhibitors (**b**), exocytosis inhibitors (**c**), DTNB (**d**), and D-lipo (**e**). Green: FITC-tagged insulin; red: endoplasmic reticulum; blue: nuclei. Scale bars, 20 μm. The inset numerical value is the Pearson's correlation coefficient (*R*) between green and red fluorescence averaged from the cells in each panel (n = 10-15). Overall, no specific correlation between the non-disassociated LG/insulin-*x* and the endoplasmic reticulum in the presence and absence of endocytosis inhibitors, exocytosis inhibitors or DTNB (*R*'s are below the threshold of >0.5 required for correlation) were observed (see further discussion in the legends of Supplementary Fig. 28).

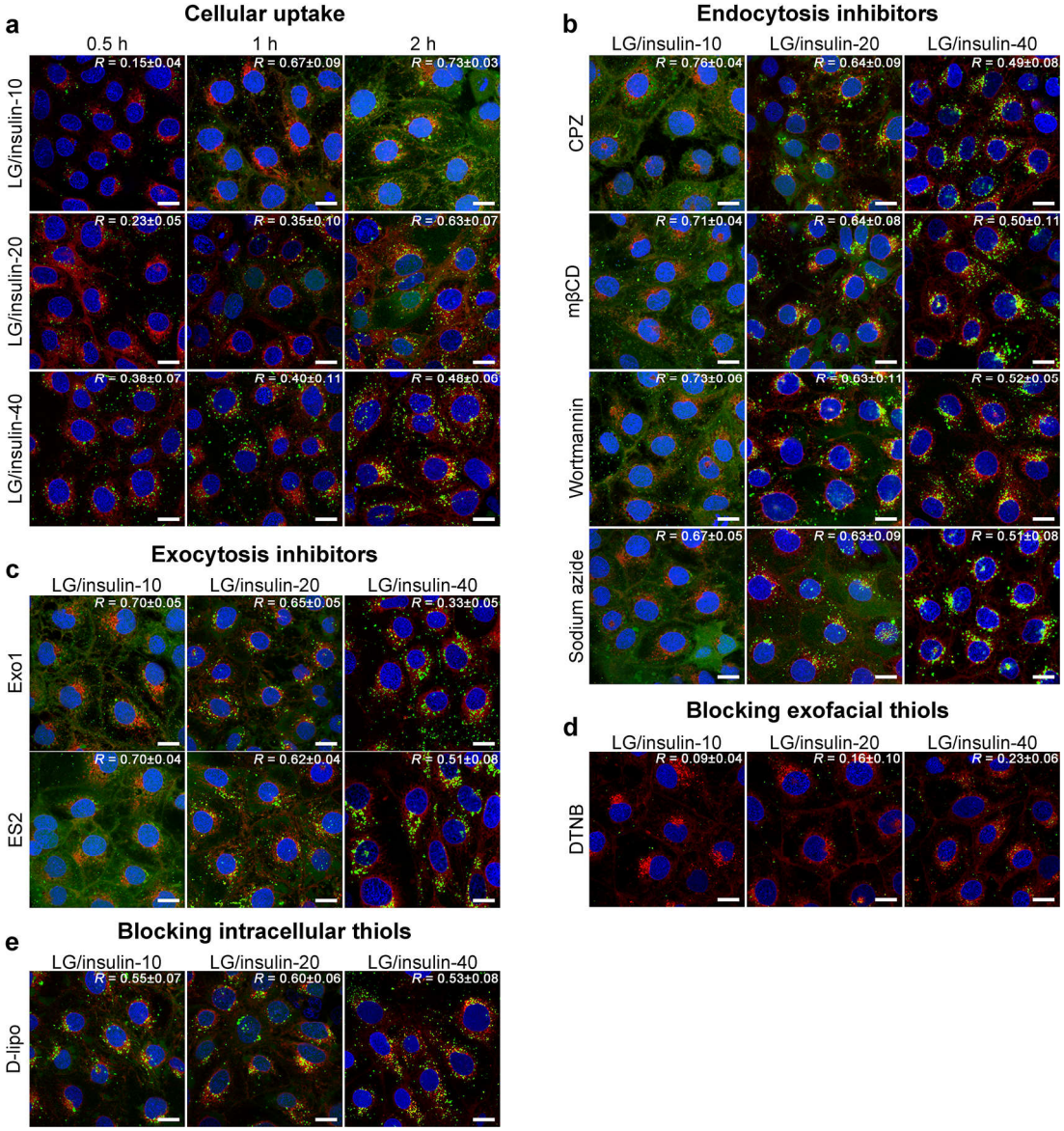

Supplementary Fig. 28 | Confocal microscopy images showing the cellular uptake of LG/insulin-*x* and the correlation of LG/insulin-*x* with the Golgi apparatus after different incubation time (**a**), and the correlation of LG/insulin-*x* with the Golgi apparatus after incubation for 2 h in the presence of endocytosis inhibitors (**b**), exocytosis inhibitors (**c**), DTNB (**d**), and D-lipo (**e**). Green: FITC-tagged insulin; red: Golgi apparatus; blue: nuclei. Scale bars, 20 μm. The inset numerical value is the Pearson's correlation coefficient (*R*) between green and red fluorescence averaged from the cells in each panel (n =9-15). Overall, mild correlation between the non-disassociated LG/insulin-*x* and the Golgi apparatus in the presence and absence of endocytosis inhibitors, exocytosis inhibitors or DTNB (*R*'s are around the threshold of >0.5 required for correlation) were observed after 2 h incubation. Together with the transepithelial results which showed that the passage of LG/insulin-*x* was slightly affected by endo/exocytosis inhibitors (Supplementary Fig. 19), the nonspecific correlation between non-dissociated LG/insulin-*x* with the endoplasmic reticulum and the mild correlation with the Golgi apparatus implicated that the endoplasmic reticulum/Golgi apparatus secretory pathway, Golgi apparatus/membrane pathway, or endocytic recycling pathway was not primarily involved in the transcellular transport of LG/insulin-*x*.

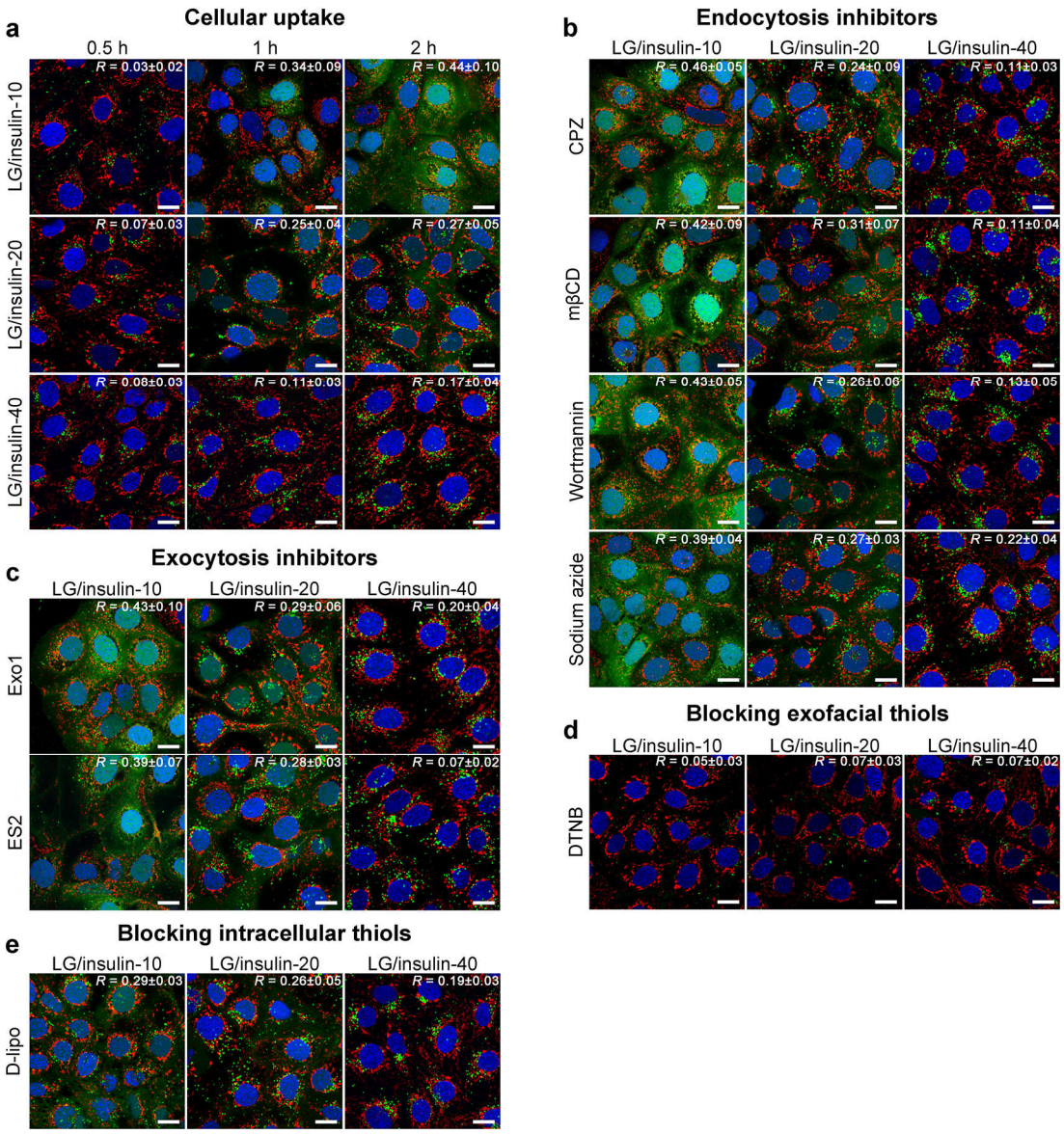

Supplementary Fig. 29 | Confocal microscopy images showing the cellular uptake of LG/insulin-*x* and the correlation of LG/insulin-*x* with mitochondria after different incubation time (**a**), and the correlation of LG/insulin-*x* with mitochondria after incubation for 2 h in the presence of endocytosis inhibitors (**b**), exocytosis inhibitors (**c**), DTNB (**d**), and D-lipo (**e**). Green: FITC-tagged insulin; red: mitochondria; blue: nuclei. Scale bars, 20 μm. The inset numerical value is the Pearson's correlation coefficient (*R*) between green and red fluorescence averaged from the cells in each panel (n = 10-16). Overall, no specific correlation between LG/insulin-*x* and mitochondria in the presence and absence of endocytosis inhibitors, exocytosis inhibitors or DTNB were observed, and this subcellular distribution was not affected by inhibitors. These results suggested LG/insulin-*x* showed no obvious tendency to accumulate at mitochondria and was not trafficked by mitochondria.

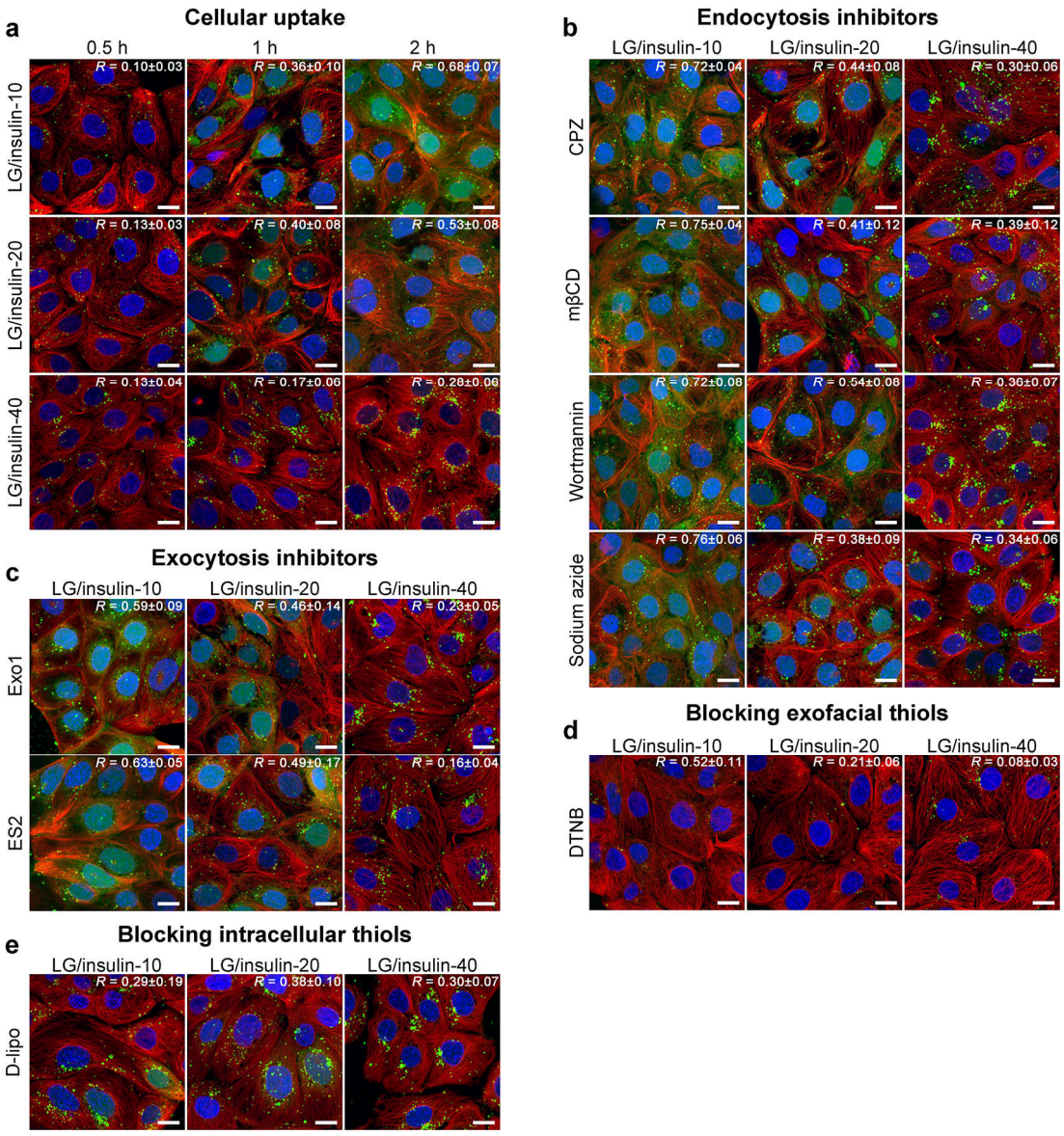

Supplementary Fig. 30 | Confocal microscopy images showing the cellular uptake of LG/insulin-*x* and the correlation of LG/insulin-*x* with microtubules after different incubation time (**a**), and the correlation of LG/insulin-*x* with microtubules after incubation for 2 h in the presence of endocytosis inhibitors (**b**), exocytosis inhibitors (**c**), DTNB (**d**), and D-lipo (**e**). Green: FITC; red: microtubules; blue: nuclei. Scale bars, 20 μm. The inset numerical value is the Pearson's correlation coefficient (*R*) between green and red fluorescence averaged from the cells in each panel (n = 9-15). Although microtubules are critical components of transcytosis machinery and have been shown to mediate the intracellular shuttling of cargoes post uptake and during exocytosis[8, 9], the non-specific correlation between the non-disassociated LG/insulin-*x* and microtubules in the presence or absence of endocytosis inhibitors, exocytosis inhibitors or DTNB indicated that the transit of the cytosolic delivered LG/insulin-*x* towards the basolateral plasma membrane was marginally mediated by the regular transcytosis pathways but more likely driven by thermal motions or aggregate cytoplasmic forces which were suggested to exert on cytosolic delivered cargoes[10, 11].

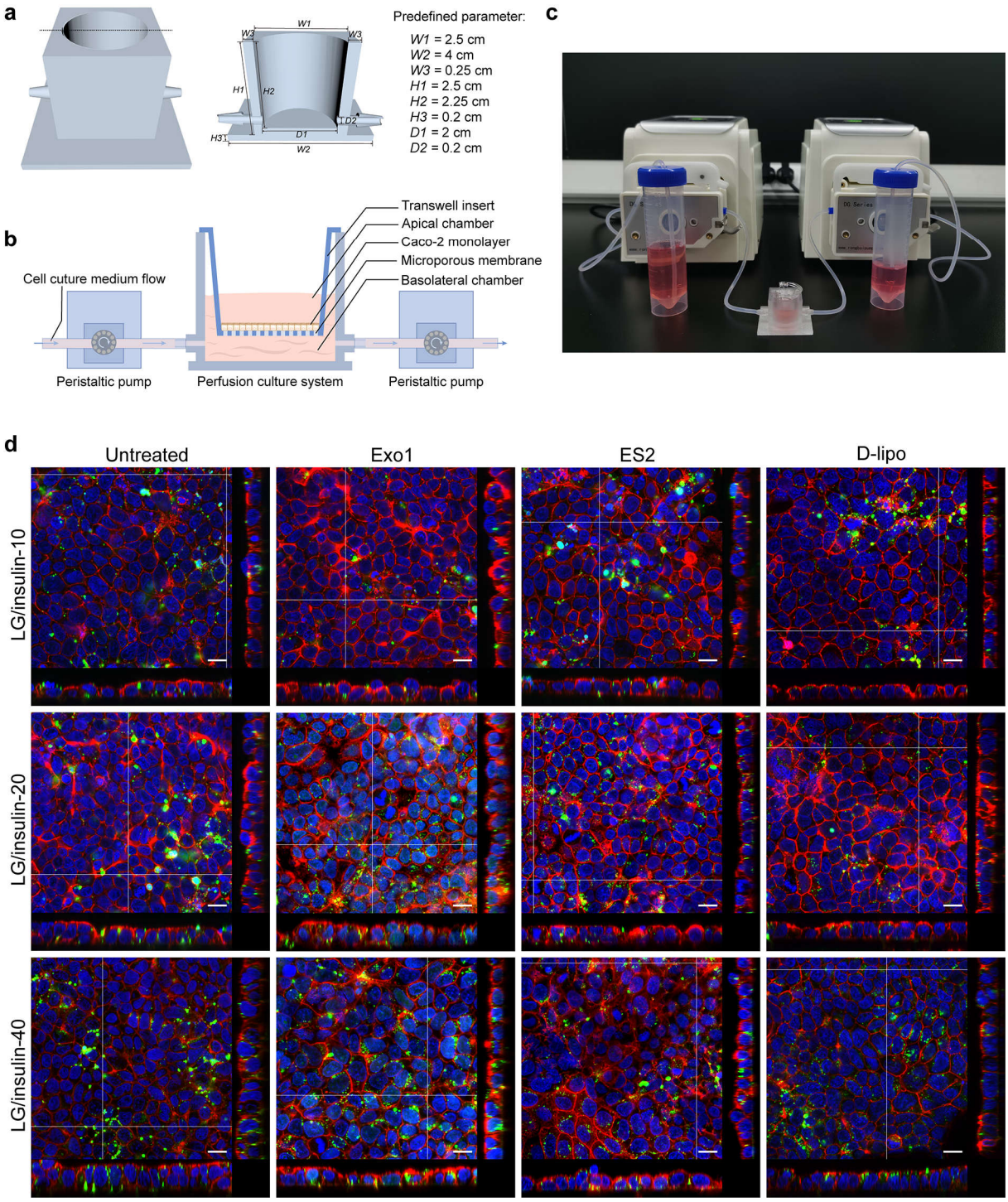

Supplementary Fig. 31 | Tracking the translocation of LG/insulin-*x* across the basal plasma membrane of Caco-2 monolayers. **a-c**, To avoid basal membrane binding by the LG/insulin-*x* rerouted back from the acceptor chamber, the transwell inserts were placed into home-made 3D-printed acceptor chambers equipped with perfusion culture medium during the procedure. **a**, Schematic of the designed 3D-printed acceptor chamber (left), cross section of the designed chamber along the indicated dash line (middle), and predefined parameter (right). Schematic illustration (**b**) and photographs (**c**) of the perfusion system. **d**, Orthogonal projections of Caco-2 monolayers after incubated with FITC-tagged LG/insulin-*x* (green) for 1 h in the absence and presence of exocytosis inhibitors (Exo1, ES2) or intracellular delivered DTNB (D-lipo). In each panel, orthogonal views show the intersection planes at the position of the white crosshair. The nuclei and plasma membrane were stained with Hoechst 33342 (blue) and Alexa Fluor-555 Wheat Germ Agglutinin (red), respectively. Scale bars, 20 μm. The *x*-*z* orthogonal views were also shown in **Fig. 2f**.

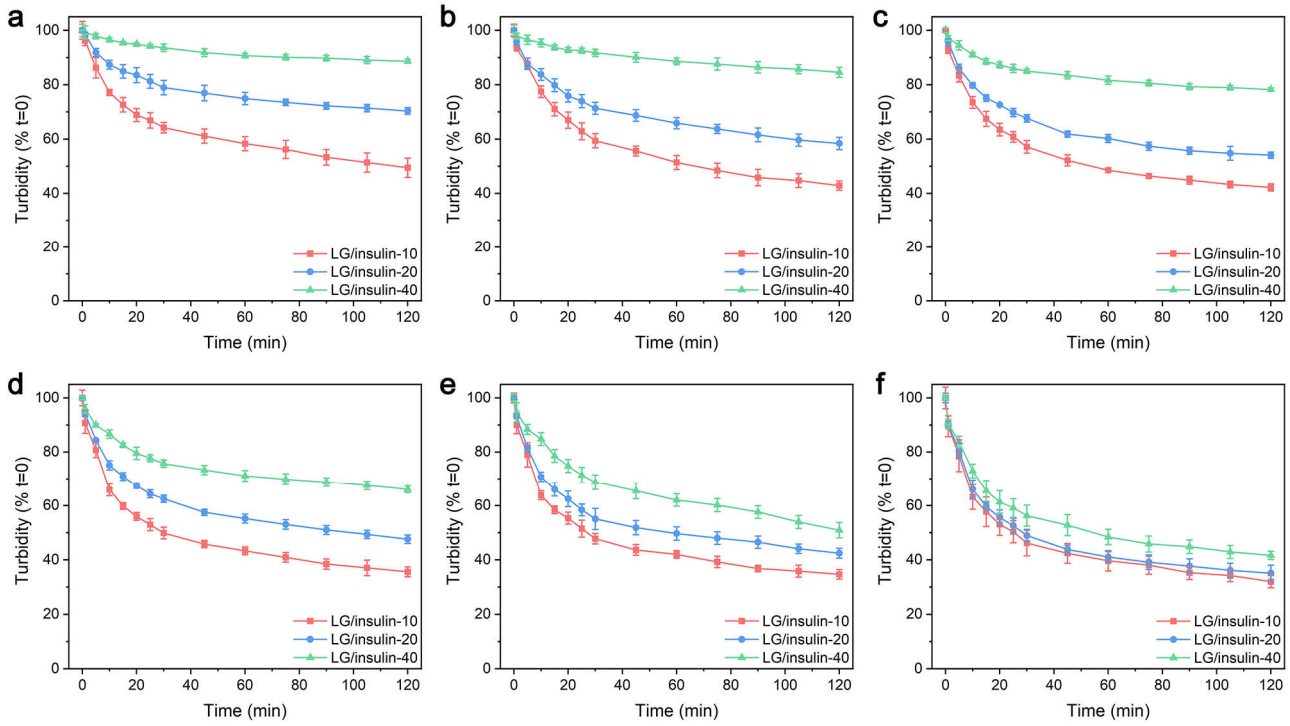

Supplementary Fig. 32 | Dissociation kinetics of LG/insulin-*x* in the presence of glutathione at different physiologically relevant levels. After adding 200 µl of LG/insulin-*x* (0.25 mg ml^{-1}) in PBS to each well of plate readers, 4 µl of freshly prepared stock solution of glutathione of different concentrations was added. After incubated at 37 ℃ for different times, changes in turbidity of the suspensions were recorded by measuring the absorbance at 600 nm by a microplate reader. A series concentrations of glutathione were studied, including (**a**) 30 µM, (**b**) 250 µM, (**c**) 500 µM, (**d**) 1.5 mM, (**e**) 4 mM, and (**f**) 8 mM, which were in the range of the glutathione levels in the blood plasma (~30 µM)[12], intestinal lumen (60–300 µM)[13], nonproliferating Caco-2 (300–600 µM)[14] or villus tip cells (250–400 µM)[15], proliferating Caco-2 cells (1.2–1.6 mM)[14], crypt cells (4–5 mM)[15] and hepatic sinusoids (7–10 mM)[16], respectively. Data points represent mean ± s.d. (n = 3 independent experiments). At the glutathione concentrations mimicking the levels of blood plasma, intestinal lumen, nonproliferating Caco-2 cells or villus epithelial cells, LG/insulin-40 dissociated much slower than LG/insulin-10 and -20. At the levels of hepatic sinusoidal glutathione pool, all coacervates dissociated quickly.

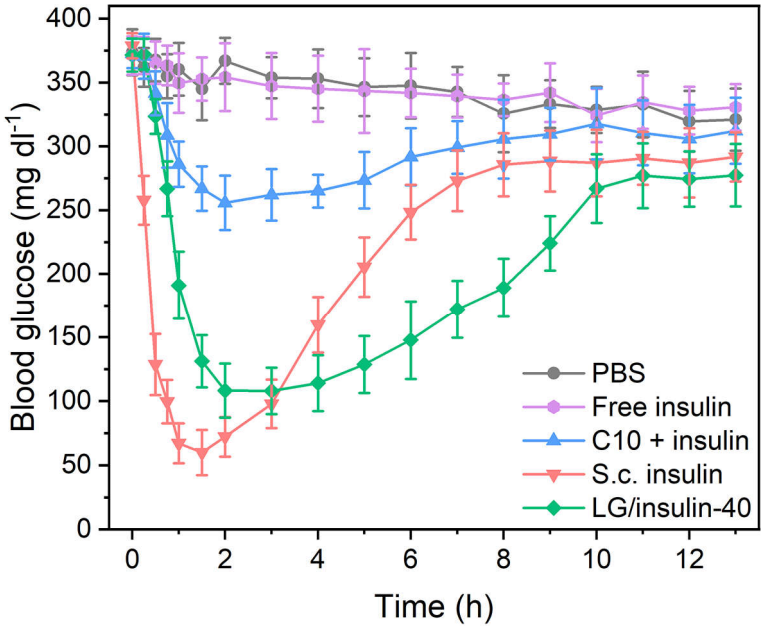

Supplementary Fig. 33 | Changes in blood glucose levels after intrajejunal injection of insulin of different formulations. Absolute values of blood glucose changes in diabetic mice after intrajejunal injection of LG/insulin-40 (20 IU kg^{-1}), free insulin (20 IU kg^{-1}), sodium caprate (C10) plus insulin (20 IU kg^{-1}), and PBS. Mice receiving s.c. insulin (5 IU kg^{-1}) were used as the control. Data points represent mean ± s.d. (n = 5 mice per group).

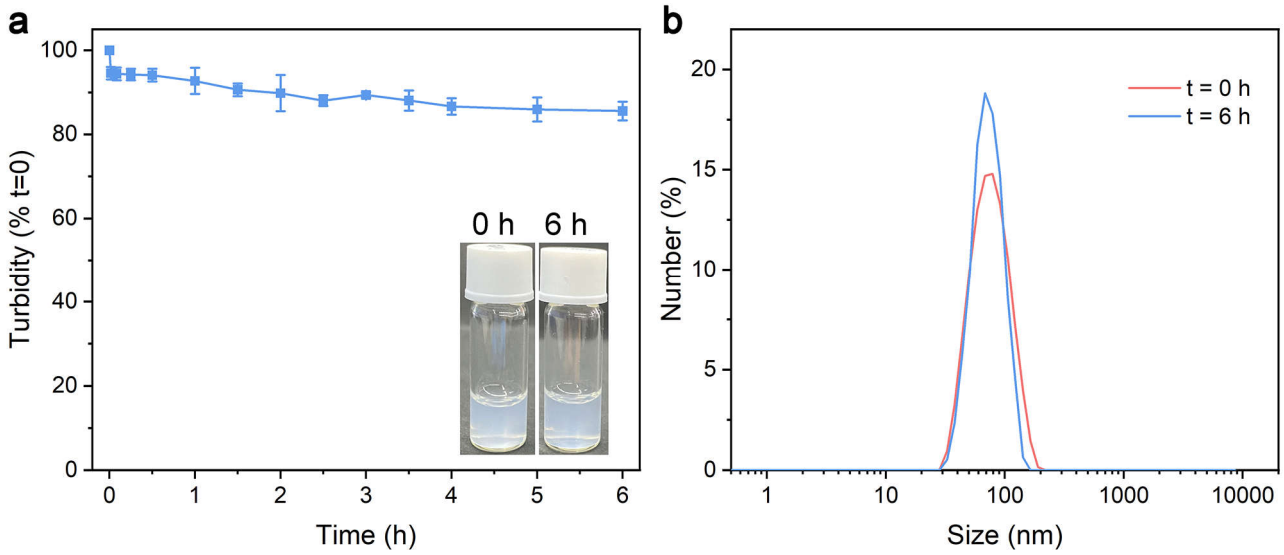

Supplementary Fig. 34 | Colloidal stability of LG/insulin-40 in simulated intestinal fluid (SIF). **a**, Changes in turbidity of LG/insulin-40 suspensions in SIF. The turbidity remained over 80% of its initial value after six-hour incubation. Data points represent mean ± s.d. (n = 3 independent experiments). Inset photographs showing that the suspensions of LG/insulin-40 in SIF remained turbid at 6 h after mixing. **b**, Hydrodynamic size distribution of LG/insulin-40 before (t = 0) and 6 h after incubation in SIF. No obvious reduction in the average hydrodynamic size was detected after incubation in the SIF. These results demonstrated the stability of LG/insulin-40 against nonspecific disassociation in the SIF.

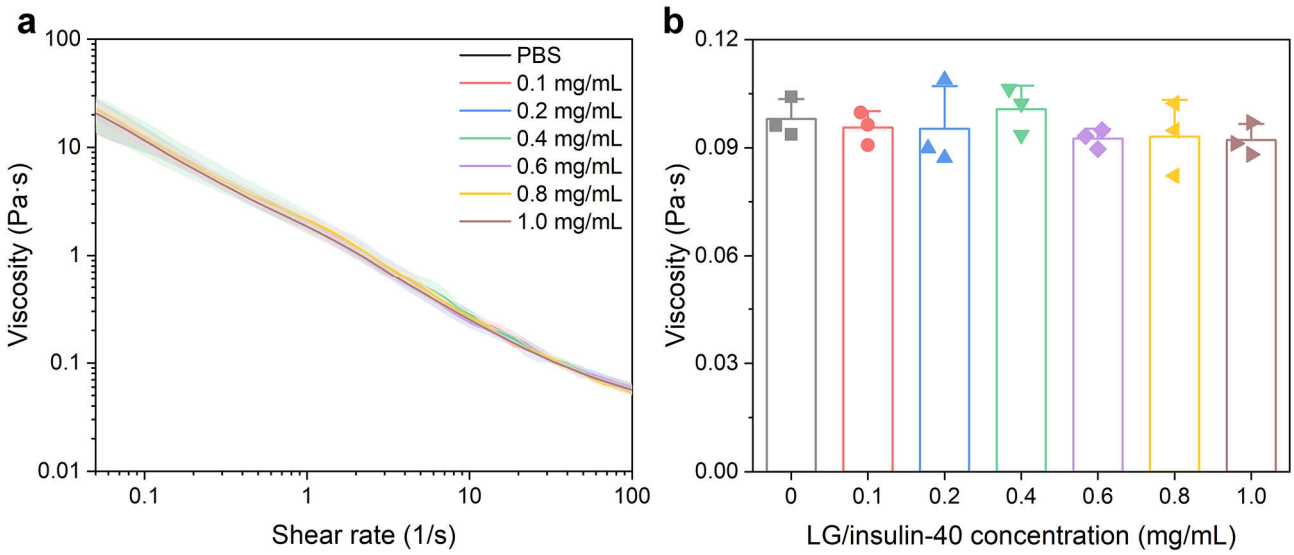

Supplementary Fig. 35 | Rheology study of the reconstituted mucus after incubated with LG/insulin-40. **a**, Viscosity of reconstituted mucus in the presence of LG/insulin-40 of different concentrations (0, 0.1, 0.2, 0.4, 0.6, 0.8, and 1.0 mg ml^{-1}) as a function of shear rate ranging between 0.05 and 100 1/s. An equivalent volume of PBS was used in the group of 0 mg ml^{-1} LG/insulin-40. **b,** Mean viscosity values of mucus at a shear rate of 39.1 1/s in the presence of LG/insulin-40 of different concentrations. The presence of LG/insulin-40 showed no notable effect on the shear-thinning behavior of mucus, which is critical for normal function of mucus in the intestine. No significant declines in the viscosity of mucus were seen after incubated with LG/insulin-40 of different concentrations for 3 h, suggesting that the transmucus delivery of LG/insulin-40 was not earned from decreasing the mucus viscosity.

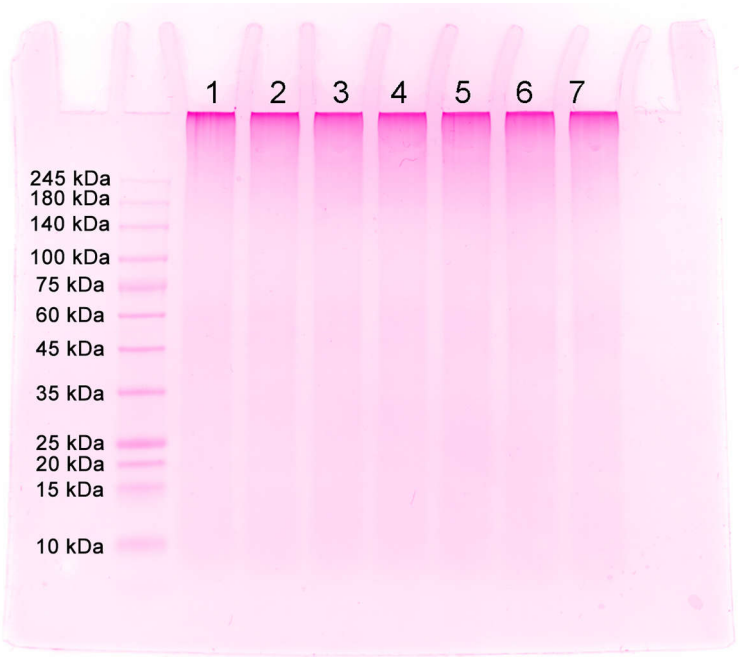

Supplementary Fig. 36 | SDS-PAGE analysis of mucins incubated with LG/insulin-40. SDS-PAGE analysis of the size of mucins after incubated with LG/insulin-40 of different concentrations for 3 h, followed by periodic acid-Schiff (PAS) staining. Lanes 1-7: lane 1, control with PBS only; lanes 2-7, mucins treated with LG/insulin-40 at concentrations of 0.1, 0.2, 0.4, 0.6, 0.8, and 1.0 mg ml^{-1}, respectively. Compared to the control group, no observable reduction in mucin size was detected at each concentration, implying that the transmucus delivery of LG/insulin-40 was not gained from the mucolytic effect.

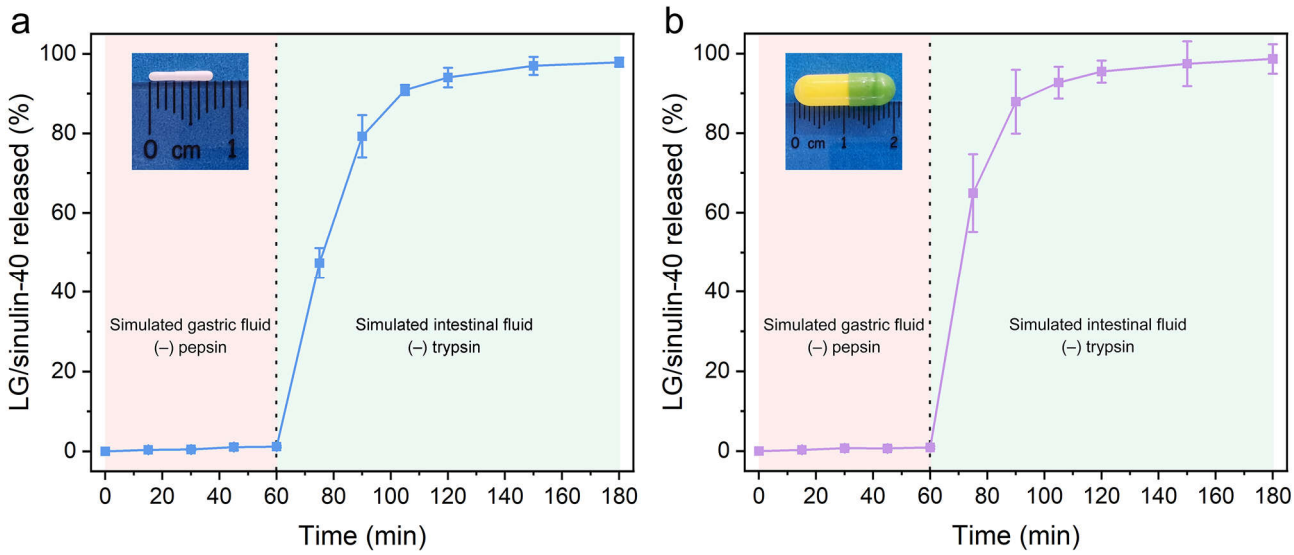

Supplementary Fig. 37 | Release kinetics of LG/insulin-40 from enteric capsules. The release profiles of LG/insulin-40 from (**a**) size-M (enteric coated, used for mice) and (**b**) size-2 (used from Bama minipigs) capsules in the simulated gastric fluid (SGF) and simulated intestinal fluid (SIF) without the corresponding digestive enzymes. Inset photographs in **a** and **b** are LG/insulin-40-loaded size-M (**a**, inset) and size-2 (**b**, inset) capsules, respectively. Release of LG/insulin-40 was not detected in the SGF but was quick in the SIF. Data points represent mean ± s.d. (n = 3 in dependent experiments).

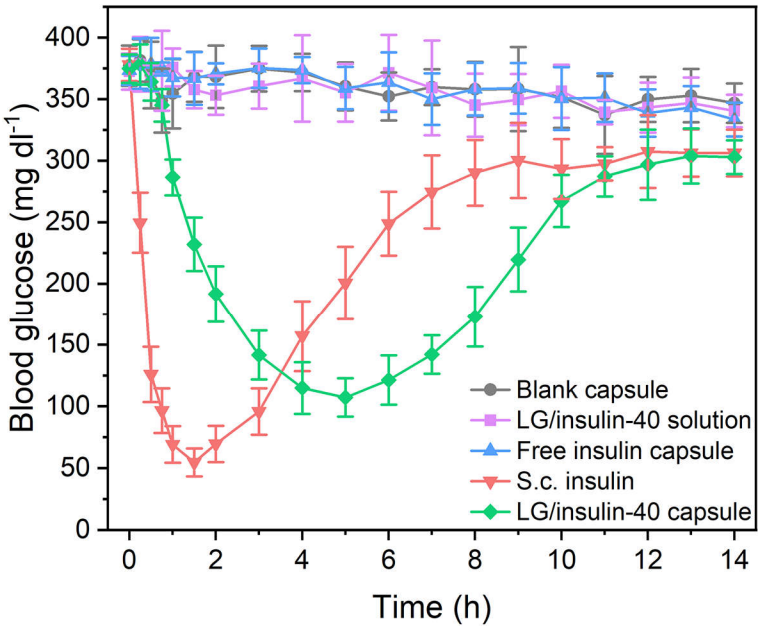

Supplementary Fig. 38 | Oral insulin delivery with LG/insulin-40-loaded enteric capsules (size M) in diabetic mice. Absolute values of the changes in blood glucose levels of diabetic mice after oral gavage of LG/insulin-40-loaded capsules (20 IU kg^{-1}), free insulin-loaded capsules (20 IU kg^{-1}), LG/insulin-40 solutions (20 IU kg^{-1}) and blank capsules. Mice treated with s.c. insulin (5 IU kg^{-1}) were used as the control. Data points represent mean ± s.d. (n = 5 mice per group).

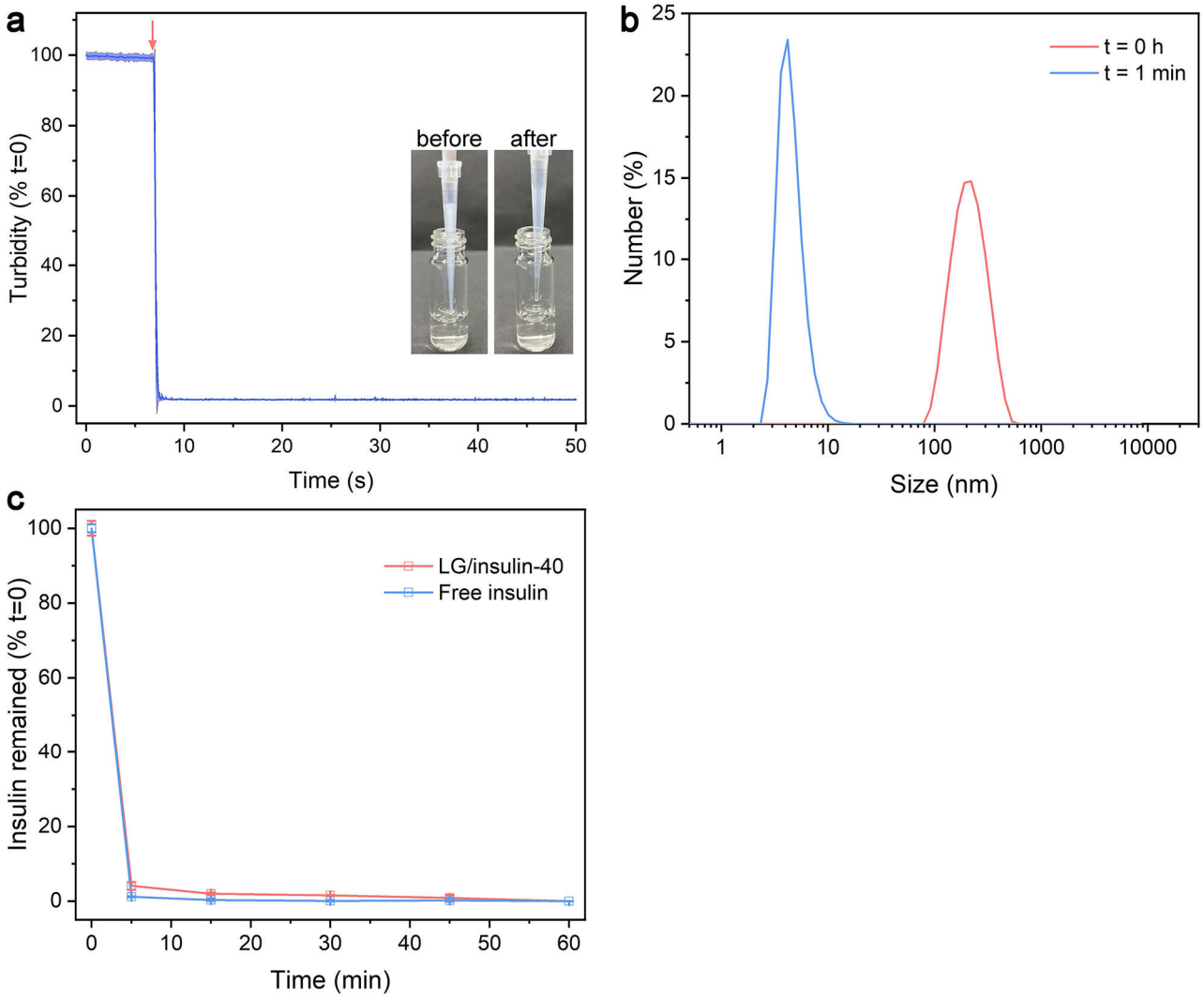

Supplementary Fig. 39 | Stability of LG/insulin-40 in simulated gastric fluid (SGF). **a**, Changes in turbidity of LG/insulin-40 suspensions upon mixing with the SGF. The red arrow indicated the time points of mixing. Inset shows the suspension of LG/insulin-40 before and right after dropping into the SGF. The solution became transparent instantly after addition into the SGF, indicating that LG/insulin-40 dissociated quickly in simulated gastric fluid. This was due to that at pH 2.3, the carboxyl groups of insulin amino acid residues became protonated, which disrupted the salt bridges formed between poly(disulfide)s and insulin and thereby led to the disassembly of the complex coacervates. Data points represent mean ± s.d. (n = 3 independent experiments). **b**, Hydrodynamic size distribution of LG/insulin-40 before (t = 0) and 1 min after added to the SGF. After adding LG/insulin-40 into the SGF, only the hydrodynamic size corresponding to that of insulin was detected, which was due to the dissociation of the complex coacervates and release of insulin. **c**, Percentage of insulin remained after incubation of LG/insulin-40 in the SGF. Over 95% of insulin were degraded in the SGF after 5 min incubation. Free insulin was used as a control. Data points represent mean ± s.d. (n = 3 independent experiments).

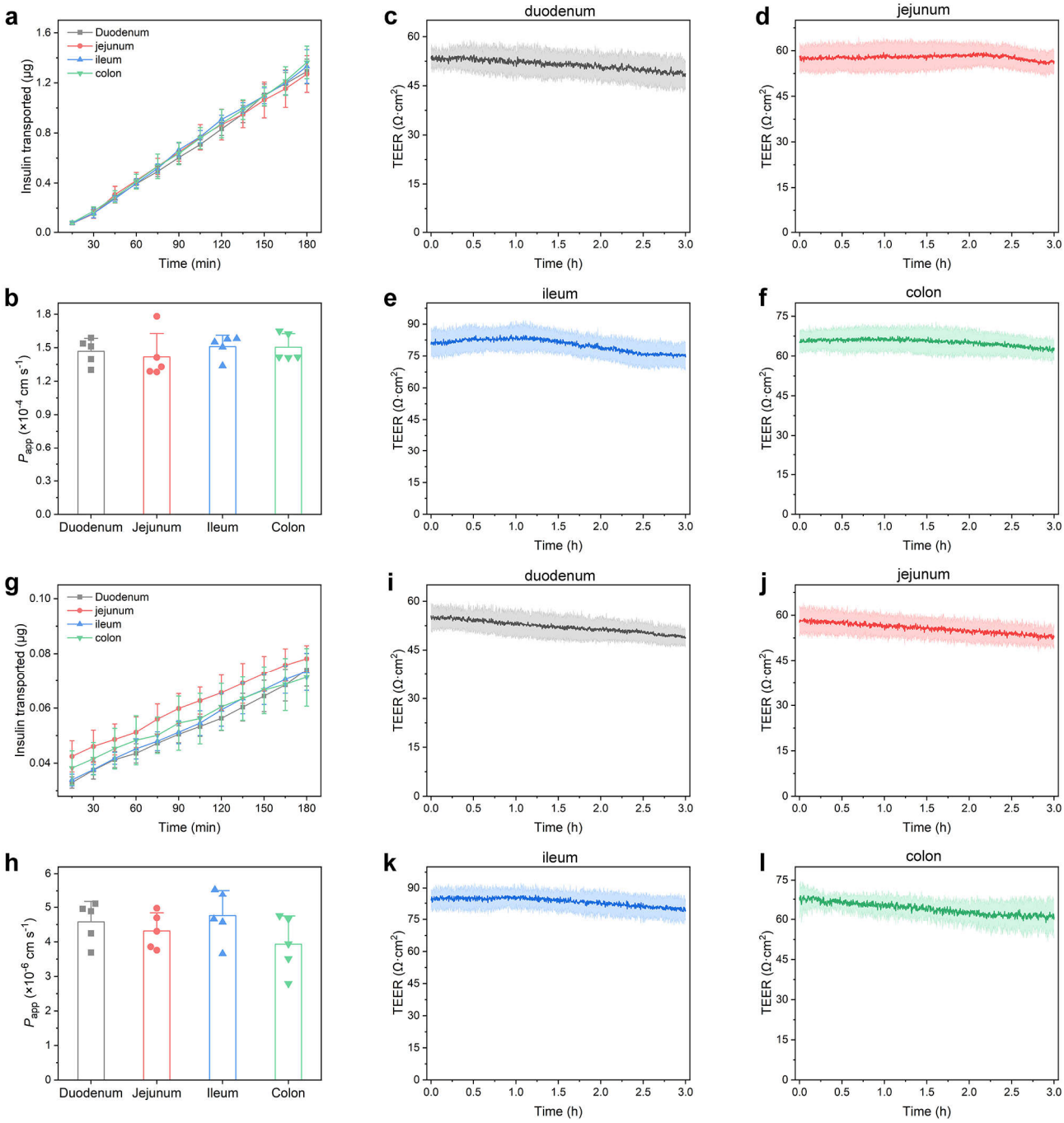

Supplementary Fig. 40 | Study of the *ex vivo* absorptive transport of LG/insulin-40 across different intestinal segments with an Ussing chamber system. **a**, Cumulative transport profiles showing the absorptive transport of LG/insulin-40 across the duodenum, jejunum, ileum, and colon mucosae. **b**, P_{app} values derived from the data in **a**. No significant differences in permeation efficiencies of LG/insulin-40 across different intestinal regions were recorded. The TEER of each intestinal segments, *i.e.*, duodenum (**c**), jejunum (**d**), ileum (**e**), and colon (**f**), were continuously monitored, which indicated that LG/insulin-40 exerted no substantial effect on the tissue integrity. Panels **g–l** are the corresponding data obtained with free insulin under the same experimental conditions. Data points represent mean ± s.d. (n = 5 mice per group). Compared to LG/insulin-40, free insulin showed much lower permeation through the intestinal segments.

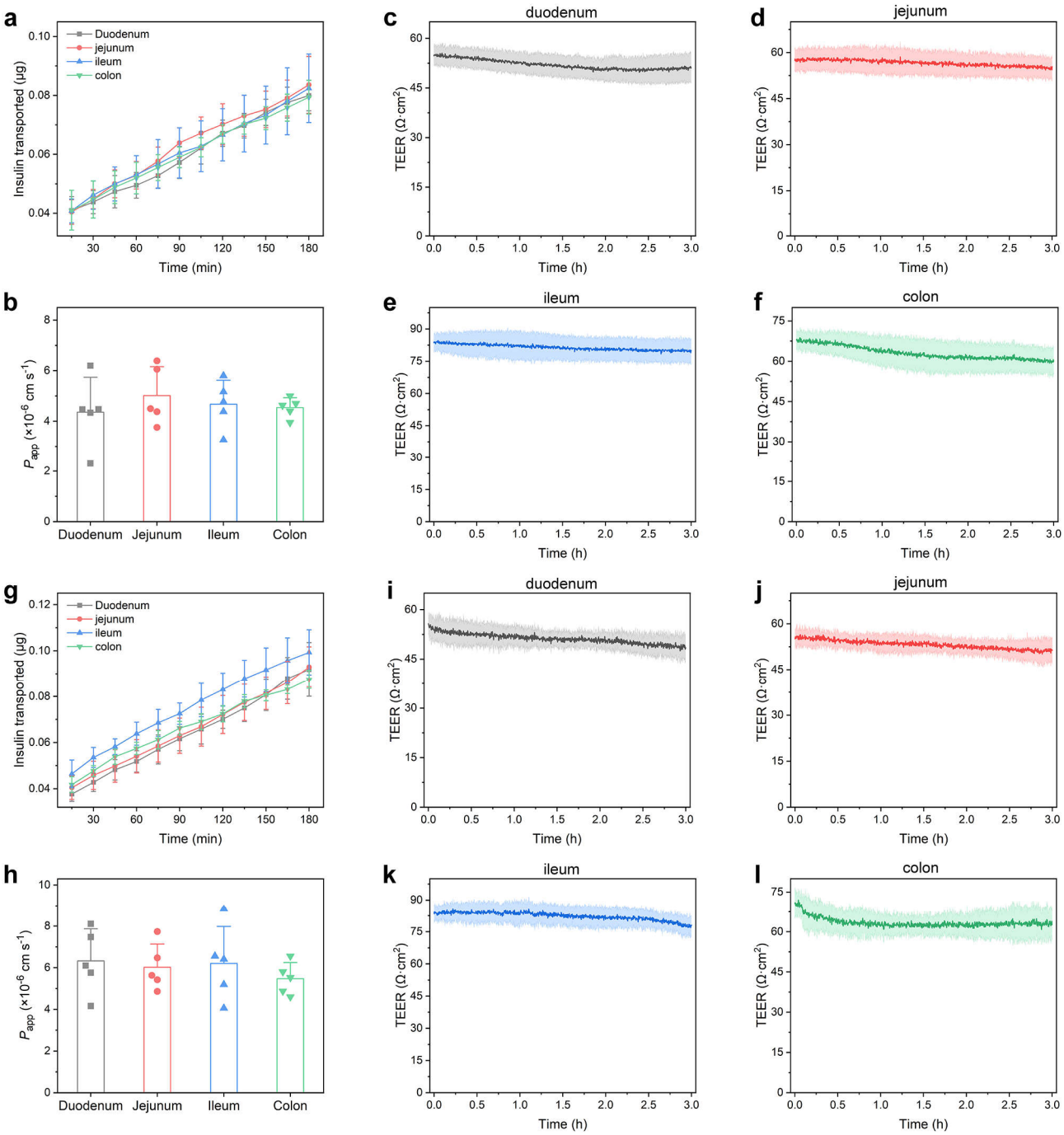

Supplementary Fig. 41 | Study of the *ex vivo* absorptive transport of LG/insulin-40 across different intestinal segments with an Ussing chamber system. Cumulative transport profiles showing the absorptive transport of LG/insulin-40 across the duodenum, jejunum, ileum, and colon mucosae with DTNB (**a**) and (**g**) DTNB-loaded fusogenic liposomes added in the donor chambers. **b**, **h**, P_{app} values derived from the data in **a** and **g**, respectively. The TEER of each intestinal segment in each group (**c–f** for the group of DTNB, **i–l** for the group of DTNB-loaded fusogenic liposomes) was continuously recorded to monitor the tissue integrity. Data points represent mean ± s.d. (n = 5 mice per group). Compared to the cumulative transport profiles and P_{app} values respectively shown in Supplementary Fig. 41, the presence of thiol-blocking reagents significantly reduced the absorptive transport of LG/insulin-40 across each intestinal segment.

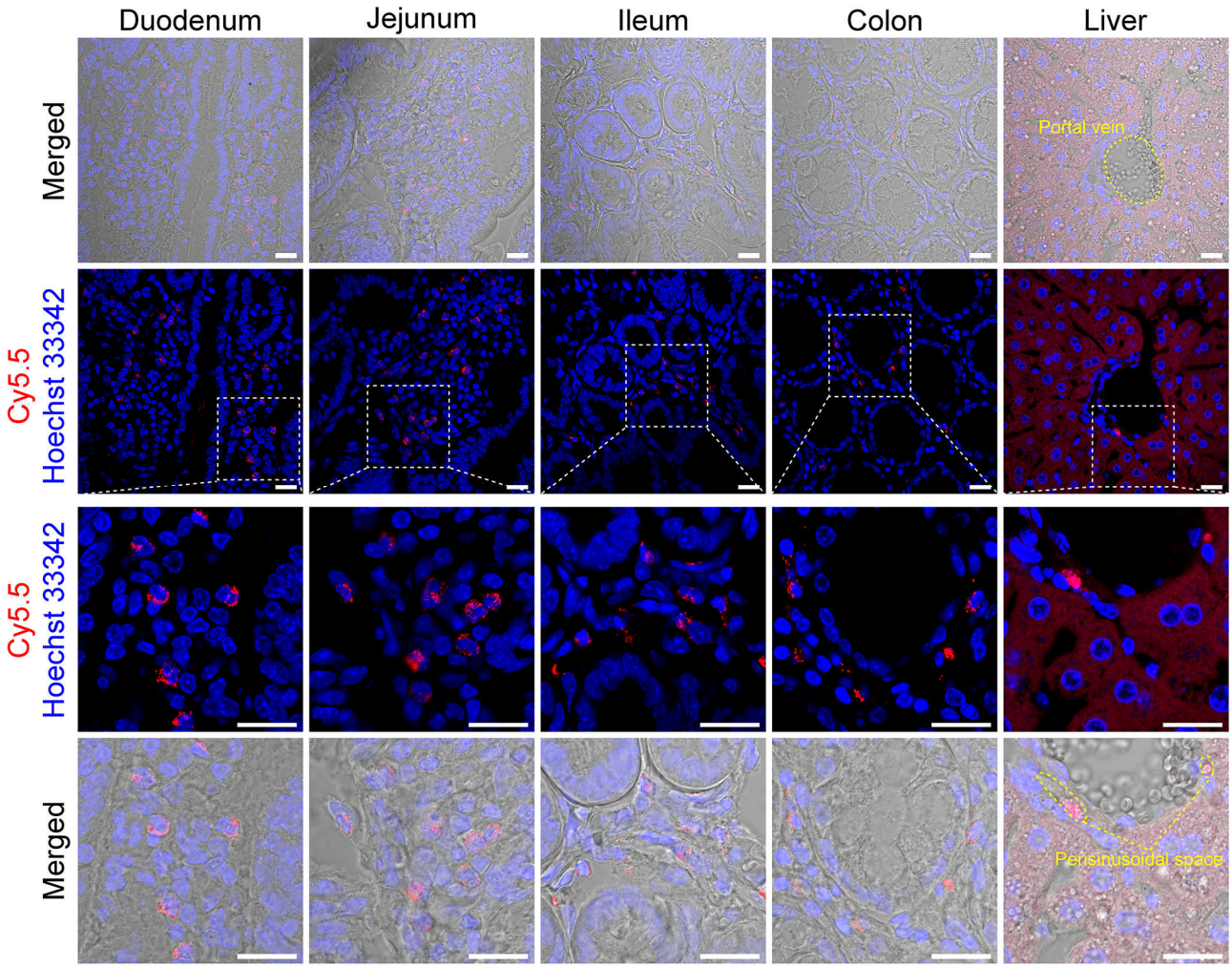

Supplementary Fig. 42 | Representative cryosection images of duodenum (1 h after dosing), jejunum (2 h after dosing), ileum (4 h after dosing), colon (6 h after dosing) and liver (4 h after dosing) showing the integrity of LG/insulin$^{Cy5.5}$-40 in different intestinal segments and in the liver. In each group, the bottom two panels represent a magnified view of the boxed area in the top second panel. Red: Cy5.5-tagged insulin; blue: Hoechst 33342. Scale bars, 20 μm. Most of LG/insulin-40 showed punctate fluorescence in epithelia, whereas few LG/insulin$^{Cy5.5\text{-}40}$ scattered in the perisinusoidal space was observed and strongly diffuse fluorescence appeared throughout the hepatocytes, indicating that LG/insulin-40 was stable during absorption but dissociated after transited to the liver. The bottom two rows of panels are also shown as Fig. 4g in the main text.

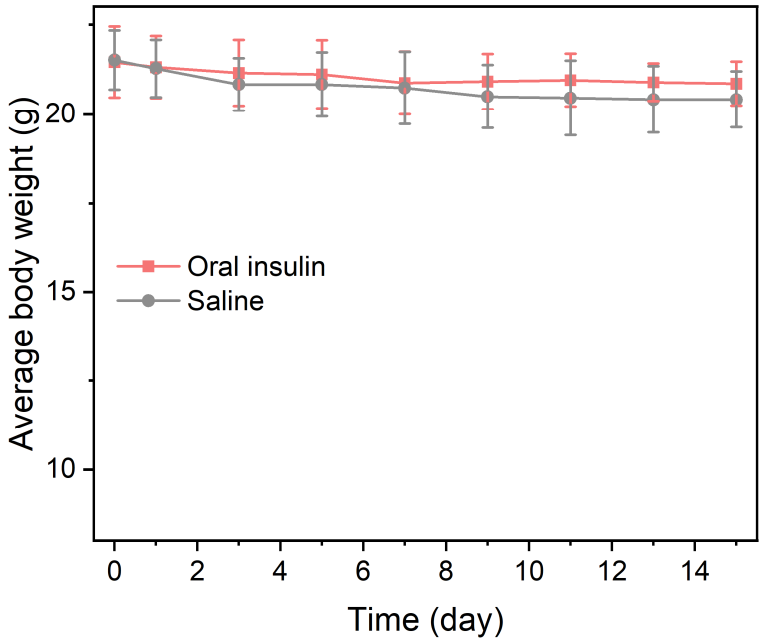

Supplementary Fig. 43 | Changes in the average body weight of diabetic mice after dosed with LG/insulin-40-loaded enteric capsules (oral insulin) twice daily for two weeks. Mice treated with saline were used as the control. Data points represent mean ± s.d. (n = 5 mice per group). Similar to the control group receiving saline, no dramatic body weight fluctuation was observed for mice treated with oral insulin, indicating that LG/insulin-40 exposed unobvious systemic toxicity over long-term dosing.

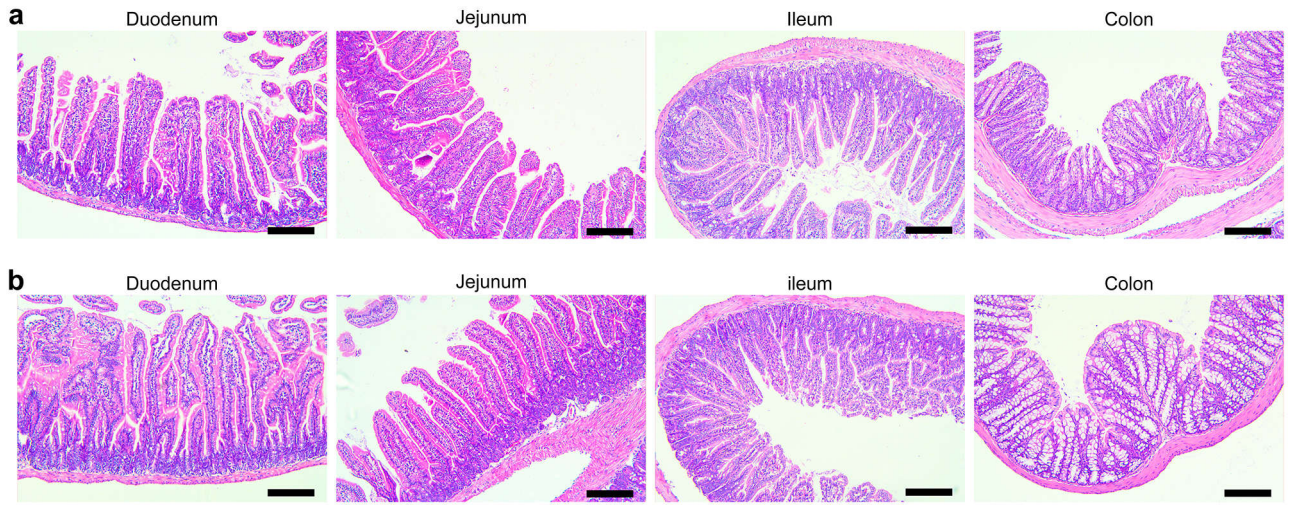

Supplementary Fig. 44 | Histological analysis of the intestinal segments of diabetic mice after dosed with oral insulin twice daily for two weeks. **a,** Hematoxylin and eosin-stained sections of duodenum, jejunum, ileum, and colon of the diabetic mice dosed with LG/insulin-40-loaded enteric capsules twice daily for two weeks. **b,** Diabetic mice treated with saline were used as the control. Scale bars, 200 μm. The general appearance of intestinal tissue sections of LG/insulin-40 treated group was similar to that of the control group. No evidence of changes in mucosal structures including thickness and size of fingerlike villi, or inflammatory reactions were observed in the experimental group. These results showcased the biocompatibility of LG/insulin-40 with intestinal tissues.

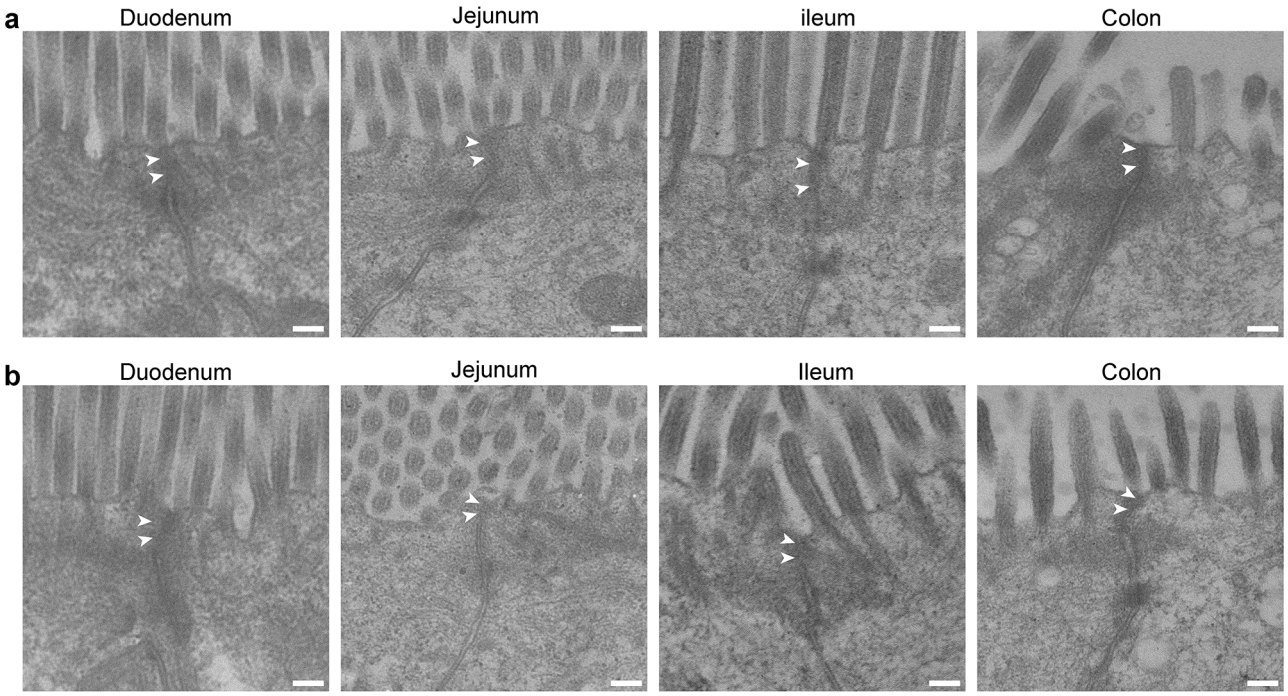

Supplementary Fig. 45 | Integrity of the intestinal epithelial tissues of diabetic mice after dosed with oral insulin twice daily for two weeks. **a**, Representative TEM images of the microstructures of intestinal tissues (duodenum, jejunum, ileum, and colon) of diabetic mice after dosed with LG/insulin-40-loaded enteric capsules twice-a-day for two weeks. **b**, Diabetic mice treated with saline were used as the control. Scale bars, 200 nm. Tight junctions were indicated by arrows. No opening of tight junctions was caused by LG/insulin-40 over long-term oral dosing.

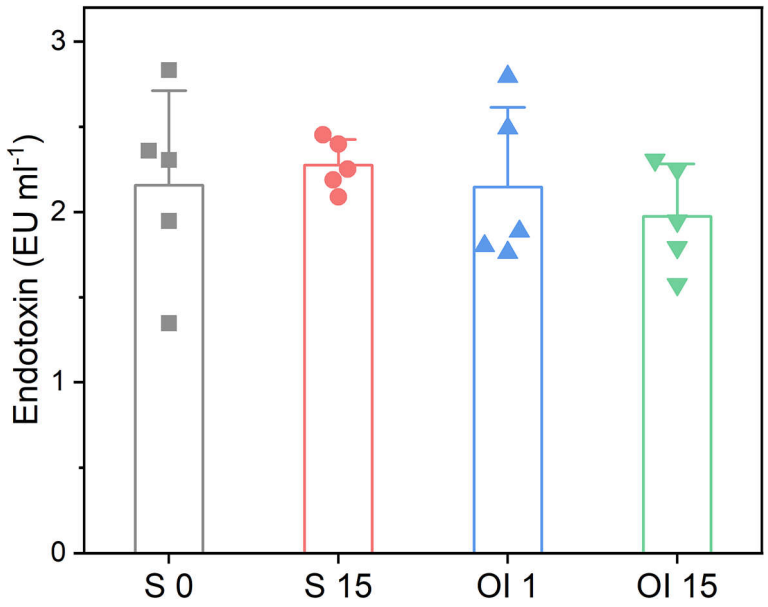

Supplementary Fig. 46 | Serum endotoxin levels of diabetic mice after dosed with oral insulin twice daily for two weeks. The levels of serum endotoxin of diabetic mice before (day 0, OI 0) and after (day 15, OI 15) dosed with LG/insulin-40-loaded enteric capsules twice daily for two weeks. Mice treated with saline were used as the control (S 0 and S 15 represent saline group on day 0 and day 15, respectively). EU, endotoxin units. Data points represent mean ± s.d. (n = 5 mice per group). Like that of the saline-treated mice, no elevation of endotoxin levels in the serum was observed over long-term dosing, suggesting that no opening tight junctions or a leaky gut was caused by LG/insulin-40.

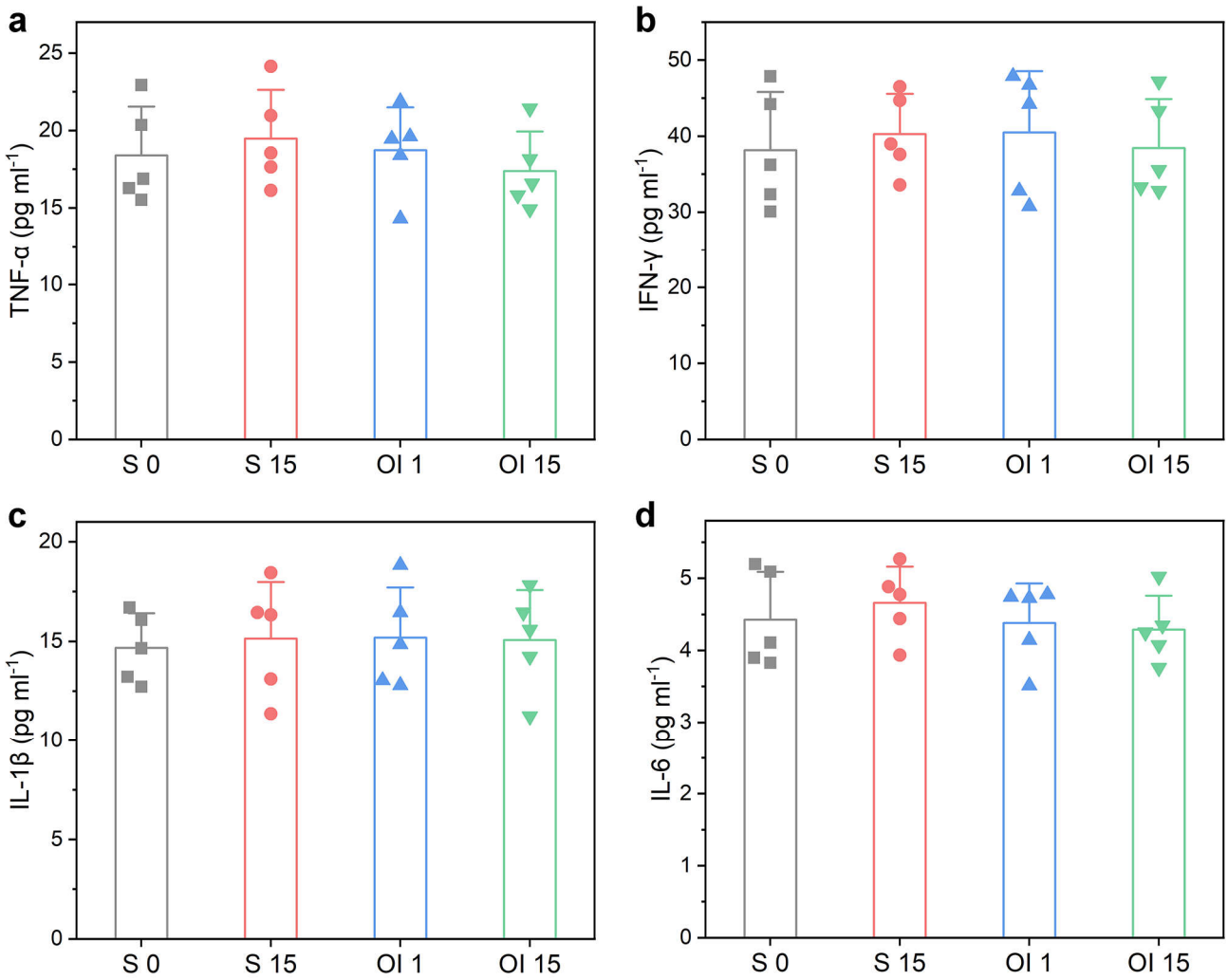

Supplementary Fig. 47 | Inflammation responses in diabetic mice after dosed with oral insulin twice daily for two weeks. **a**-**d**, Levels of proinflammatory cytokines including TNF-α (**a**), IFN-γ (**b**), IL-1β (**c**), and IL-6 (**d**) in the serum of diabetic mice before (day 0, OI 0) and after (day 15, OI 15) dosed with LG/insulin-40-loaded enteric capsules twice daily for two weeks. Mice treated with saline were used as the control (S 0 and S 15 represent saline group on day 0 and day 15, respectively). Data points represent mean ± s.d. (n = 5 mice per group). No significant differences in proinflammatory cytokine levels were detected between the experimental and control groups, indicating no inflammation was induced by long-term dosing of LG/insulin-40.

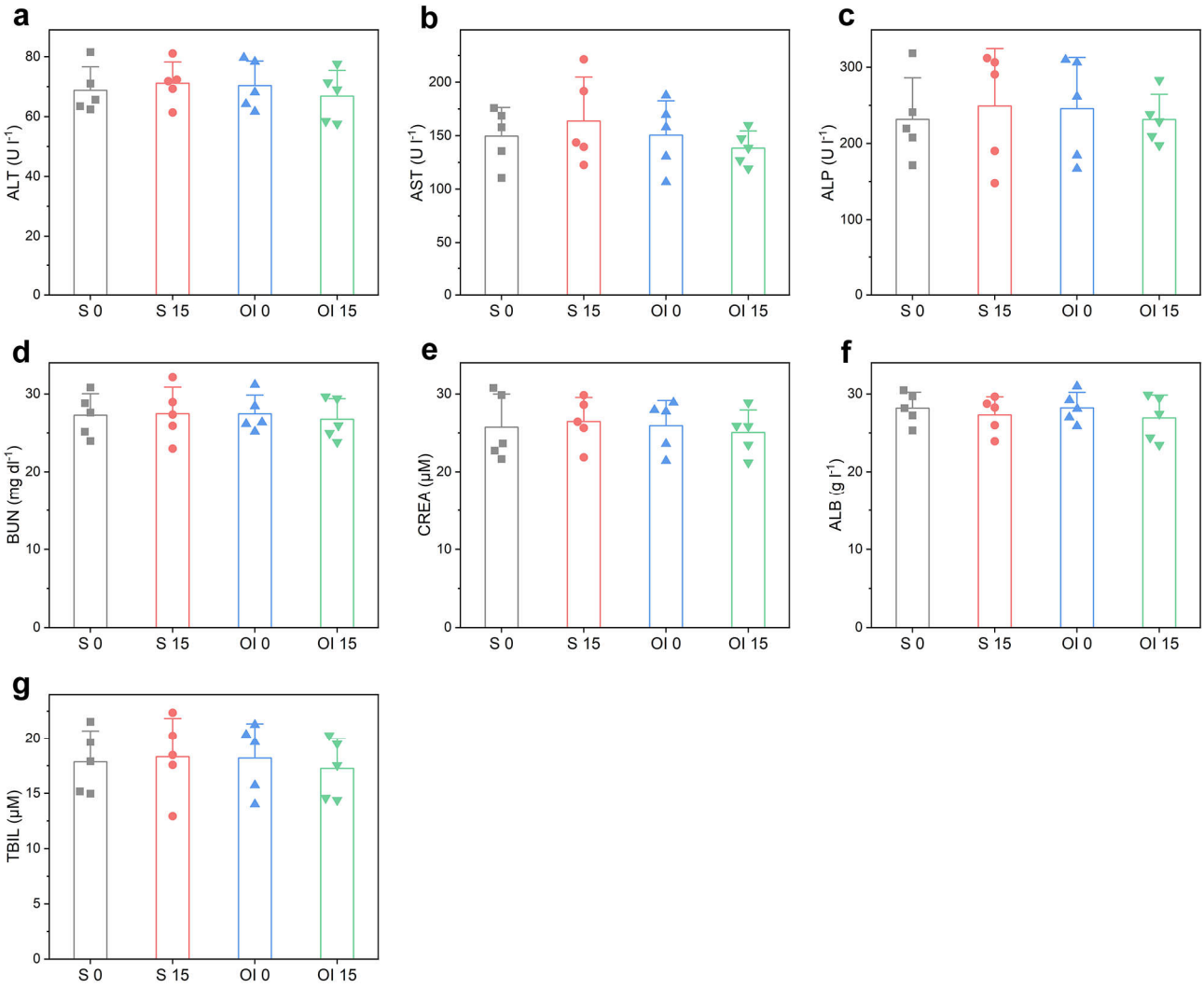

Supplementary Fig. 48 | Blood biochemical analysis of diabetic mice after dosed with oral insulin twice daily for two weeks. **a-g**, Blood biochemical indexes of diabetic mice before (day 0, OI 0) and after (day 15, OI 15) dosed with LG/insulin-40-loaded enteric capsules twice daily for two weeks. Mice treated with saline were used as the control (S 0 and S 15 represent saline group on day 0 and day 15, respectively). Serum concentrations of (**a**) alanine aminotransferase (ALT), (**b**) aspartate aminotransferase (AST), (**c**) alkaline phosphatase (ALP), (**d**) blood urea nitrogen (BUN), (**e**) creatinine (CREA), (**f**) albumin (ALB), and (**g**) total bilirubin (TBIL). Data points represent mean ± s.d. (n = 5 mice per group). No statistical differences in each blood biochemical indexes were detected between all groups. Serum AST and ALT are indicators for liver function, while CREA and BUN are indexes used to identify alternations in kidney function. Mice treated with LG/insulin-40 showed similar levels of AST, ALT, CREA, and BUN to those of the saline-treated group and those on day 0, indicating that no substantial adverse effects were exposed on liver and kidney functions by LG/insulin-40 over long-term dosing.

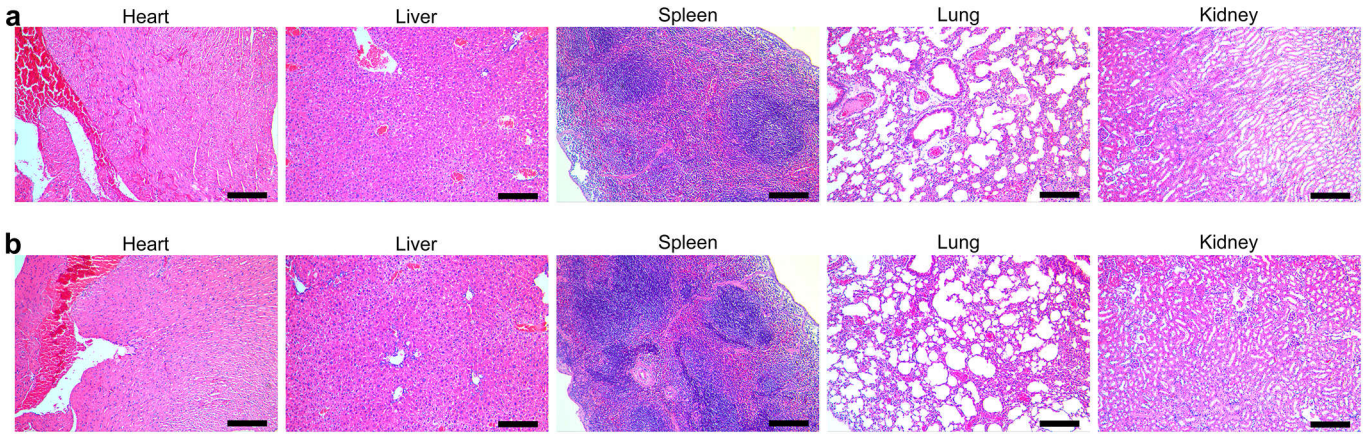

Supplementary Fig. 49 | Histological analysis of the major organs of diabetic mice after dosed with oral insulin twice daily for two weeks. **a**, Representative hematoxylin and eosin-stained sections of the major organs (heart, liver, spleen, lung, and kidneys) collected from diabetic mice which had been dosed with LG/insulin-40-loaded enteric capsules twice daily for two weeks. **b**, Diabetic mice treated with saline were used as the control. Scale bars, 200 μm. The histological sections of each major organ displayed similar appearance in LG/insulin-40 treated and control groups, evidencing the biosafety of LG/insulin-40 towards the major organs over long-term dosing.

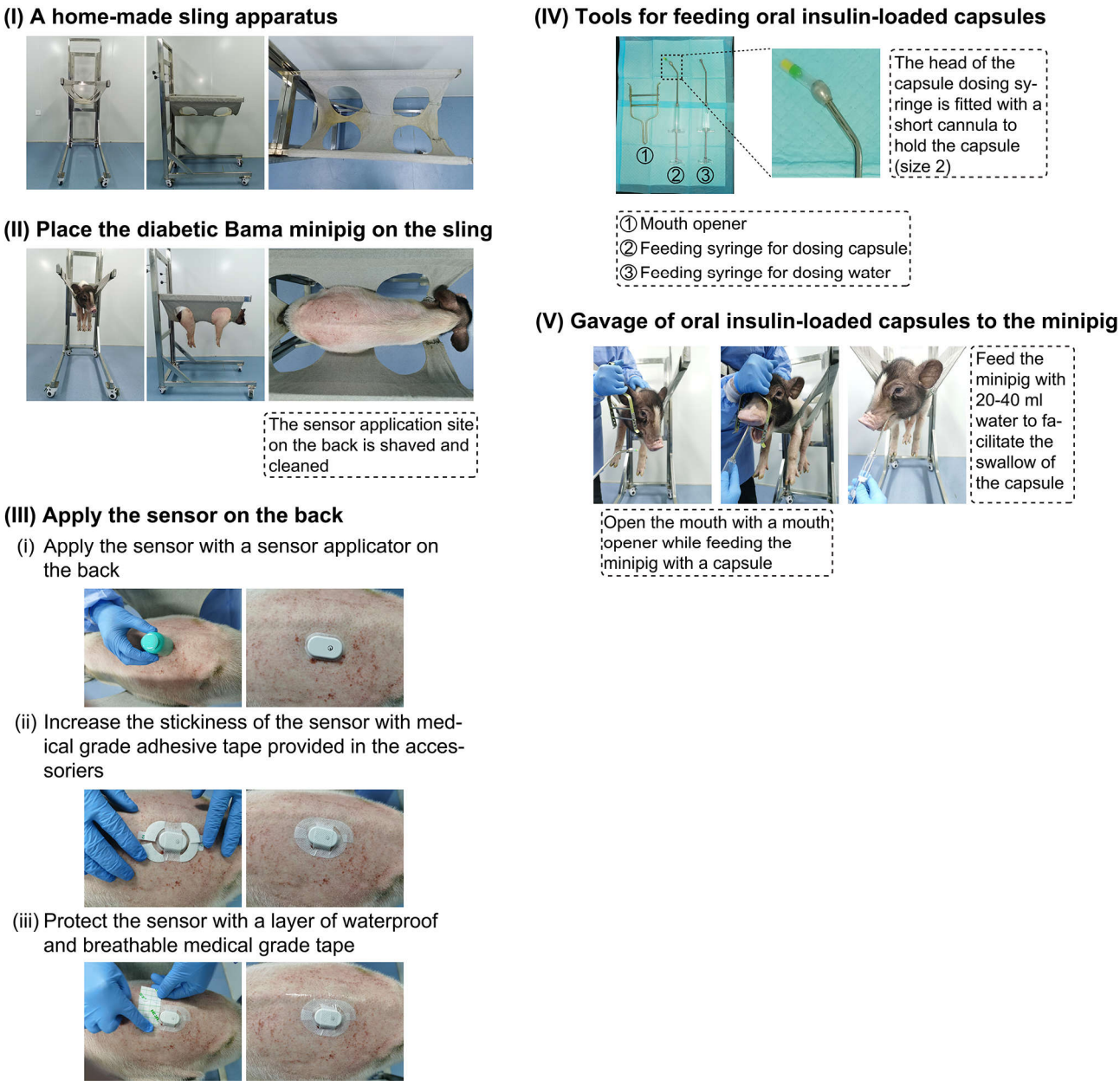

Supplementary Fig. 50 | An overview of minipig experiments. Steps **I-III**, application of the sensor of the continuous glucose monitoring system on the back of a diabetic Bama minipig, where an area that stays flat is preferred. Steps **IV-V**, oral gavage of LG/insulin-40-loaded enteric capsules to diabetic Bama minipigs with a mouth opener and a capsule dosing syringe.

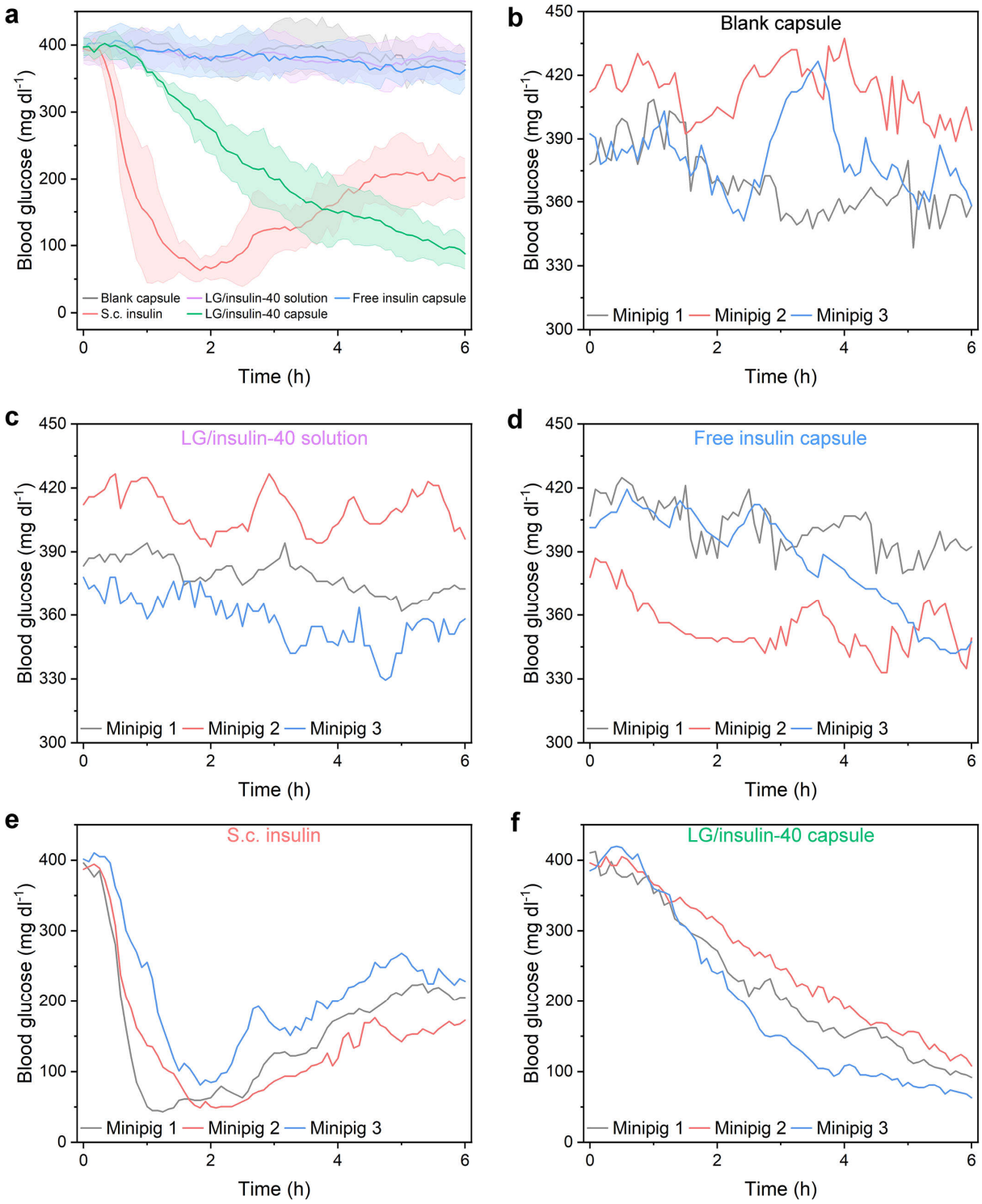

Supplementary Fig. 51 | Oral insulin delivery with LG/insulin-40-loaded enteric capsules in diabetic Bama minipigs. **a**, Absolute values of changes in blood glucose levels after oral gavage of LG/insulin-40-loaded capsules (2 IU kg^{-1}), free insulin-loaded capsules (2 IU kg^{-1}), LG/insulin-40 solutions (2 IU kg^{-1}) and blank capsules. The group receiving s.c. insulin (0.5 IU kg^{-1}) was used as the control. Data points represent mean ± s.d. (n = 3 minipigs per group). **b-f**, Changes in the blood glucose levels of individual minipigs in each group as indicated.

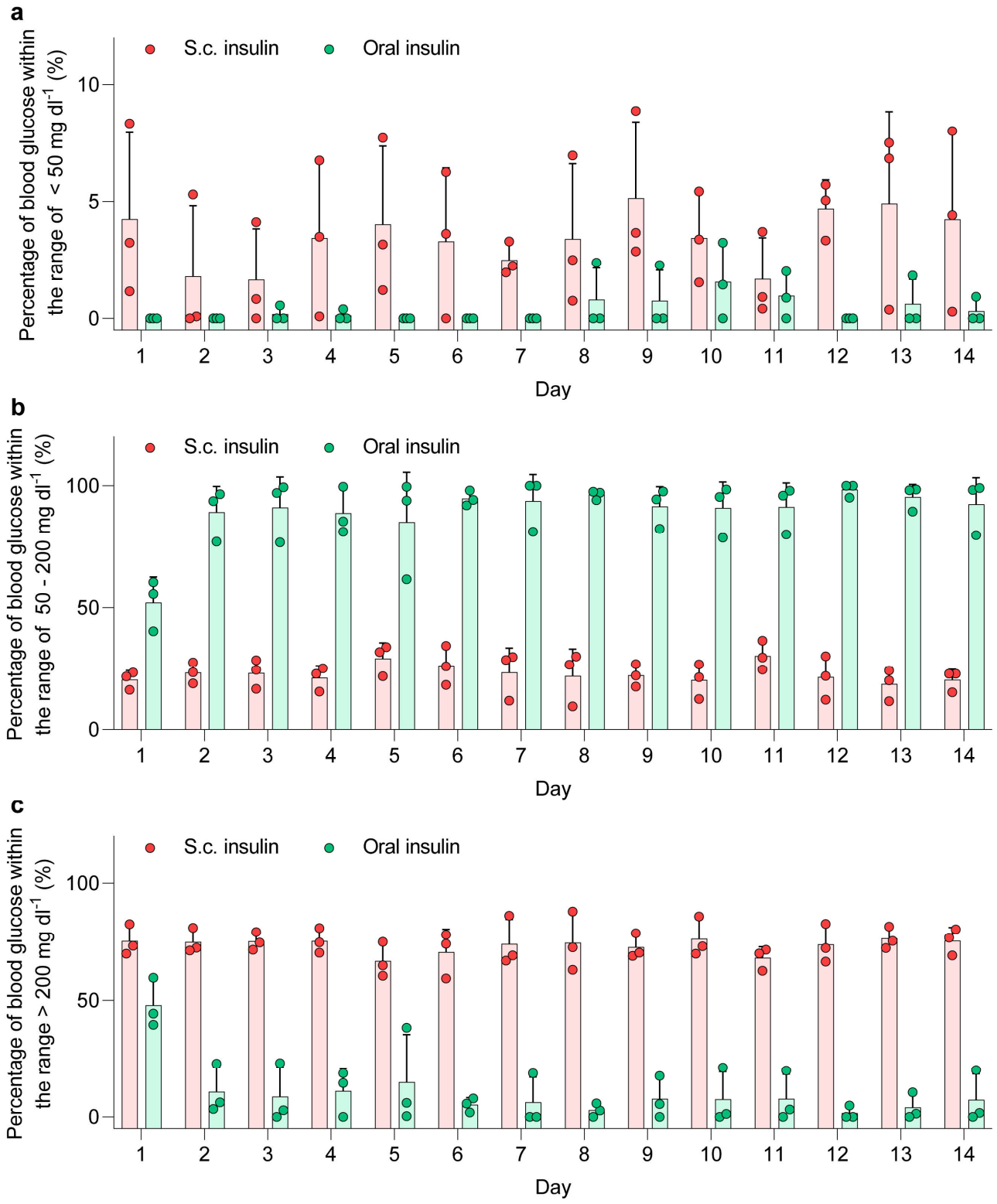

Supplementary Fig. 52 | Percentage of time spent in different given blood glucose ranges on each day during the two-week consecutive treatment. Values were extracted from the data shown in Fig. 5f. Compared to the group receiving s.c. insulin, minipigs dosed with oral insulin experienced few events of hypoglycemia (**a**, BGLs < 50 mg dl^{-1}) and spent much longer time in the blood glucose range of 50-200 mg dl^{-1} (**b**) and much less time in the hyperglycemic status (**c**, BGLs > 200 mg dl^{-1}). Data points represent mean ± s.d. (n = 3 minipigs per group).

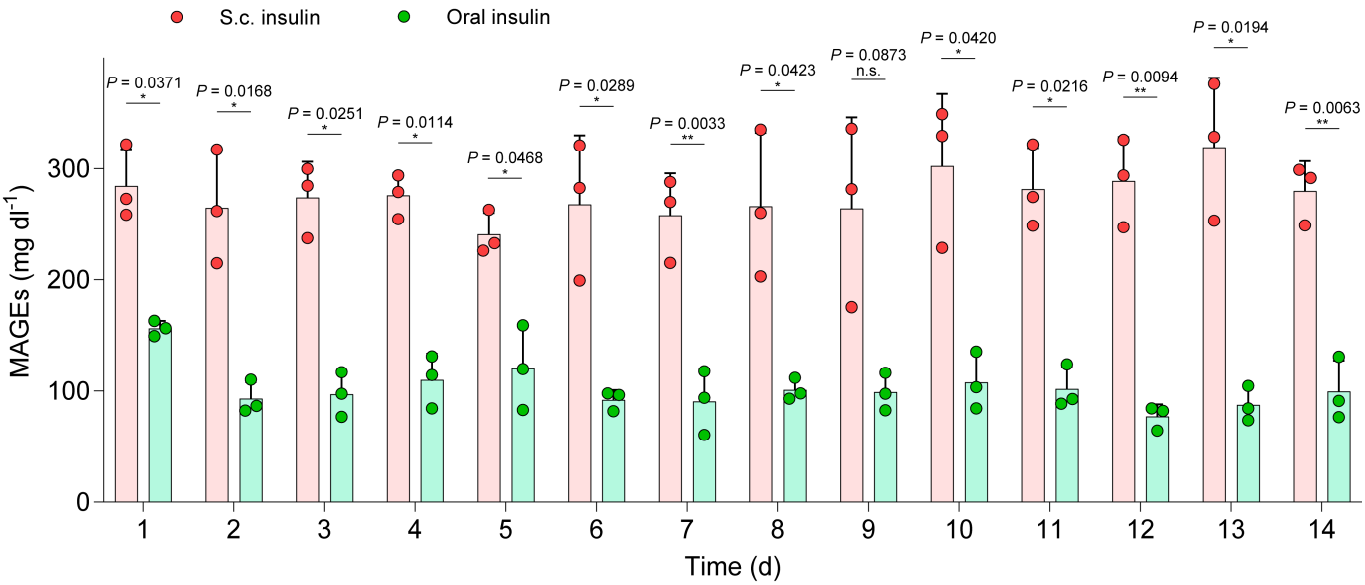

Supplementary Fig. 53 | Analysis of the daily glycemic variability of diabetic minipigs during the two-week consecutive treatment. Mean amplitude of glucose excursions (MAGEs) from day 1 to day 14 in the group treated with oral insulin versus the group treated with s.c. insulin. The MAGEs were much lower in the group treated with oral insulin than those in the group treated with s.c. insulin on each day, indicating that the oral insulin caused less daily glycemic fluctuations. Data points represent mean ± s.d. (n = 3 minipigs per group). Statistical significance was calculated *via* two-tailed Student's *t*-test. **P* < 0.05, ***P* < 0.01. n.s., not significant.

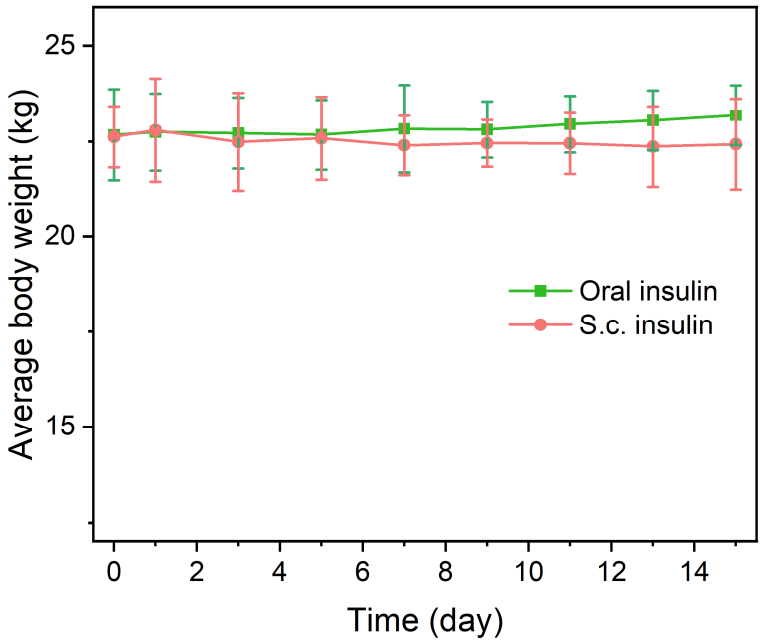

Supplementary Fig. 54 | Changes in the average body weight of diabetic minipigs during the two-week consecutive treatment with oral insulin or s.c. insulin. Data points represent mean ± s.d. (n = 3 minipigs per group). No dramatic body weight fluctuation for minipigs treated with oral insulin were recorded during the treatment course, suggesting unobvious systemic toxicity were posed by LG/insulin-40 over long-term dosing.

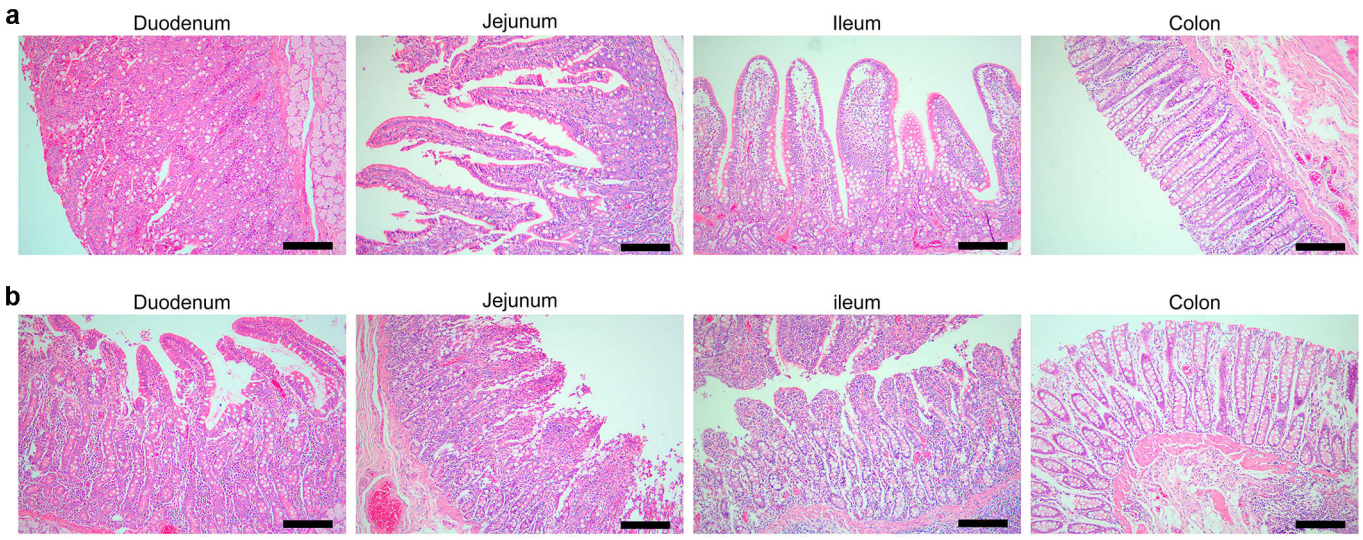

Supplementary Fig. 55 | Histological analysis of the intestinal segments of diabetic minipigs after two-week consecutive treatment. Representative hematoxylin and eosin-stained sections of duodenum, jejunum, ileum, and colon of diabetic minipigs after dosed with oral insulin (**a**) and s.c. insulin (**b**). Scale bar, 200 μm. Compared to the control group, no abnormalities in mucosal structures or signatures of inflammatory reactions were observed in the experimental group. These results showcased the biosafety of LG/insulin-40 towards the intestinal tissues of minipigs.

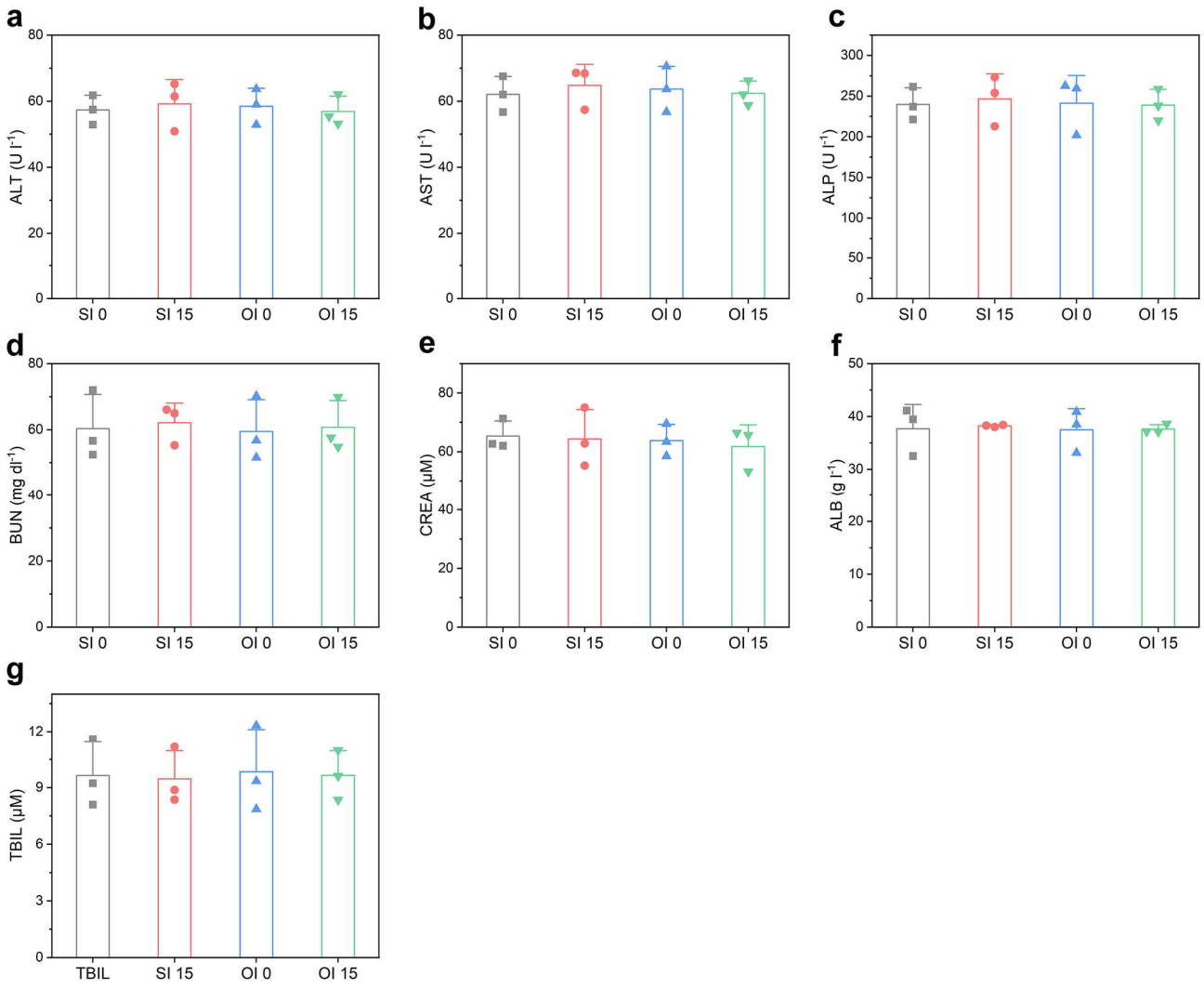

Supplementary Fig. 56 | Blood biochemical analysis of diabetic minipigs after two-week consecutive treatment. **a-g**, Blood chemical indexes of diabetic minipigs before (day 0; OI 0) and after (day 15; OI 15) treated with oral insulin twice daily for two weeks. Diabetic minipigs treated with s.c. insulin were used as the control (SI 0 and SI 15 represent s.c. insulin-treated group on day 0 and day 15, respectively). Serum levels of (**a**) ALT, (**b**) AST, (**c**) ALP, (**d**) BUN, (**e**) CREA, (**f**) ALB, and (**g**) TBIL. Data points represent mean ± s.d. (n = 3 minipigs per group). No statistical differences in each blood biochemical indexes were detected between the experimental and control groups. Minipigs treated with oral insulin showed similar levels of AST, ALT, CREA, and BUN to those of the s.c. insulin-treated group and those on day 0, suggesting that multi-day oral dosing of LG/insulin-40 exposed no observable adverse effects on the liver and kidney functions over long-term dosing.

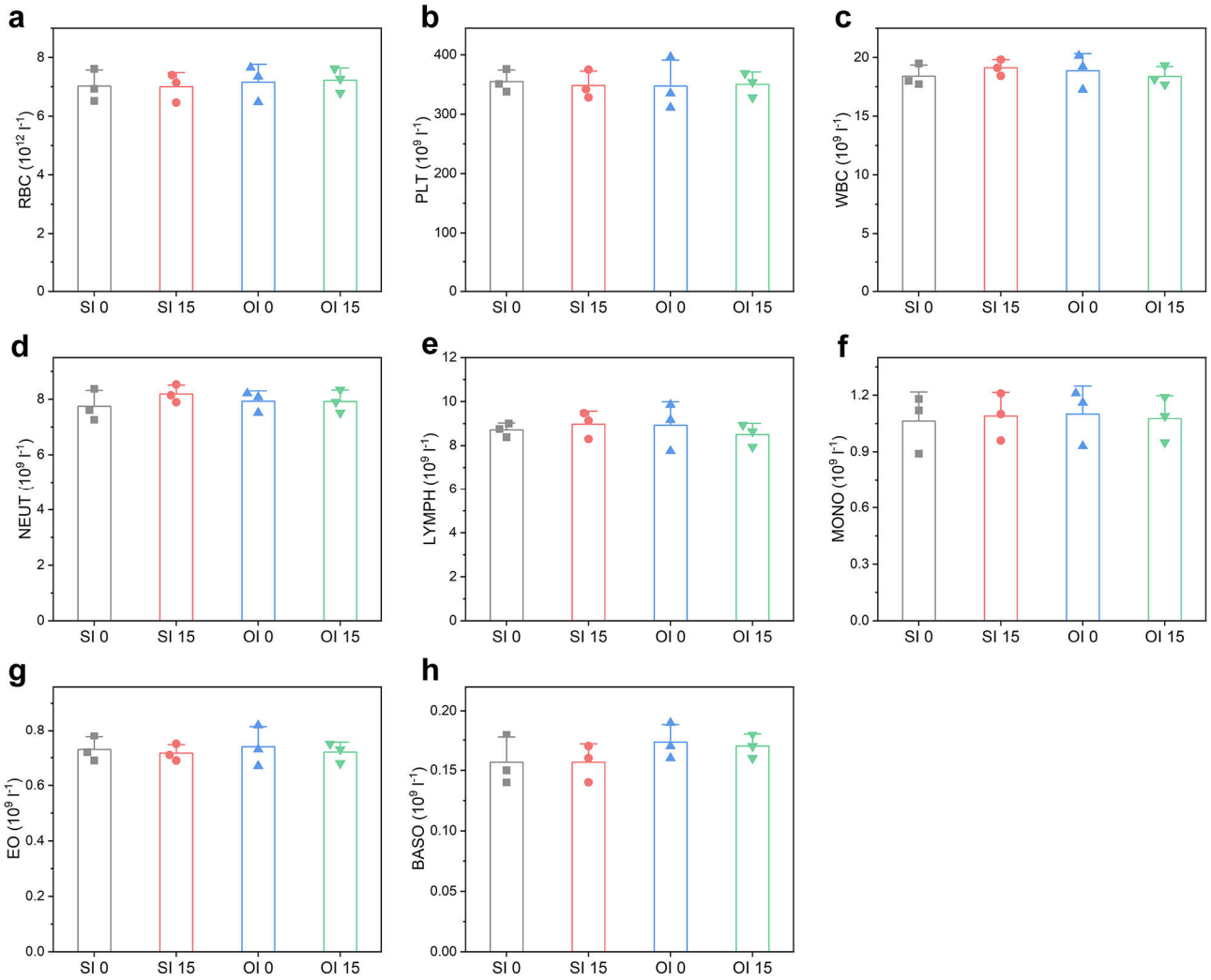

Supplementary Fig. 57 | Hematology analysis of diabetic minipigs after two-week consecutive treatment. **a-h**, Complete blood count of diabetic minipigs before (day 0; OI 0) and after (day 15; OI 15) treated with LG/insulin-40-loaded enteric capsules twice daily for two weeks. Diabetic minipigs treated with s.c. insulin were used as the control (SI 0 and SI 15 represent s.c. insulin-treated group on day 0 and day 15, respectively). **a**, Red blood cell (RBC) count; **b**, platelet (PLT) count; **c**, white blood cell (WBC) count; **d**, neutrophil (NEUT) count; **e**, lymphocyte (LYMPH) count; **f**, monocyte (MONO) count; **g**, eosinophile (EO) count; **h**, basophil (BASO) count. Data points represent mean ± s.d. (n = 3 minipigs per group). There were no obvious statistical differences in complete blood count between the two groups or changes after two-week consecutive treatment, suggesting that no immune response or systemic inflammation was caused over multi-day dosing of the oral insulin.

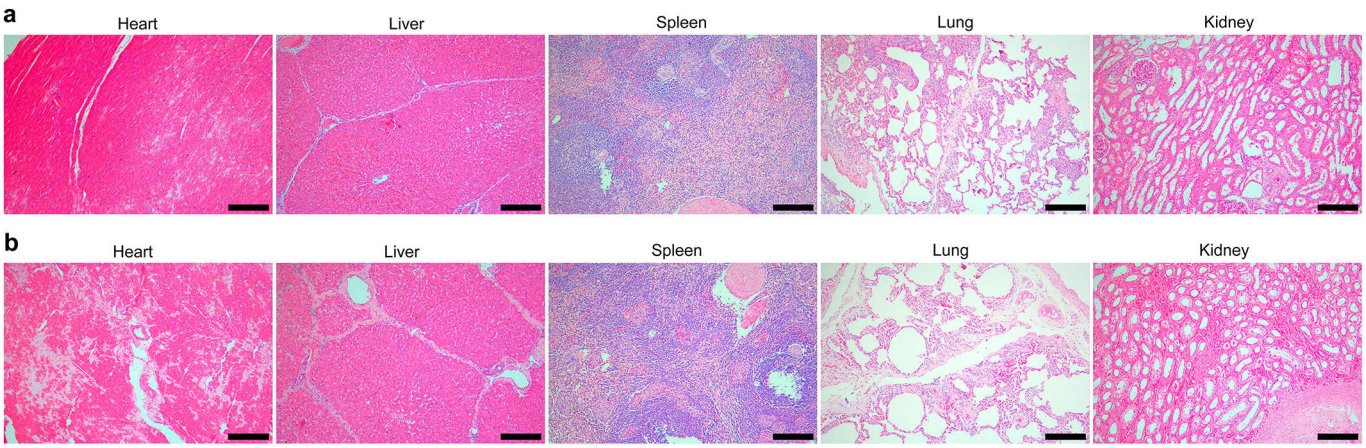

Supplementary Fig. 58 | Histological examination of the major organs of diabetic minipigs after two-week consecutive treatment**. a**, Representative hematoxylin and eosin-stained sections of the major organs (heart, liver, spleen, lung, and kidneys). **b**, Diabetic minipigs treated with s.c. insulin were used as the control. Scale bar, 200 μm. Compared to those of the control group, the histological sections of each organ displayed similar appearance after multi-day oral administration of LG/insulin-40 with no obvious abnormal pathologies, evidencing the biosafety of LG/insulin-40 towards the major organs.

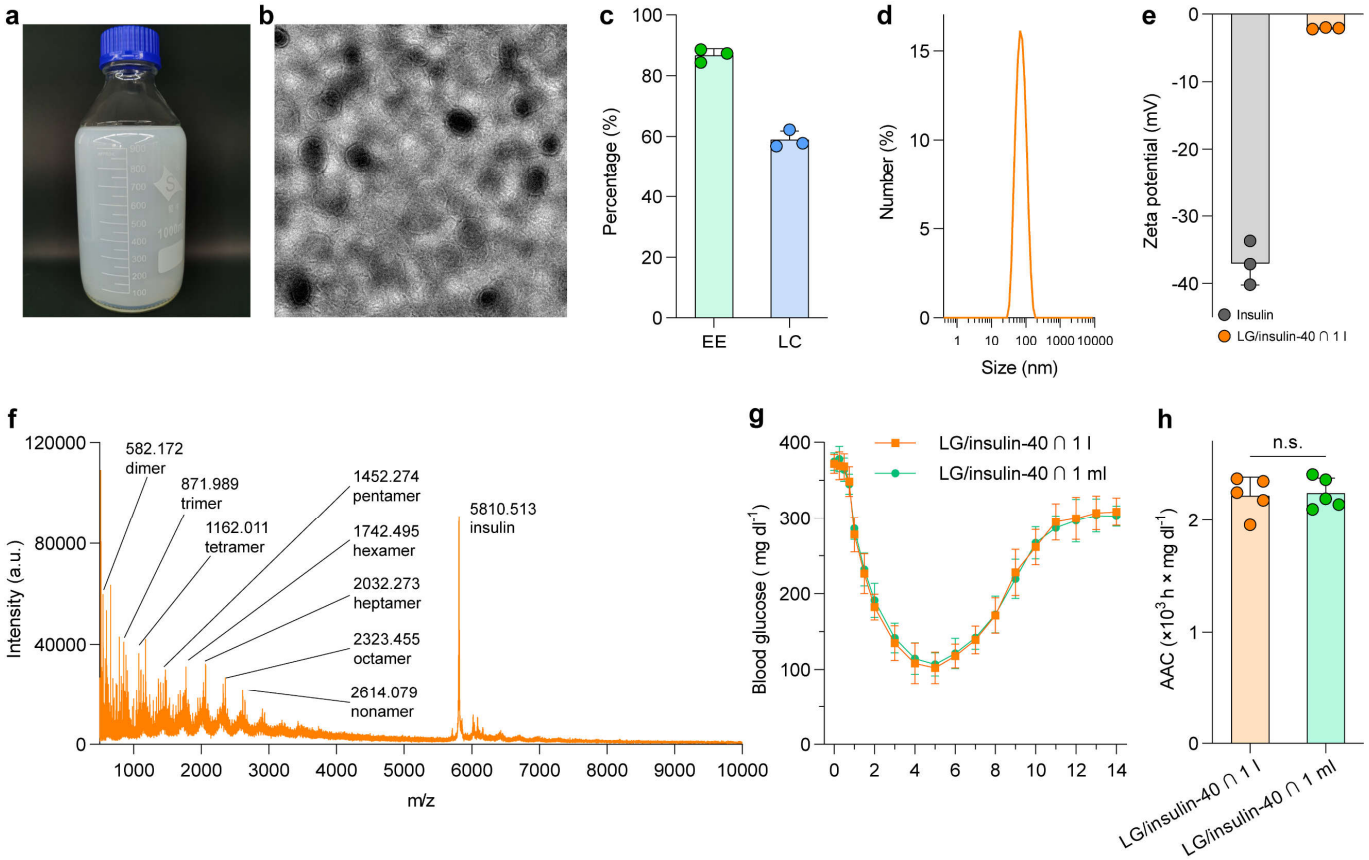

Supplementary Fig. 59 | Scale-up preparation of LG/insulin-40. **a**, Photograph showing the suspension of LG/insulin-40 formulated in a volume of 1 liter (LG/insulin-40 ∩ 1 l). **b-e**, Representative Cryo-TEM image (**b**), the encapsulation efficiency (EE) and loading capacity (LC; **c**), the dynamic light scattering analysis (**d**), the zeta-potential (**e**), and the MALDI-TOF mass spectrum (**f**) of LG/insulin-40 prepared from a formulation volume of 1 liter. For panel **e**, data points represent mean ± s.d. (n = 3 independent experiments). LG/insulin-40 prepared from a larger formulation volume reproduced the physiochemical characteristics of those prepared from a small volume. **g,** Profiles of changes in blood glucose levels of diabetic mice after oral gavage of LG/insulin-40 ∩ 1 l and LG/insulin-40 prepared from a formulation volume of 1 ml (LG/insulin-40 ∩ 1 ml) with enteric capsules (20 IU kg^{-1}). **h**, Integrated areas above the blood glucose curves from **g**. Similar pharmacological availabilities were produced by LG/insulin prepared from enlarged and small volumes. Data points represent mean ± s.d. (n = 5 mice per group). Statistical significance was calculated *via* two-tailed Student's *t*-test. n.s., not significant.

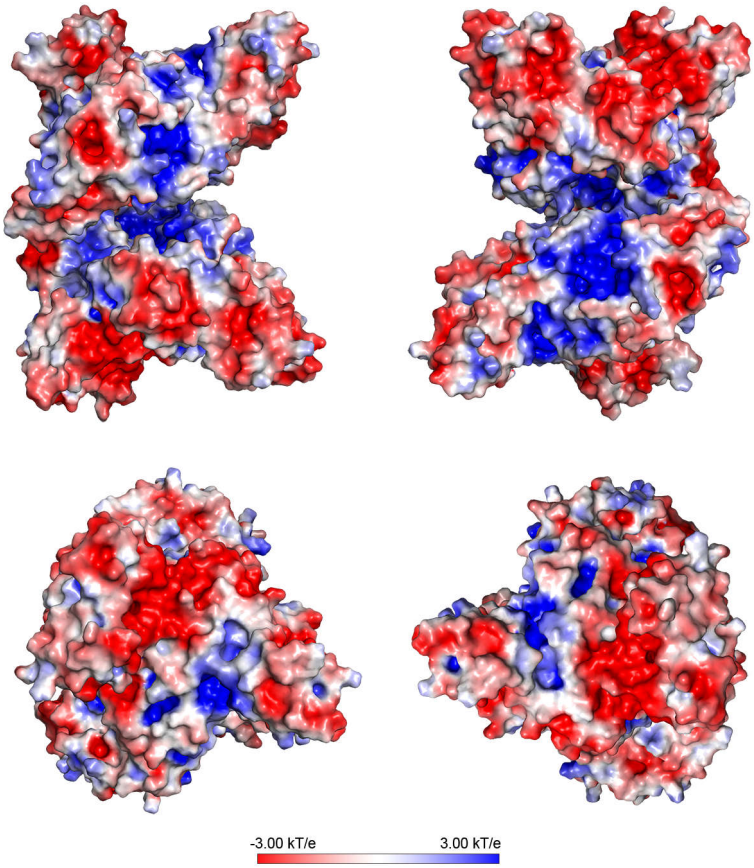

Supplementary Fig. 60 | The calculated electrostatic surface potential of HSA viewed from different directions. Red and blue colors represent negatively and positively charged domains, respectively; *k, T,* and *e* denote the Boltzmann constant, temperature, and magnitude of the electron charge, respectively. The images were generated by PyMOL using 1AO6 PDB file. Similar to insulin, HSA can bind LGs *via* electrostatic interactions between its negatively charged patches and the positively charged heads of LGs, leading to the *in-situ* formation of complexes.

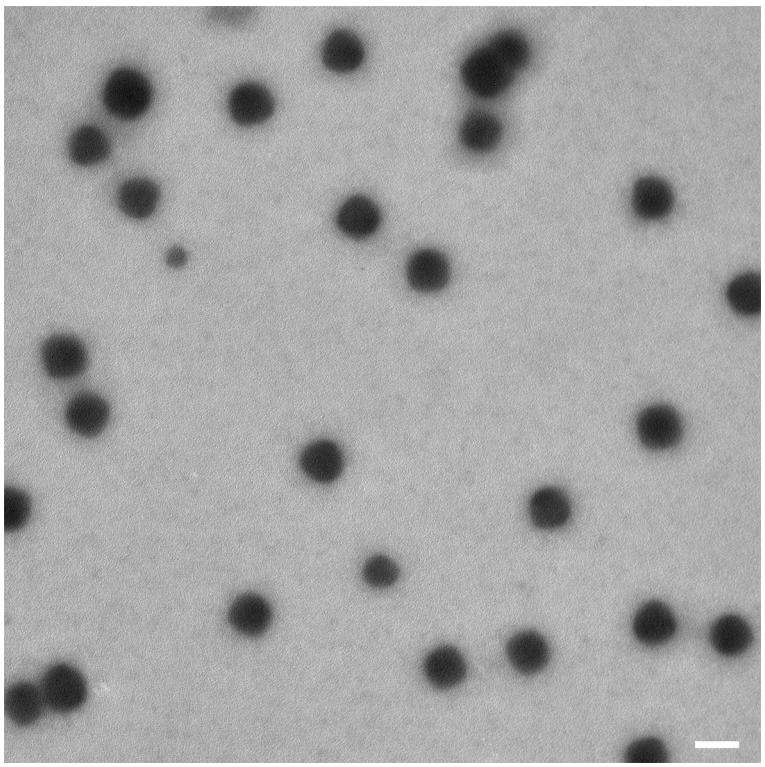

Supplementary Fig. 61 | Representative TEM image of the poly(disulfide)s-formulated HSA prepared by mixing LG monomers and HSA in aqueous solution at a staring molar ratio of 200:1 (LG/HSA-200). Scale bar, 200 nm. The samples were negatively stained by phosphotungstic acid.

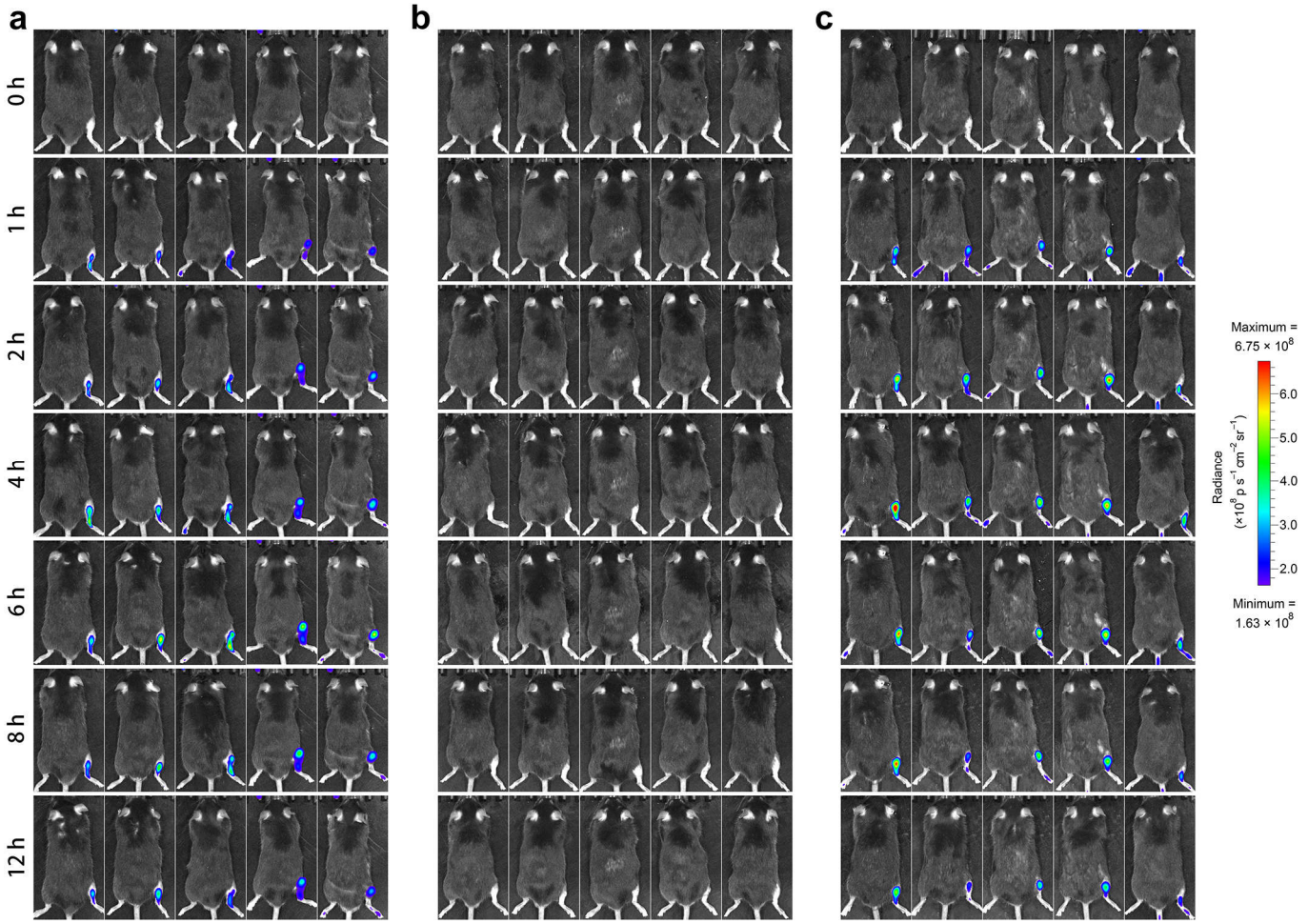

Supplementary Fig. 62 | Oral delivery of poly(disulfide)s-formulated HSA. *In vivo* imaging of tumor-bearing mice at different time points after oral gavage of enteric capsules loaded with Cy5.5-tagged HSA/LG-200 (20 mg kg^{-1}; **a**) or free Cy5.5-tagged HSA (20 mg kg^{-1}; **b**). **c**, Intravenous injection of Cy5.5-tagged HSA (4 mg kg^{-1}) was used as a control. Signals of Cy5.5 gradually appeared in the tumor after oral administration of Cy5.5-tagged HSA/LG-200. The accumulation of Cy5.5-tagged HSA in group **a** proved that poly(disulfide)s could be potentially extended to fabricate oral formulations of biomacromolecular therapeutics.

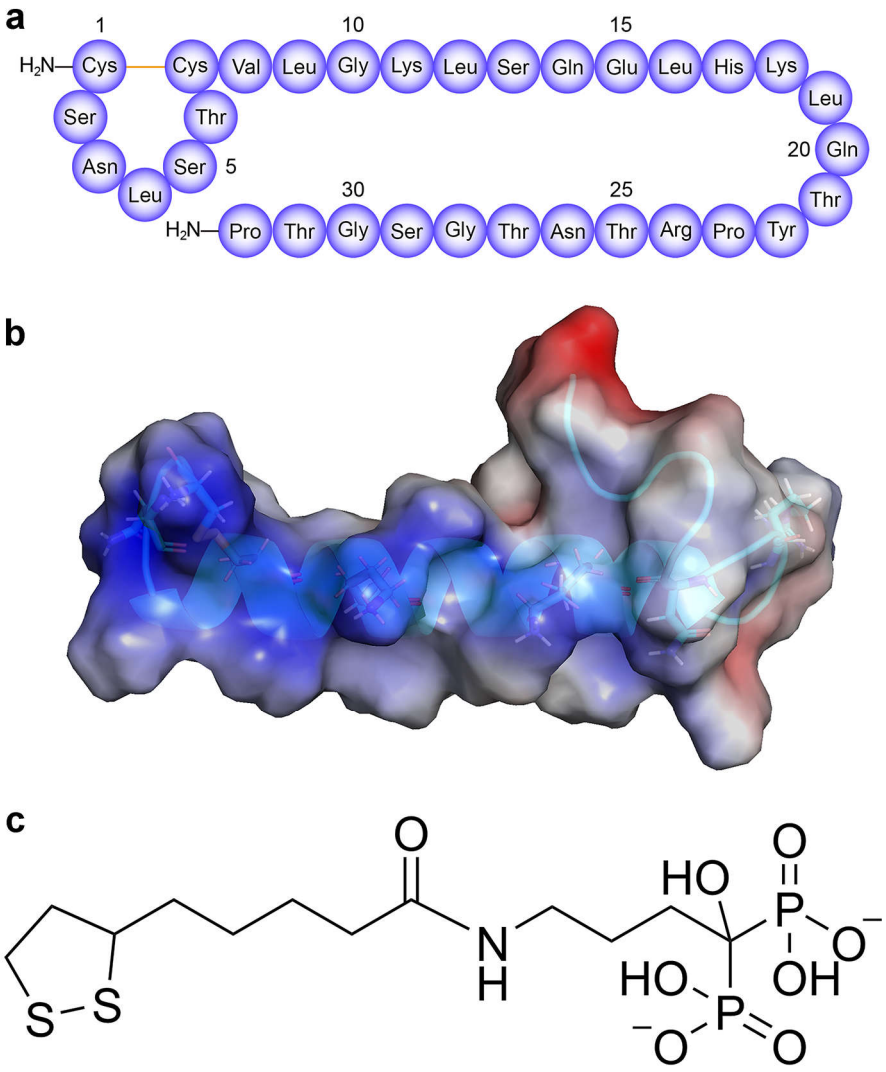

Supplementary Fig. 63 | Formulation of oral sCT using alendronate-conjugated lipoic acid (AL) as the poly(disulfide)s monomer. **a**, The amino acid sequence of sCT. **b**, Ball-and-stick presentation of the six positive charge-bearing amino acid residues (*i.e.*, Cys^{1}, Lys^{11}, His^{17}, Lys^{18}, Arg^{24}, and Pro^{32}) lying on the sCT surface. H and N atoms are in gray and blue, respectively. The calculated electrostatic surface potential of sCT colored from -3 kT/e (dark red) to + 3 kT/e (dark blue), where *k, T,* and *e* are the Boltzmann constant, temperature, and magnitude of the electron charge, respectively. The image was generated by PyMOL using 2GLH PDB file. **c**, The chemical structure of ionized AL monomer at pH 7.4. The positively charged patches on sCT surface could bind the negatively charged AL monomers to bring them into proximity and induce *in-situ* polymerization to form complexes.

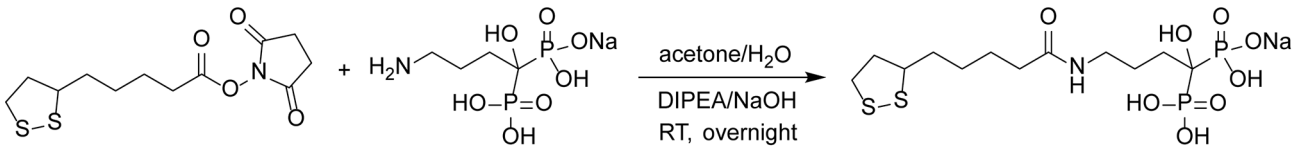

Supplementary Fig. 64 | Schematic illustration of the procedures for synthesizing the AL monomer.

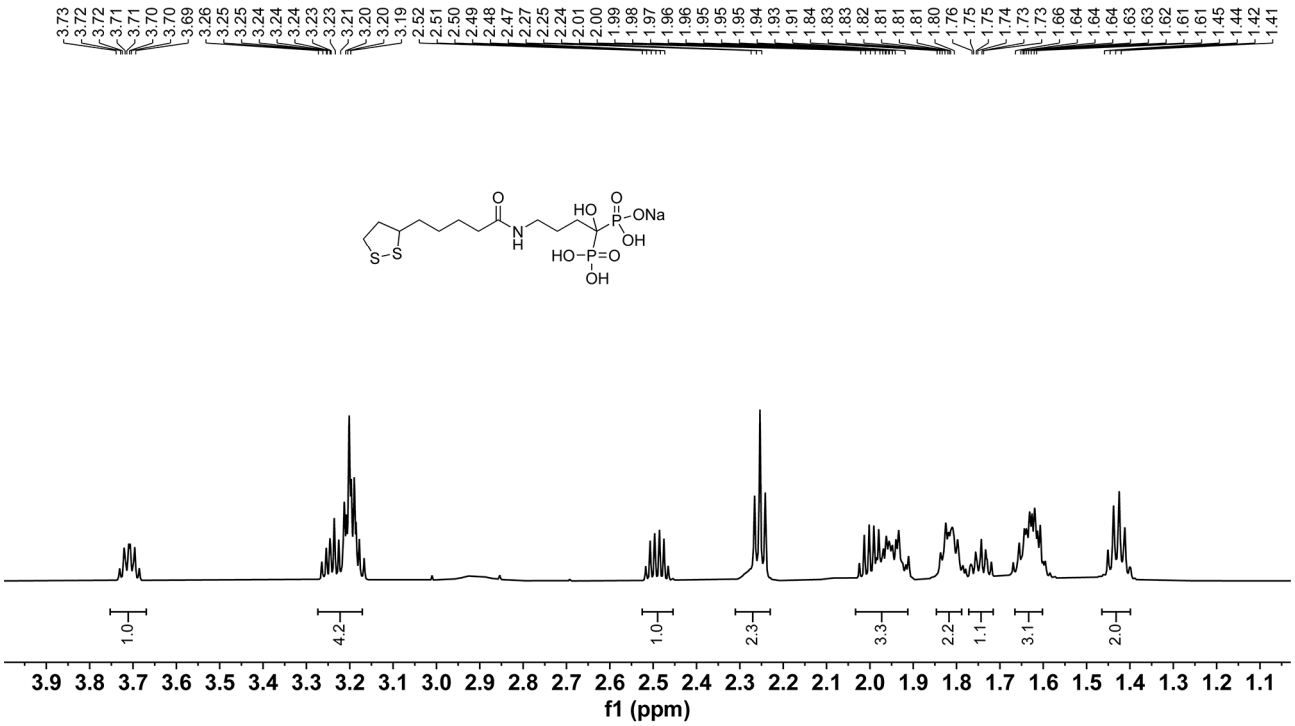

Supplementary Fig. 65 | ^{1}H NMR (600 MHz, in D_2O) spectrum of the AL monomer. δ (ppm): 3.71 (dq, *J* = 8.6, 6.2 Hz, 1H), 3.28 – 3.15 (m, 4H), 2.49 (dq, *J* = 12.3, 6.0 Hz, 1H), 2.25 (t, *J* = 7.4 Hz, 2H), 2.03 – 1.91 (m, 3H), 1.86 – 1.71 (m, 4H), 1.63 (ddd, *J* = 11.4, 9.0, 5.5 Hz, 3H), 1.43 (q, *J* = 7.7 Hz, 2H).

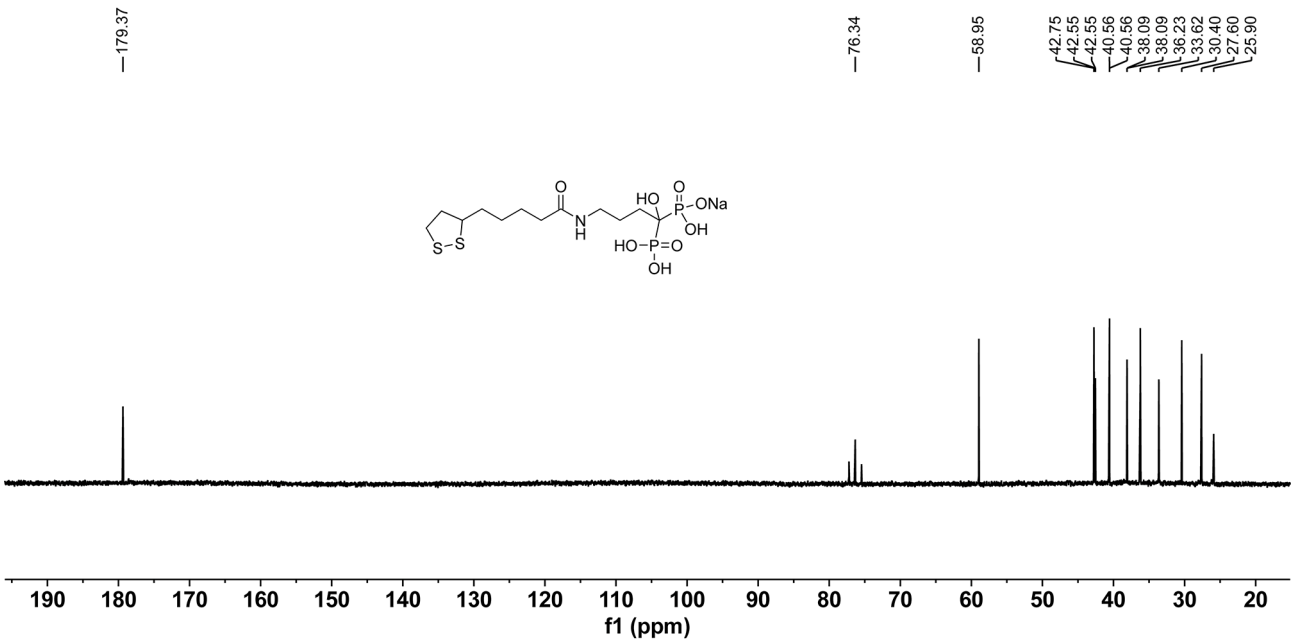

Supplementary Fig. 66 | ^{13}C NMR (600 MHz, D_2O) spectrum of the AL monomer. δ (ppm): 179.37, 76.34, 58.95, 42.75, 42.55, 40.56, 38.09, 36.23, 33.62, 30.40, 27.60, 25.90.

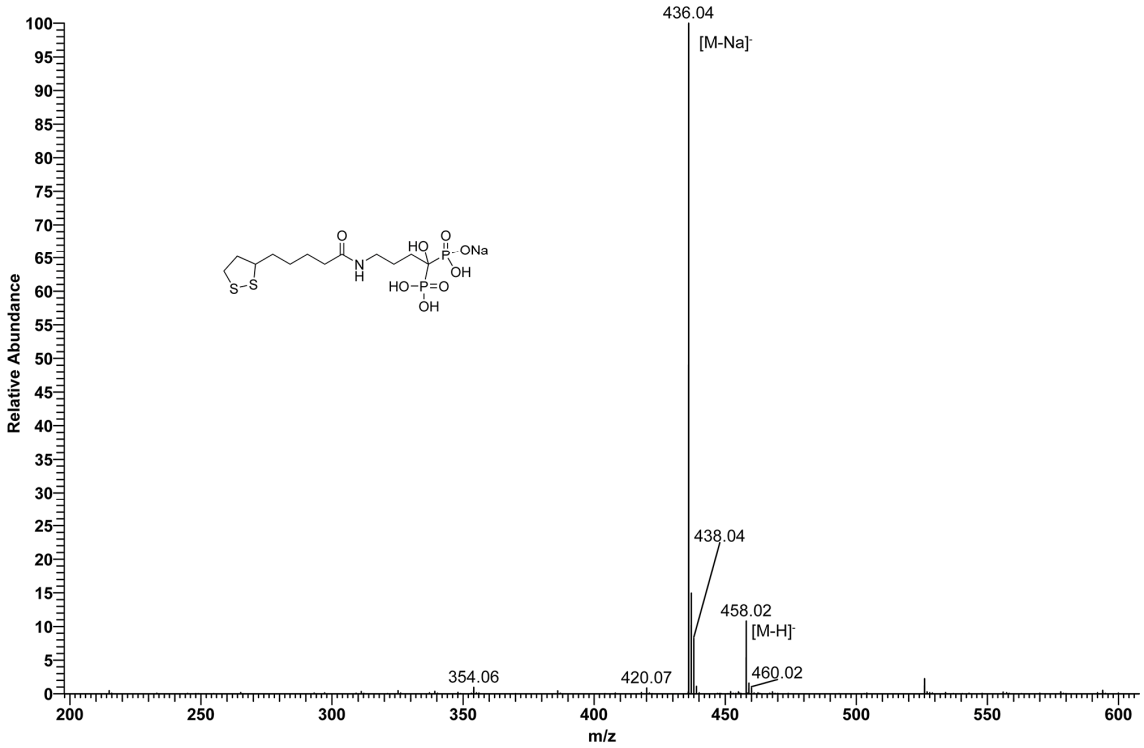

Supplementary Fig. 67 | Mass spectrum (ESI, H_2O) of the AL monomer which is matched by the peak at 436.04 ($[M\text{-}N_a]^-$).

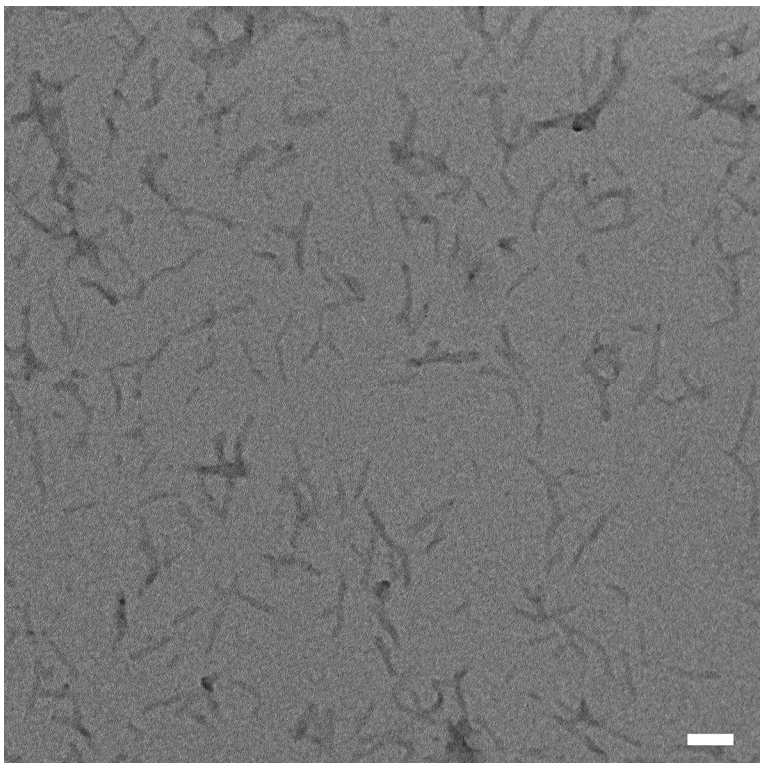

Supplementary Fig. 68 | Representative TEM image of the poly(disulfide)s-formulated sCT prepared by mixing AL monomers and sCT in aqueous solution at a staring molar ratio of 20:1 (AL/sCT-20). Scale bar, 100 nm. The samples were negatively stained by phosphotungstic acid.

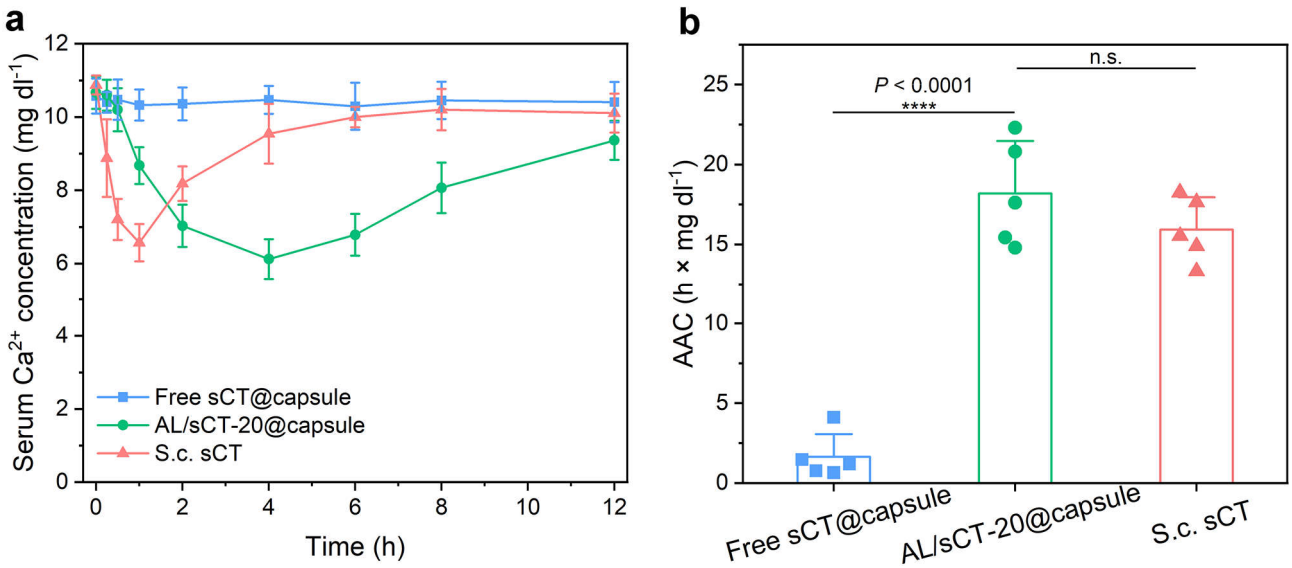

Supplementary Fig. 69 | Evaluation of the pharmacological efficacy of AL/sCT-20 in mice. **a**, Serum calcium levels of mice after oral gavage of AL/sCT-20 (0.25 mg kg^{-1}) using enteric capsules (AL/sCT-20@capsule), or free sCT-loaded enteric capsules (free sCT@capsule; 0.25 mg kg^{-1}). Subcutaneously injected sCT (0.05 mg kg^{-1}; s.c. sCT) was used as a control. **b**, Integrated areas above the serum calcium curves from **a** showing the pharmacodynamic performance of AL/sCT-20, which yielded a relative pharmacological availability of about 22.8%. Data points represent mean ± s.d. (n = 5 mice per group). Statistical significance was calculated with one-way ANOVA with Tukey's multiple comparisons test. ****$P < 0.0001$. n.s., not significant. The hypocalcemia effect elicited by the orally delivered poly(disulfide)s formulated-sCT suggested that poly(disulfide)s could be expanded to develop oral biologics beyond insulin, which could be readily achieved by changing the head groups ligated to the lipoic acid.

Supplementary Table S1 | Cost analysis of LG monomers. An estimate of the total cost to synthesize LG monomers from commercially available chemicals is calculated below. Detailed synthetic procedures were described in the Methods section. Note: as all experiments were conducted with lab accessible instruments, the corresponding cost was not included.

Chemicals	**Supplier**[#]	**Product No.**	**Cost (US$/package)**	**Cost per batch (US$/feeding or yield)**
(±)-α-Lipoic acid	Sigma-Aldrich	T5625-50G	$572.00	$47.25/4.13 g
1,1'-Carbonyldiimidazole	Sigma-Aldrich	115533-100G	$300.00	$12.18/4.06 g
Anhydrous dichloromethane	Sigma-Aldrich	270997-2L	$122.00	$16.78/275 ml
Ethylenediamine	Sigma-Aldrich	E26266-1L	$59.60	$0.60/10 ml
Sodium chloride	Sigma-Aldrich	S9888-5KG	$198.00	$4.28/108 g
Anhydrous sodium sulphate	Sigma-Aldrich	238597-2.5KG	$221.00	$0.66/7.5 g
1H-pyrazole-1-carbox-amidine hydrochloride	Sigma-Aldrich	40256-50G	$211.00	$8.65/2.05 g
Methanol	Sigma-Aldrich	179337-4L	$153	$0.76/20 ml
Diethyl ether	Sigma-Aldrich	296082-1L	$115.00	$28.75/250 ml
LG monomers				**$119.91/1.78 g**

As calculated, the chemicals needed for synthesis of 1 gram of LG monomers cost about 67.4 US$. According to the encapsulation efficiency and loading capacity yielded by our formulation procedure (Fig. 1d), 1 gram of LG monomers could be used to formulate about 9,136 IU of oral insulin (LG/insulin-40). If a diabetic patient took about 100 IU of this oral insulin each time, the required excipient monomers would cost only about 0.7 US$ per dose.

[#]The cost would be fluctuated if other chemical suppliers were chosen.

Supplementary References

1. Hubatsch, I., Ragnarsson, E.G.E. & Artursson, P. Determination of drug permeability and prediction of drug absorption in Caco-2 monolayers. *Nat. Protoc.* **2**, 2111-2119 (2007).
2. Chen, Z. et al. Synthetic beta cells for fusion-mediated dynamic insulin secretion. *Nat. Chem. Biol.* **14**, 86-93 (2018).
3. Danylchuk, D.I., Jouard, P.-H. & Klymchenko, A.S. Targeted Solvatochromic Fluorescent Probes for Imaging Lipid Order in Organelles under Oxidative and Mechanical Stress. *J. Am. Chem. Soc.* **143**, 912-924 (2021).
4. Lamson, N.G., Berger, A., Fein, K.C. & Whitehead, K.A. Anionic nanoparticles enable the oral delivery of proteins by enhancing intestinal permeability. *Nat. Biomed. Eng.* **4**, 84-96 (2020).
5. Hill, N.R. et al. Normal Reference Range for Mean Tissue Glucose and Glycemic Variability Derived from Continuous Glucose Monitoring for Subjects Without Diabetes in Different Ethnic Groups. *Diabetes Technol. Ther.* **13**, 921-928 (2011).
6. Chen, Z. et al. A Multinuclear Metal Complex Based DNase-Mimetic Artificial Enzyme: Matrix Cleavage for Combating Bacterial Biofilms. *Angew. Chem. Int. Ed.* **55**, 10732-10736 (2016).
7. Boyd, D.B. Structural and spectral properties of the disulfide linkage in proteins and other molecules. *Int. J. Quantum Chem.* **8**, 13-19 (1974).
8. Wu, L. et al. Transport Mechanisms of Butyrate Modified Nanoparticles: Insight into "Easy Entry, Hard Transcytosis" of Active Targeting System in Oral Administration. *Mol. Pharm.* **15**, 4273-4283 (2018).
9. Apodaca, G. Endocytic Traffic in Polarized Epithelial Cells: Role of the Actin and Microtubule Cytoskeleton. *Traffic* **2**, 149-159 (2001).
10. Guo, M. et al. Probing the Stochastic, Motor-Driven Properties of the Cytoplasm Using Force Spectrum Microscopy. *Cell* **158**, 822-832 (2014).
11. Derivery, E., Bartolami, E., Matile, S. & Gonzalez-Gaitan, M. Efficient Delivery of Quantum Dots into the Cytosol of Cells Using Cell-Penetrating Poly(disulfide)s. *J. Am. Chem. Soc.* **139**, 10172-10175 (2017).
12. Jiang, X. et al. Noninvasive monitoring of hepatic glutathione depletion through fluorescence imaging and blood testing. *Sci. Adv.* **7**, eabd9847 (2021).
13. Samiec, P.S., Dahm, L.J. & Jones, D.P. Glutathione S-Transferase in Mucus of Rat Small Intestine. *Toxicol. Sci.* **54**, 52-59 (2000).
14. Nkabyo, Y.S., Ziegler, T.R., Gu, L.H., Watson, W.H. & Jones, D.P. Glutathione and thioredoxin redox during differentiation in human colon epithelial (Caco-2) cells. *Am. J. Physiol. - Gastrointest. Liver Physiol.* **283**, G1352-G1359 (2002).
15. Cornell, J.S. & Meister, A. Glutathione and gamma-glutamyl cycle enzymes in crypt and villus tip cells of rat jejunal mucosa. *Proc. Natl. Acad. Sci. USA* **73**, 420-422 (1976).
16. Jiang, X., Du, B. & Zheng, J. Glutathione-mediated biotransformation in the liver modulates nanoparticle transport. *Nat. Nanotechnol.* **14**, 874-882 (2019).